



Faculty of Sciences
Department of Geography

Nasem Badr El Din

Assessing environmental change of an arid region at multi-spatial scales using remote sensing and GIS

Promoter

Prof. Dr. Rudi Goossens

Dissertation submitted in accordance
with requirements for the degree of
doctor of Science: Geography, 2013

Front cover:

Egypt from space, taken by Chris Hadfield (Canadian astronaut)

Copyright: Nasem Badr El Din, 2013

Published by:

Department of Geography, Ghent University

Krijkslaan 281-S8, 9000 Gent, Belgium

© All rights reserved

Promoter:

Prof. Dr. Rudi Goossens

Ghent University, Department of Geography

Members of the examination committee

Prof. Dr. ir. Alain De Wulf - (Chairman)

Ghent University, Department of Geography

Prof. Dr. Anton Van Rompaey

KULeuven, Department of Earth and Environmental Sciences

Prof. Dr. Ioannis Gitas

Aristotle University of Thessaloniki, Faculty of Forestry and Natural Environment

Laboratory of Forest Management and Remote Sensing

Prof. Dr. Morgan De Dapper

Ghent University, Department of Geography

Prof. Dr. Philippe De Maeyer

Ghent University, Department of Geography

Prof. Dr. Veerle Van Eetvelde

Ghent University, Department of Geography

"Man must rise above Earth to the top of the atmosphere and beyond, for only then will he fully understand the world in which he lives" - Socrates (469-399 BC)



Acknowledgment

Many persons and institutes have contributed to this research since it began in 2009. Each contribution has in some way enriched the process and facilitated my ability to bring this research to successful outcomes. I gratefully acknowledge the support of all those who have assisted me in this effort, but I will also make specific mention of those persons whose contributions have been especially significant to my work.

It would not have been possible to complete this task without the help and guidance of my supervisor, Professor Rudi Goossens, I'm grateful for the independence, sufficient freedom, responsibilities and friendly working environment he has given me during my thesis work. I am very grateful to work with Dr. Amaury Frankl, Dr. Jaime Uria-Diez, Dr. J.Mateu, Cornelis Stal, and Dr. Magdy El-Bana. Also, many thanks to my dear colleagues Marijn Hendrickx, Miro Jacob, Timothy Nuttens, Sil Lanckriet, and Klaas Annys for sharing ideas and nice discussions. Also, many thanks to Helga Vermeulen, Wim Van Roy, Michiel Van den Berghe, and Tineke De Keyser for being very helpful.

Many thanks to my dear friends Ali Youssef, Youssef Zidan, Dr. Khalid Mostafa, Ir. Motaz Mousa, Sami Ismail, Ahmed Magdy, Ashraf Rootel, Mohamed Safroot, and Dr. Ahmed Ramadan for being very supportive and helpful. Also, I'm very grateful to Hedwig Bockstal and Jouris and Christine Dubois-Vandewyngaerde. Many thanks to Prof. Dr. Ingmar Unkel for his advices and care during my PhD.

I owe a deep gratitude to my wife Sara El-Esawe, who always supported me to go for my dreams. And a big apology to my daughter Habeba for being sometimes busy or not at home to play with her. Also, Special thanks go to my family, for their support and encouragement.

Part of this thesis was supported by Agricultural Research and Development Fund (ARDF) in Egypt. Sincere thanks to the research staff at the soil and water department, Faculty of Environmental Agricultural Sciences in Suez Canal University.

I apologise to those that I forgotten to mention here.

Summary

Desertification is responsible for depleting natural resources, which is globally happening in an alarming rate. It is considered as the major environmental change that affects about 40% of the world dry lands, which are populated by approximately one billion humans. In this research the main objective was to explore new methodologies and indicators, which can be implemented in an arid environment using remote sensing, GIS and field survey to obtain information about the desertification status. The case studies of this research were all conducted in Egypt, where about 95% of the land are deserts and extremely arid. The population of Egypt is about 85 million with a population growth rate of 1.92%, and approximately 95% of population lives on only 4% of the national territory.

The Soil-Adjusted Vegetation Index (SAVI) was chosen as an indicator to monitor the desertification change in regional scale for assessing the spatio-temporal dynamics of vegetation cover in Egypt. A multi-temporal satellite data of MODerate resolution Imaging Spectroradiometer (MODIS) were used to estimate SAVI and Land Surface Temperature (LST). In this particular research we focused on assessing the trend of the vegetation cover change in the seasons of January, March, June, September and December for the years 2002, 2005, 2008 and 2011. The magnitude of the vegetation cover change in periods 2002-2005, 2005-2008 and 2008-2011 at ≤ 100 and > 100 meters elevation were analyzed. A major increase in the vegetation cover occurred in the period 2002-2005, which was about 3400 km², as a result of two national mega-projects (Toshka Project and El-Salam Canal). In contrast, vegetation cover decreased by 5500 km² in March during the period 2005-2008, coinciding with the period when the management of the mega-projects failed. Three sites were chosen in this investigation (Kom Ombo, El-Oweinat and Nile Delta) in order to observe the difference of desertification dynamics and to understand relationship between the vegetation cover distribution and other environmental variables.

The Sinai Peninsula was the second case study for monitoring the desertification change. The MODIS-Based disturbance index (MBDI) was improved by estimating the annual long-term variation in the ratio of maximum LST and SAVI on a pixel-by-pixel basis. A significant relation was found between the mean-maximum SAVI and mean-maximum LST in the dry season. The response of the MBDI to land degradation was assessed by comparing the obtained soil salinity data to the algorithm outcomes. The results showed that the proposed new satellite-based algorithm detected the spatial extent of prime land degradation in an arid environment.

A spatio-temporal study was done to assess and monitor the Land Use and Land Cover (LULC) change in the arid region of El-Arish in North Sinai. In the past 11 years a dramatic changes of environment have been recorded in case studies. The Post Classification Comparison (PCC) method was used to observe the changes using multi-temporal Landsat satellite images, which were captured in the years 1999, 2001, 2005, and 2010. The overall accuracy of the produced thematic images was assessed regarding to the quantity and allocation disagreements.

Many researchers found that Google images are valuable for environmental studies. We developed a new method for assessing the spatial distribution of the Halophytic Species (HS) in an arid coastal environment of El-Zaraniq Protected Area in North Sinai Governorate. The obtained information was based on the field survey assumptions that explained plant-pixel relationship in

this particular case study. Three different types of digital image processing techniques were implemented and validated in order to obtain accurate HS spatial distribution. The spatial structure was modeled using stochastic point processes, in particular a hybrid family of Gibbs processes. A new model is proposed which is handled a hard-core structure at very short distances, together with a cluster structure in short-to-medium distances and a Poisson one for larger distances. This model found to fit the data perfectly well.

Anti-desertification policies and advanced agricultural management are highly required in Egypt to decrease any environmental crises and food shortage. Therefore, the satellite-based algorithm is able to recognize the difference between the natural variability and instantaneous/non-instantaneous desertification symptoms in an arid environment. Thus, soil and water management were the keys of land development and positive LULC dynamics. Changing agricultural policies and using carefully the available water resources are highly required in Egypt to prevent severe food shortage in the near future.

Samenvatting

Desertificatie is in belangrijke mate medeverantwoordelijk voor de uitputting van onze natuurlijke bronnen. Deze wereldwijde uitputting zit momenteel in een alarmerende fase. Er wordt algemeen aangenomen dat in 40% van de aride gebieden, waar ongeveer één miljard mensen wonen, desertificatie de grootste milieuverandering is. De hoofddoelstelling van dit onderzoek was het ontwikkelen en analyseren van nieuwe methodologieën en indicatoren van desertificatie, gebruikmakend van teledetectie, GIS en terreinwerk. Dit onderzoek werd toegepast op verschillende studiegebieden in Egypte. Egypte bestaat voor 95% uit woestijn, het land heeft ongeveer 85 miljoen inwoners met een jaarlijkse bevolkingsaan groei van 1.92% en ongeveer 95% van deze bevolking leeft op slechts 4% van het grondgebied.

Om de tijdruimtelijke vegetatiedynamieken in Egypte te bepalen werd de Soil-Adjusted Vegetation Index (SAVI) gekozen als indicator om de desertificatie te monitoren. Multi-temporele satellietdata van de MODerate resolution Imaging Spectroradiometer (MODIS) werd gebruikt om de SAVI-index en Land Surface Temperature (LST) in te schatten. In dit onderzoek focusten we op de bepaling van de tendens in vegetatiebedekking voor de maanden januari, maart, juni, september en december in de jaren 2002, 2005, 2008 en 2011 in drie studiegebieden (Kom Ombo, El-Eweinat en de Nijldelta). De mate van verandering in vegetatiebedekking in de perioden 2002-2005, 2005-2008 en 2008-2011 voor hoogtes ≤ 100 en > 100 m werd hierbij geanalyseerd. De grootste toename in vegetatiebedekking (ongeveer 3400 km²) vond plaats in de periode 2002-2005 als gevolg van twee nationale infrastructuurprojecten (Toshka Project en El-Salam kanaal). In de periode 2005-2008 gebeurde echter een afname van vegetatie in de maand maart van 5500 km². Deze afname viel samen met de periode waarin het management van deze grote projecten faalde. De monitoring van de desertificatie zorgde er voor dat de relatie tussen de verspreiding van de vegetatiebedekking en andere milieuvariabelen begrepen kon worden.

Een tweede case studie voor het monitoren van desertificatie in functie van de aride milieucondities werd uitgevoerd op het Sinäi-schiereiland. De MODIS-Based Disturbance Index (MBDI) werd geoptimaliseerd door de jaarlijkse variaties in de verhouding tussen de maximale LST en SAVI pixelgewijs op langere termijn te vergelijken. Tussen de gemiddelde jaarlijkse maximum SAVI and LST in het droge seizoen was deze relatie significant. Om de invloed van de MBDI op de landdegradatie in te schatten werd de verkregen data over bodemsaliniteit vergeleken met de uitkomst van het MBDI-algoritme. Het voorgestelde nieuwe algoritme, gebaseerd op satellietdata, detecteert de ruimtelijke spreiding van landdegradatie in een aride milieu al in het eerste stadium.

Een tijdruimtelijke studie om de de Land Use and Land Cover (LULC) te monitoren werd uitgevoerd in de aride regio rond de stad El-Arish in Noord-Sinäi. Volgens verschillende rapporten vonden er tijdens de voorbije elf jaar ingrijpende veranderingen plaats. We gebruikten de Post Classification Comparison (PCC) om deze veranderingen waar te nemen, gebruikmakend van multi-temporele Landsat satellietbeelden van de jaren 1999, 2001, 2005 en 2010, waarna ook de globale nauwkeurigheid van de geproduceerde thematische kaarten werd geanalyseerd.

Vele onderzoekers stellen dat Google Earth-beelden nuttig kunnen zijn voor milieustudies. Wij ontwikkelden een nieuwe methode om de ruimtelijke distributie van de Halophytic Species (HS) in het aride litorale milieu van 'El-Zaraniq Protected Area' in Noord-Sinäi te detecteren. Op basis van

veldwerk werden assumpties opgesteld die de plant-pixel relatie in dit specifieke geval beschreven. De ruimtelijke spreiding van de HS kon verkregen en gevalideerd worden met gebruik van drie verschillende digitale beeldverwerkingstechnieken. Het hybrid family of Gibbs proces, een stochastisch puntproces, werd toegepast om hun ruimtelijke structuur te modelleren. Het nieuwe model dat wordt voorgesteld, behandelt een hardcore-structuur voor zeer korte afstanden tussen de verschillende habitats, een clusterstructuur voor korte tot middellange afstanden en een Poison-structuur voor grotere afstanden en levert uitstekende resultaten op.

Een beleid gericht op anti-desertificatie en geavanceerd landbouwmanagement in Egypte is meer en meer noodzakelijk om eender welke milieucrisis in te dijken of een voedseltekort te vermijden. Door het gebruik van op satellietdata gebaseerde algoritmes konden we het verschil in natuurlijke variabiliteit en de symptomen van een al dan niet onmiddellijke desertificatie in een aride omgeving in een vroeg stadium herkennen. Bodem- en watermanagement zijn de sleutel tot landontwikkeling en positieve LULC-dynamieken. Egypte heeft hiervoor dringend nood aan een veranderende landbouwpolitiek en een bewust gebruik van de beschikbare waterbronnen. Dit onderzoek reikt daarvoor een aantal methodologieën en indicatoren aan en draagt aldus bij om Egypte te beschermen tegen een ernstig voedseltekort of een milieucrisis in de nabije toekomst.

Table of Contents

<i>Acknowledgment</i>	v
<i>Summary</i>	vi
<i>Samenvatting</i>	viii
<i>Table of Contents</i>	x
<i>List of acronyms and symbols</i>	xiii

Chapter 1

General introduction	1
1.1 Global interest of desertification	2
1.1.1 Natural impact	4
1.1.2 Human impact.....	6
1.2 Technology for monitoring environmental changes in arid regions: remote sensing and GIS.....	7
1.2.1 Remote sensing and GIS: tools for environmental monitoring	8
1.2.2 Remote sensing and GIS integration system.....	10
1.3 New approaches for assessing desertification in arid lands.....	12
1.3.1 Bi-stable ecosystem dynamics.....	12
1.3.2 Satellite-based Environmental modeling	13
1.3.3 The spatial pattern analysis.....	13
1.4 General objective	14
1.5 Research objectives per chapter	14
1.6 Thesis structure and organization.....	16
1.7 References.....	18

Chapter 2

Egypt dry lands: A general description	23
2.1 Overview	25
2.2 Geological characteristics	26
2.3 Geographical Characteristics.....	26
2.4 Soil-Vegetation Relationships	28
2.5 Climate	31
2.5.1 Hyperarid provinces	31
2.5.2 Arid provinces.....	31
2.6 References.....	32

Chapter 3

Assessing the spatio-temporal dynamics of vegetation cover as an indicator of desertification in Egypt using multi-temporal MODIS satellite images	33
3.1 Introduction	35
3.2 Study area description.....	36
3.3 Materials and methods	39
3.3.1 Remote sensing and meteorological datasets.....	39

3.3.2	Field survey	40
3.3.3	Data analysis	42
3.3.4	Accuracy assessment of SAVI distributions.....	44
3.3.5	The vegetation covers feedbacks as desertification indicator.....	44
3.4	Results and discussion.....	45
3.4.1	Spatio-temporal patterns in vegetation cover spatial distribution along with elevation	45
3.4.2	Vegetation covers distribution along with elevation at two significant seasons	47
3.4.3	Spatio-temporal patterns in vegetation cover spatial distribution along with climatic condition (LST and P)	49
3.4.4	Trends of the vegetation cover in Egypt (2002-2011)	51
3.4.5	Bi-stable system for assessing desertification dynamics.....	52
3.5	Conclusions and perspectives	56
3.6	References	57

Chapter 4

A satellite-based disturbance index algorithm for monitoring mitigation strategies effects on desertification change in an arid environment..... 61

4.1	Introduction	63
4.2	Materials and methods	64
4.2.1	Study area description and field survey	64
4.2.2	Statistical analysis.....	68
4.2.3	Remote sensing data	69
4.2.4	MBDI improvement for monitoring desertification change.....	69
4.2.5	Assessing the MBDI algorithm	72
4.3	Results and discussions	73
4.3.1	Mean-maximum LST and SAVI relationship	73
4.3.2	MBDI application for desertification recovery detection.....	77
4.4	Conclusion	79
4.5	References	80

Chapter 5

Monitoring Land Use / Land Cover Change Using Multi-Temporal Landsat Satellite Images in Arid Environment: A Case Study of El-Arish, Egypt..... 83

5.1	Introduction	85
5.2	Study area description and field survey	86
5.3	Materials and methods	88
5.3.1	Data sets	88
5.3.2	Image pre-processing	88
5.3.2.1	Geometric correction.....	88
5.3.2.2	Image enhancement	89
5.3.2.3	ETM+ SLC off and gap filling	89
5.3.3	Supervised classification.....	90
5.3.4	Post-Classification Comparison (PCC).....	90
5.3.5	Classification accuracy assessment	90
5.4	Results and discussions	91
5.4.1	LULC trend of changes over decade	93
5.4.2	Causes of LULC change trajectory	94
5.5	Conclusion	97
5.6	References	98

Chapter 6

Object-based image analysis for monitoring the spatial distribution of a halophytic species in an arid coastal environment	101
6.1 Introduction	103
6.2 Case study description, field survey and data collection	104
6.3 Materials and methods	106
6.3.1 Image pre-processing	106
6.3.1.1 Image enhancement	107
6.3.1.2 Geometric correction	107
6.3.2 Object - pixels relationship	107
6.3.2.1 Roberts Cross Edge Detector (RCED)	109
6.3.2.2 Dilate Operator (DO)	109
6.3.2.3 Erode Operator (EO)	109
6.3.3 Data validation	109
6.3.4 Spatial analysis and statistical modelling	112
6.4 Results and discussions	113
6.4.1 Soil salinity and microtopography relationship	113
6.4.2 HS spatial distribution along with EC and pH	114
6.5 Conclusion	120
6.6 References	121

Chapter 7

General conclusions and recommendations	123
7.1 General conclusion	125
7.2 Bi-stable ecosystem balance for assessing desertification status	127
7.3 MODIS Based Disturbance Index (MBDI) for monitoring the desertification development	129
7.4 A decade of LULC change in El-Arish city	131
7.5 Google Earth images for spatial pattern analysis	133
7.5.1 Object-pixel relationship and extraction in arid environment	133
7.5.2 Integration system based analysis for HS spatial distribution	134
7.6 Suggestions for future research	135
7.7 Clues for decision makers on the use of the research findings	136
7.8 References	137
Appendix A	CD rom
Appendix B	CD rom

List of acronyms and symbols

Bwh	Arid-desert-hot Climate
DN	Digital Number
DO	Dilate Operator
DOS	the Dark Object Subtraction
e	the regression error
EC	Electric Conductivity (dS/m)
EO	Erode Operator
EROS	the Earth Resources Observation and Science
ETM+	the Enhanced Thematic Mapper Plus
ETM+ SLC off	the Scan Line Corrector failed of Landsat 7 images
EVI	Enhanced Vegetation Index
FAO	Food and Agriculture Organization
GCP	Ground Control Point
GIS	Geographic Information System
GMTED2010	Global Multi-resolution Terrain Elevation Data 2010
GPS	Global Positioning System
HS	Halophytic Species
KML	Keyhole Markup Language
L	the soil brightness correction factor
LDCM	Landsat Data Continuity Mission
LST	Land Surface Temperature
LULC	Land Use and Land Cover
MBDI	the MODIS-Based Disturbance Index
MODIS	The Moderate Resolution Imaging Spectroradiometer
MRT	the MODIS Re-projection Tool
MSS	Multispectral Scanner System
NASA	the National Aeronautics and Space Administration
NCDC	the National Climatic Data Center
NDVI	the Normalized Difference Vegetation Index
NOAA	the National Oceanic and Atmospheric Administration
NRCS	Natural Resources Conservation Service
P	Precipitation (mm)
PCC	Post-Classification Comparison
pH	is a measure of the acidity or basicity of an aqueous solution
r	Pearson's correlation analysis
RCED	Roberts Cross Edge Detector
RMSE	Root Mean Square Error
RMSSE	Root Mean Square Standardized Error
SAVI	Soil-Adjusted Vegetation Index
SIWSI	the Shortwave Infrared Water Stress Index
TM	Thematic Mapper
UNCCD	the United Nations Convention to Combat Desertification
USGS	U.S. Geological Survey

USSCS	the United States Soil Conservation Services
VI	Vegetation Indices
WIST	Warehouse Inventory Search Tool
x	the environmental variable
α and β	the regression coefficients
ρ_{NIR}	the reflectance value of the near infrared band
ρ_{RED}	the reflectance of the red band

Chapter 1

General introduction

1.1 Global interest of desertification

The term of desertification was originally introduced by Aubreville (1949). Today, the most common definition is the one that was introduced by the United Nations Convention to Combat Desertification (UNCCD) as “land degradation in arid, semi-arid and dry sub-humid areas, resulting from various factors, including climatic variations and human activities” (United Nations 1994; Vogt et al. 2011). Also, it is defined as the process whereby the productivity of land was reduced, this land deterioration involves changes in vegetation cover by reduction, replacement, and destruction (Kassas 1977).

Desertification in arid and semi-arid regions was globally recognized as a serious environmental threat, which covered about 40% of the world lands that are populated by approximately 1 billion humans (Thomas 2011; United Nations 2011; Verón et al. 2006; Yang et al. 2005), about 52% of this dry land used for agriculture, and moderately to severely affected by soil degradation, due to drought and desertification, which is responsible for the loss of about 12 million ha each year, where 20 million tons of grain could have been grown (United Nations Convention to Combat Desertification (UNCCD) 2012), see Figure 1.1

Understanding the impacts of human activities and climatic variations on desertification requires innovative way of assessing the dynamics and the interactions of the biophysical and societal feedbacks in multiple spatial and temporal scales (Okin et al. 2009b; Reynolds et al. 2007). In the extreme environmental conditions of arid lands these interactions are highly significant, so that slight irregularities in one component of the ecosystem are likely to lead to substantial variations in others (Linstädter and Baumann 2012; Thomas 2011), and the interrelationships between soils, vegetation and atmosphere are so interconnected that, in an ecological perspective, they can hardly be considered as separate entities (Bregt et al. 2002; Gratani et al. 2012; Ozkan and Mert 2011).

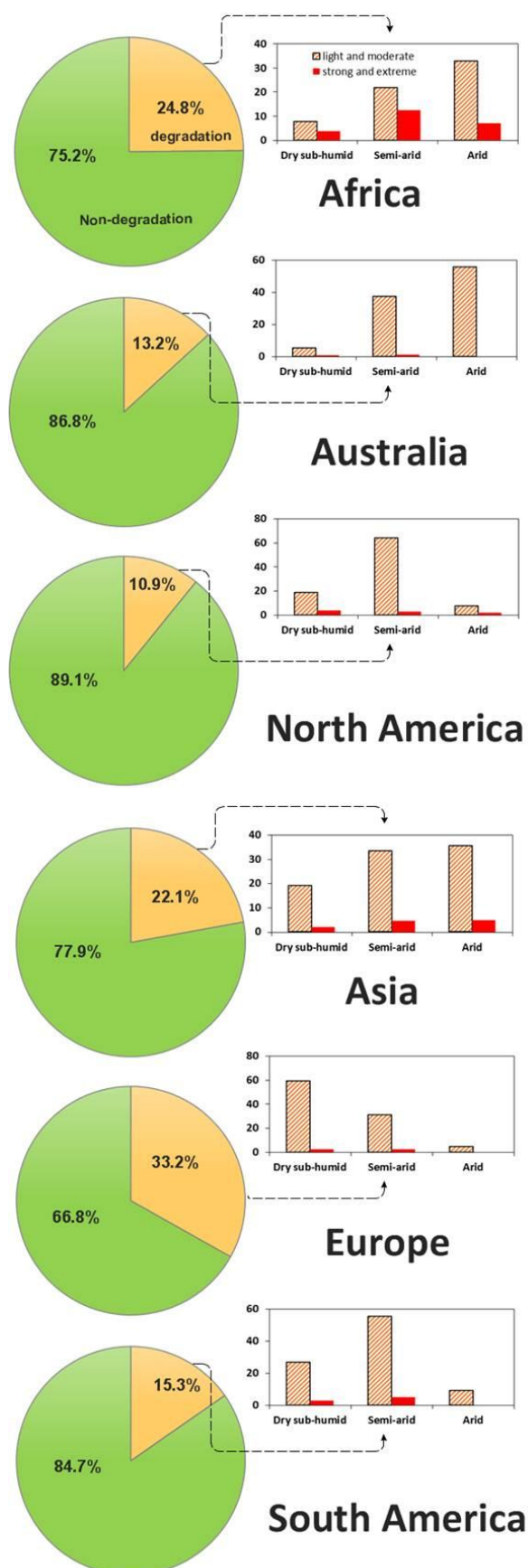


Figure1.1 World distribution of affected land by degradation (%), and degree of soil degradation by region in sensitive dry-lands (%); After (Le Houerou 1996; UNEP 1992)

1.1.1 Natural impact

The natural (biophysical) impact is considered a direct cause of desertification and land degradation in arid environment, which is mostly representing the drastic reduction or destruction of the perennial vegetation cover (Le Houerou 1977; Kassas 1995; United Nations 2011). When the soil surface is not protected for a long time by vegetation cover, it became vulnerable to the impact of water and wind soil erosion, salinization, and waterlogging in topographic depressions (Le Houerou 1996). As shown in Figure 1.2, all causes and processes of desertification are connected to each other, making a complex and intricate processes of land degradation in arid environmental condition. D'Odorico et al. (2013) reported that Worldwide agricultural lands degraded by erosion, salinization, and waterlogging were causing the irretrievable loss of an estimated 6 million hectares each year. Both water and wind erosion affecting negatively the land productivity by reducing the water availability, soil fertility, and organic matter. During water erosion, most of the water is lost due to rapid runoff, and water infiltration rate may be reduced as much as 90%, which cause water scarcity for the crops in good rainfall years. Also, soil organic matter is one of the important agent that improve the physical and chemical soil properties, such as increasing the infiltration rate, water retention, soil structure, and cation exchange capacity (Gilabert M.A. et al. 2002; Natural Resources Conservation Service (NRCS) 1999). Salinization cause more permanent soil degradation, which reduced crop growth and yield (Rozema and Flowers 2008), the soil salinization refers to the accumulation of water-soluble salts on the soil surface. Also, more often associated with the soil sodicity (Na^+ ions represent more than 15% of the exchangeable cations) (Natural Resources Conservation Service (NRCS) 1999), which is found in about 50% of the world's salt affected soils (Buchanan 2007; Martinez Beltran and Licona Manzur 2005). The sodicity degraded the physical soil properties by destroying the soil structure, reduce the porosity, and soil permeability (Rengasamy et al. 2003).

1.1.2 Human impact

The indirect causes of desertification are mainly resulted from human activities and changing of life styles (Le Houerou 1996; Wessels et al. 2004). The increase demand of water and energy, poor land management strategies and inappropriate technology, led to reduce or destroy the vegetation cover and the eco-system balance in the arid environment (Reynolds et al. 2003). Laity (2008) stated that the anthropological activities are strongly associated with the political and economic systems, as shown in Figure 1.3.

The resulting anthropogenic stresses include: (1) physical land restructuring (soil dredging, constructing dams, earth-moving operations, artificial lakes creation), (2) the introduction of exotic species, (3) the industrial outcomes such as the discharge of toxic substances to soil and water, (4) over-cultivation, deforestation, and overstocking, and (5) over consumption to the water resources (intensive irrigation, and drawdown of groundwater) (Rapport and Whitford 1999).

Human activities are depending on the political and economic conditions of each country and not necessarily harmful to natural resources, for example desertification hazards in most of the developing countries found to be more correlated to the density of rural human and livestock populations, unlike the industrial countries, which are found to be well-developed in land management techniques, public awareness and concern to the environmental protection (D'Odorico et al. 2013; Millennium Ecosystem Assessment 2005).

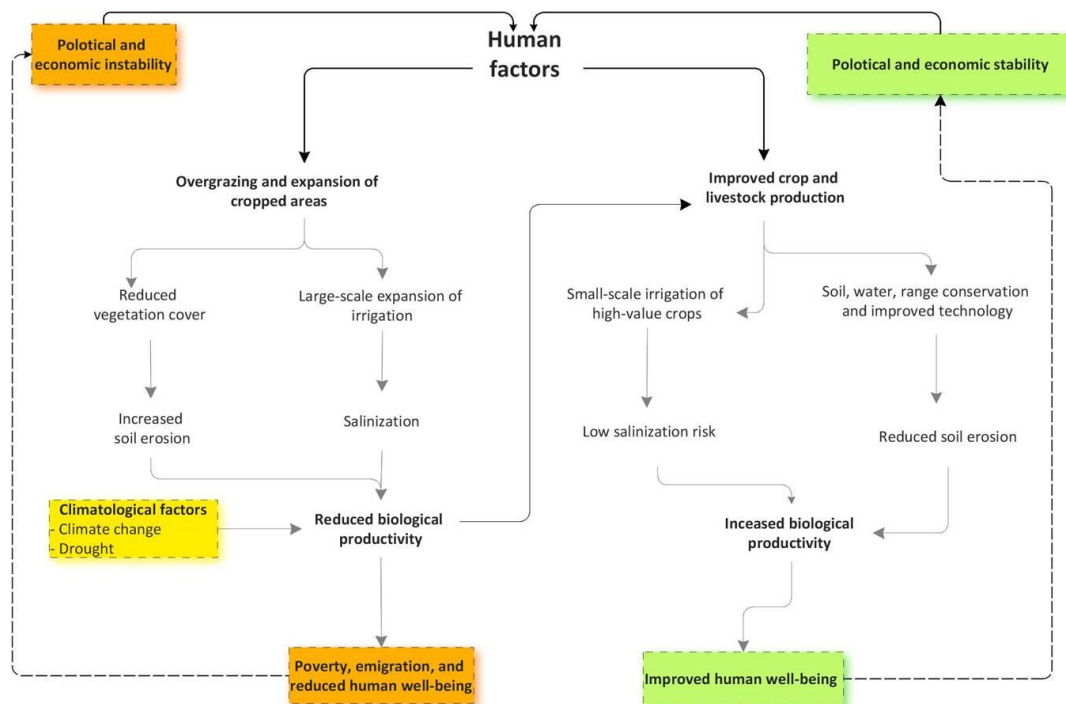


Figure 1.3 Schematic description of human impact on desertification development, After (Millennium Ecosystem Assessment 2005)

1.2 Technology for monitoring environmental changes in arid regions: remote sensing and GIS

Remote sensing data provide repetitive and consistent information in different spatial and spectral ranges. It is invaluable data source for monitoring short and long-temporal changes and the impacts of human and environment dynamics (Schowengerdt 2007). Some of the important applications of remote-sensing technology are stated as follow (Van Westen 2002):

- Environmental assessment and global change detection (desertification, deforestation, soil erosion, urban growth, atmospheric ozone depletion, and natural hazards);
- renewable natural resources (wetlands, soils, forests, oceans);
- nonrenewable resource exploration (minerals, oil, and natural gas);
- mapping (topography, land use, and urban planning); and
- military surveillance and reconnaissance (strategic policy, tactical assessment)

Natural hazards occurred as extreme and sudden events which harm and threat human, agriculture, environment, and urbanization (Adamo and Crews-Meyer 2006; Jongman et al. 2012; Perotto-Baldivieso et al. 2011; Schepanski et al. 2012). The success of the mitigation depends on the obtained information, such as the expected frequency, character, and magnitude (Van Westen 2002). Remote sensing is the ideal tool for monitoring the natural hazards, since it offers information at different spatial and temporal scales, which is requires a huge dataset of multi-temporal and spatial data, with the combination of other data sources, such as maps, field measurement, and statistical data (Le Hégarat-Masclé et al. 2005; Khalifa and Arnous 2010; Nagendra et al. 2012; Singh and Kumar 2012; Zucca et al. 2012). Therefore, the remote sensing applications and GIS have become important for natural hazard management, as shown in Table 1.1 Many types of information that are needed in natural disaster management have an important spatial component such as maps, aerial photography, satellite imagery, GPS data, rainfall data, etc., and many of these data have different projection and co-ordinate systems, and need to be brought to a common map-basis, in order to superimpose them (Weng 2010).

Table 1.1. Classification of the natural hazard in a gradual scale between purely natural and human-made, (Van Westen 2002).

Natural	Some human influence	Mixed natural/Human influence	Some natural influence
<ul style="list-style-type: none"> • Earthquake • Tsunami • Volcanic eruptions • Snow storm • Wind storm • Cyclone 	<ul style="list-style-type: none"> • Flood • Dust storm • drought 	<ul style="list-style-type: none"> • Landslides • Erosion • Desertification • Wildfire • Sea level rise • Greenhouse effect 	<ul style="list-style-type: none"> • Crop disease • Acid rain • Ozone depletion • Coral reef decline • Insect infestation

1.2.1 Remote sensing and GIS: tools for environmental monitoring

Remote sensing was defined as the acquisition of physical data of an object without direct contact with the object of interest (Richards 2013), it has been developed from a qualitative science towards a quantitative science in order to meet the needs of different data users (Los et al. 2002).

The first earth observation trail was in the year 1858 by balloonist Gaspard-Félix Tournachon, known as "Nadar". In 1972, repetitive and systematic earth observations were acquired with the launch of Landsat 1 Multispectral Scanner System (MSS) (Lyon et al. 1998), renamed from ERTS-1, four additional MSS systems missions followed Landsat 1, two Thematic Mapper (TM) systems, and the Enhanced Thematic Mapper Plus (ETM+) in the Landsat series (Chen et al. 2011; Sun et al. 2011b; Yang et al. 2012a), and recently in 11th February, 2013 a new version of Landsat satellite was launched called Landsat Data Continuity Mission (LDCM), this new satellite will provide satellite images with better spatial and spectral properties (Irons et al. 2012; Pahlevan and Schott 2012). Recently many sensors shown a vast improvements in the quantity and quality of information that can be gathered for the earth's surface observation (Ichoku et al. 2012; Martin 2008; Nakayama et al. 2007; Richards 2013; Weng 2010; Weng 2008), as shown in Figure 1.4

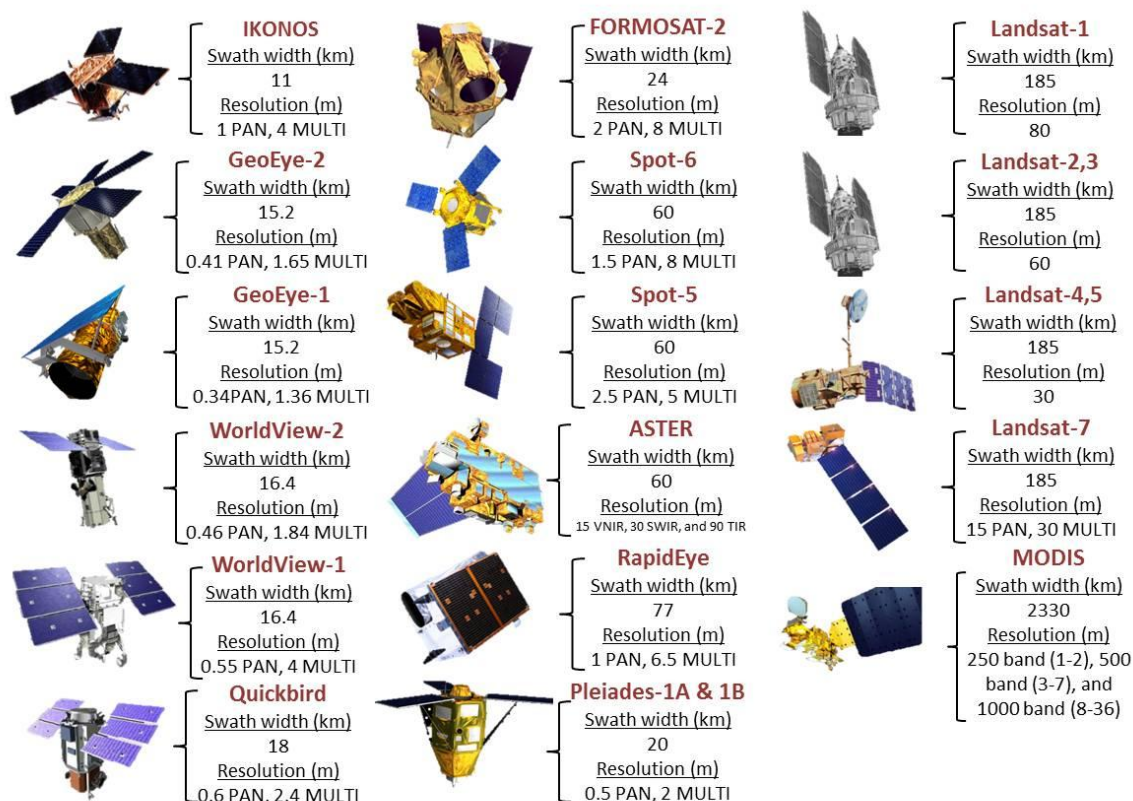


Figure 1.4 Short description of most used satellites in the environmental research

In last decade the geographical information system (GIS) was massively expanded and developed technology though software tools that become more sophisticated and easier to use, as well as more effective toolbox for large spatial-data analysis (Al-Adamat et al. 2003; Batty and Xie 1994; Brown et al. 2005; Gemitzi and Tolikas 2007; Santini et al. 2010).

The remote sensing data that used for monitoring the environmental variation provide a useful information source about the vegetation cover change, movements of desert boundaries, land degradation dynamics, and indications of environmental conditions that are associated with the outbreak of pests and disease (Los et al. 2002).

A very large set of measures for environmental analysis has been developed during the past two decades and their response to the spatial structure, and scale of the land surface has been described and quantified (Honnay et al. 2003). Satellite indices such as the Normalized Difference Vegetation Index (NDVI), Enhanced Vegetation Index (EVI), Soil-Adjusted Vegetation Index (SAVI), Land Surface Temperature (LST), and the Shortwave Infrared Water Stress Index (SIWSI) have previously shown a promise results for several environmental investigations (Aboelghar et al. 2012; Bannari et al. 1995; Honnay et al. 2003; Huete 1988; Mildrexler et al. 2009; Mildrexler et al. 2007; Sjöström et al. 2009). It is essential to perform accuracy assessment of the data that derived from remotely sensed

analysis, which determines the quality and reliability of the obtained information (Foody 2010; Foody 2002; Kim 2013; Woodcock et al. 2002)

1.2.2 Remote sensing and GIS integration system

The integration of remote sensing and GIS tools has been considered as the most effective tool in spatial analysis and environmental modeling, and has received widespread attention in the recent years (Ganapuram et al. 2009; Joshi et al. 2013; Nagendra et al. 2012; Yiran et al. 2012).

Remotely sensed data, GIS thematic layers, and field survey measurements are the three essential datasets sources for environmental change research. Remote sensing data provides multispectral, multi-resolution, and multi-temporal information, which is a valuable source for monitoring and assessing the environmental change processes and biophysical and socio-economic variables (Nagendra et al. 2012; Zhou et al. 2008). GIS is a dynamic tool for importing, modeling, and exporting data from the various sources necessary for land surface feature identification, change detection, and database development (Ehlers 2007; Forzieri et al. 2012; Silva et al. 2012; Singh and Kumar 2012; Sun et al. 2011a; Yousif and Bubenzer 2013). Gao (2002) summarized different types of integration between the remote sensing, GIS, and field survey into four conceptual models: linear, interactive, hierarchical, and complex integration. As shown in Figure 1.5, these approaches were widely applied to natural resources management and environmental research (De Freitas and Tagliani 2009; Pueyo and Alados 2007; Weickert et al. 1999). Ehlers (2007) and Weng (2010) proposed three levels of integration between remote sensing, GIS, and field measurements described as follow:

- Level I (separate and equal integration): Separate databases. Two software modules involved on data exchange. It has the ability to move the results of low-level image processing (e.g., thematic maps, extracted lines, and points) to the GIS tool box and overlay the results to layouts of image processing (Adiat et al. 2012; Choi et al. 2011; De Freitas and Tagliani 2009).
- Level II (seamless integration): Two software modules will be involved in interface and simultaneous layout display, such as incorporating vector data directly into image processing, and entity-like control over remote sensing image components (e.g., themes). It has the ability to accommodate hierarchical entities (e.g., “house” at one level, “block” at another, and “city” at another), and (spatially, radiometrically, spectrally, and temporally) inhomogeneous data in a coherent manner (Haq et al. 2012; Sutcu 2012; Thomson and Hardin 2000; Wu et al. 2006; Zinck et al. 2001).
- Level III (total integration): In this integrated system, a single model will combine all information in the GIS and remote sensing; one software will handle both object- and field-based measurements. The remote sensing data will become an integral part of the processes

of the GIS analysis (Bastawesy et al. 2008; Chowdary et al. 2008; Ghoneim et al. 2012; Magesh et al. 2012; Pradhan 2001; Wasige et al. 2013).

Generally, the three main components of the integration system are depending on each other as shown in Figure 1.5; GPS is the tool that field survey will depend on to collect ground control points (GCP) for aerial and satellite images rectification, which will combined with other data into a GIS-database and used further for subsequent analyses and modeling (Foody 2002; Richards 2013). The integration processes start with image preprocessing in order to improve subjectively the satellite data for better analysis and visualization via manipulating the histogram of the image in order to increase the contrast, filtering to remove noise, and principle component analysis for providing the maximum possible contrast especially from the multispectral images (Chavez 1988; Petrou and Bosdogianni 1999; Yang et al. 2012b). Recently different calibration utilities have been developed through remote sensing software, such as ENVI, Erdas Imagine, and IDRISI, these software apply calibration factors to most of the satellite sensors, such as AVHRR, MSS, QuickBird, TM, and WorldView-1 data, in order to use a variety of atmospheric correction techniques (Siart et al. 2009). The field survey start with obtaining GCP for geo-referencing the enhanced satellite image, and collecting field samples (soil, water, plant, ... etc.) for laboratory analysis and building database with using GIS tools, such as Arc GIS, R, GRASS GIS, Quantum GIS, ILWIS, and Whitebox GAT. Remotely sensed data can be used to extract thematic and metric information, making it ready for input into GIS, which provides better environment for spatial analysis and modeling (van der Meer et al. 2012)

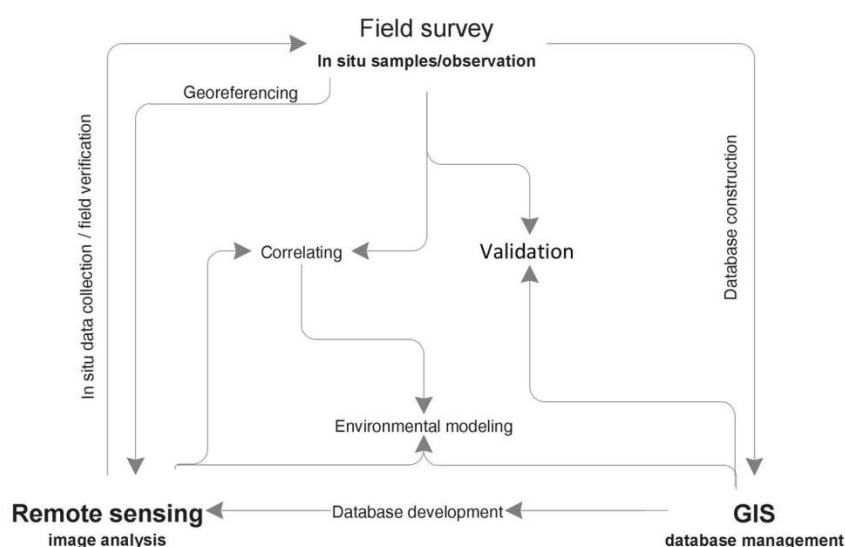


Figure 1.5 Schematic draw of general flow-process in integration system, Adapted from (Weng 2010)

1.3 New approaches for assessing desertification in arid lands

1.3.1 Bi-stable ecosystem dynamics

Desertification process is associated with a transition between two stable states in the bi-stable ecosystem dynamics, which is explained in most of the desertification theories in arid environment (D'Odorico et al. 2007; Okin et al. 2009a; Okin et al. 2009b), as shown in Figure 1.6, the two stable states would correspond to a vegetated “non degraded” state and an desertified “degraded” state, these states would be the stable configurations of the system (D'Odorico et al. 2013). The states of bi-stable systems have only a limited resilience to disturbances, which is not necessarily allow the system to naturally return back to its initial configuration (Baartman et al. 2007; Gunderson 2000). If a disturbed system is beyond the critical threshold, where it is losing massively vegetation cover areas, these system move toward to the alternative stable state of degraded land, and it would be difficult to revert back to its initial state (Walker and Salt 2006).

the ability of feedbacks to induce bi-stability in ecosystem dynamics has been shown by a number of minimalist process based models, and most of the vegetation dynamics are modeled regarding to the effect of the feedback between vegetation and its limiting resources or disturbance system (D'Odorico et al. 2013; D'Odorico et al. 2007; DeLonge et al. 2007). different feedback mechanisms have been invoked by a number of desertification theories, These mechanisms typically involve processes responsible for (i) changes in soil properties and land degradation; (ii) the coupling between vegetation and climate; or (iii) shifts in plant community composition.

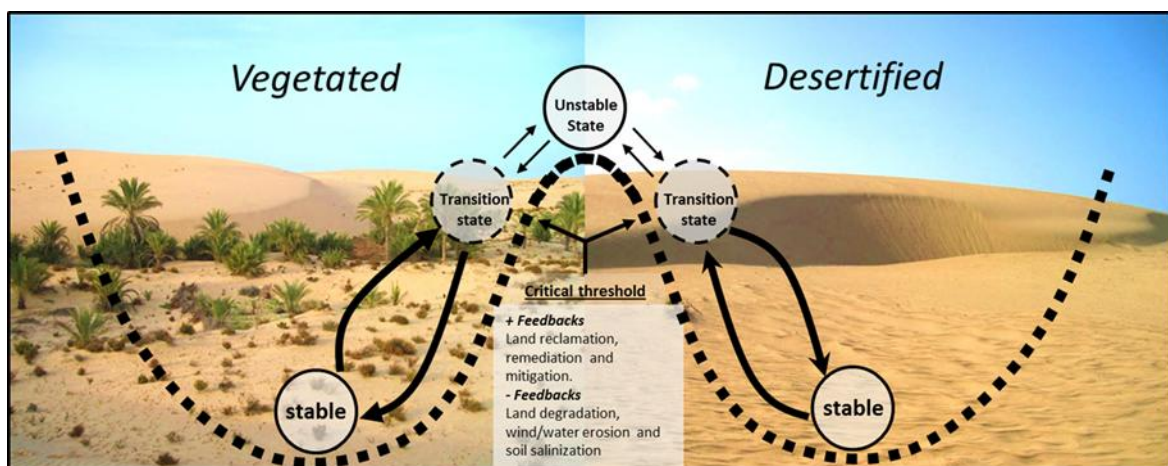


Figure 1.6 Illustration draws of the bi-stable ecosystem balance for an arid environment, both sections (vegetated and desertified) are hosting the transition and stable states, the critical threshold containing (positive and negative) environmental feedbacks. Positive feedbacks are the drivers that influence the system positively to move to the vegetated section, where the negative feedbacks are the drivers that cause more land degradation and orient the system to move to the desertified section.

1.3.2 Satellite-based Environmental modeling

In the recent years the remotely-sensed data contributed in monitoring and assessing natural resources in arid environment, and become the best source of data for studying the environmental change at different spatial scales, due to the availability of the remotely sensed data from different sensors of various platforms with a wide range of spatiotemporal, radiometric and spectral resolutions (Melesse et al. 2007; Nagler et al. 2009; Thenkabail et al. 2004). a variety of models have a growing need for improved environmental datasets to better approach biophysical parameterization, and a significant advances have recently been made in the development of large-area databases in order to support models for environmental assessment in regional and local scales (Reed et al. 2002). Also, satellite-based models for earth surface observation have become an indispensable tool for environmental change research, especially in remote areas (AghaKouchak and Nakhjiri 2012; Chen et al. 2014; Jiménez et al. 2009; Langer et al. 2013; Santos et al. 2007).

1.3.3 The spatial pattern analysis

The spatial-temporal dimensions of any ecological phenomena in arid environment have always been inherent in the conceptual framework of ecology, and recently it has been incorporated explicitly into ecological theory, sampling/experimental design and spatial modeling (Getzin et al. 2006; Haining 2004; Ripley 1981). The spatial structure has become to be essential in understanding the complexity of arid ecological patterns (Dale 1999; Fortin and Dale 2005). spatial pattern analysis is the best descriptor of the horizontal structure in plant communities' and has been used in various ecosystems (López et al. 2010). Spatial pattern within vegetation cover distribution may range from small to large scale; however, it is necessary to understand the links between plant interactions and local environmental drivers (Brooker et al. 2012).

1.4 General objective

Desertification has received substantial scholarly, institutional and political attention and controversial discussions since the late-1960s and early 1970s following the Sahel drought (Rhodes 1991). In Aug. 28, 1977 the desertification became publicly known as the major environmental hazard that occurred in arid regions (Verón et al. 2006). Desertification found in remote locations, where field survey is expensive and difficult to obtain continuous measurements or to transport samples for laboratory analysis, with the advantage of witnessing rapid development in remote sensing data, spatial pattern analysis, and GIS analysis tools. The main objective of this thesis is to introduce new methodologies and indicators that can be used to monitor and assess the environmental change in Egypt at different spatial scales. The overall aims are:

- To understand the spatial and temporal dynamics of the vegetation cover distribution at regional scale of Egypt;
- To propose a new satellite-based algorithm for assessing the desertification change at sub-regional scale of Sinai Peninsula;
- To evaluate the land use/land cover change at moderate spatial scale of El-Arish in Sinai Peninsula; and
- To assess the spatial pattern of the halophytic species (HS) at small spatial scale of El-Zaraniq Protected Area in El-Arish.

1.5 Research objectives per chapter

Monitoring and assessing the desertification in Egypt as an example of arid environment is developed during this thesis, which is based on multi-temporal satellite data at different spatial scales.

Starting with understanding the vegetation cover distribution at regional scale of Egypt. **Chapter 3** entitled “Assessing the spatio-temporal dynamics of the vegetation cover as an indicator of desertification in Egypt using multi-temporal MODIS satellite images”. The specific objectives for this chapter are the following:

- To investigate spatio-temporal vegetation cover dynamics of Egypt as a direct indicator of desertification development, by establishing trends of vegetation cover change in the period 2002-2011;
- To monitor the vegetated and desertified areas as a result of the bi-stable ecosystem dynamics over the periods 2002-2005, 2005-2008 and 2008-2011 at three different sites in Egypt; and
- To assess the desertification developments at these chosen locations in Egypt with the relationship of the vegetation cover distribution along with precipitation, LST and elevation.

Based on the findings of the previous chapter, a sub-regional spatial scale of Sinai Peninsula is chosen to apply a new method for assessing the desertification change in **Chapter 4** “A satellite-based disturbance index algorithm for monitoring mitigation strategies effects on desertification change in an arid environment”, the objectives of this study are the following:

- To propose a new satellite-based disturbance index algorithm for monitoring ago-ecosystem changes in arid environmental conditions in the years 2002, 2005, 2008 and 2011;
- To assess the relationship between the land surface temperature and vegetation cover at different sites in the Sinai Peninsula Egypt; and
- To provide useful information about mitigation strategies effects on dry lands.

Next, zooming in to the most desertification-affected site at moderate spatial scale in Sinai, **Chapter 5**, entitled “Monitoring land use/land cover change using multi-temporal Landsat satellite images in an arid environment: a case study of El-Arish, Egypt”. In this chapter, the integration between the supervised maximum likelihood classification method and visual interpretation of remote sensing data is used to provide a multi-temporal land use/land cover (LULC) maps for the years 1999, 2001, 2005, and 2010. The objectives of this study are the following:

- To provide a multi-temporal LULC maps for years 1999, 2001, 2005, and 2010;
- To assess the trends of LULC changes in El-Arish of Egypt; and
- To identify the causes of change in the case study for each studied period.

Image processing and GIS are integrated to study the spatial distribution of the local halophytic species (HS) at El-Zaraniq Protected Area in El-Arish, in **Chapter 6**, which is entitled “Object-based image analysis for monitoring the spatial distribution of a halophytic species in an arid coastal environment”. The objectives of this chapter are to:

- To improve Google Earth image using different digital image processing operators, in order to obtain the spatial distribution of the local halophytic species (HS);

- To understand the impact of the local environmental variables on HS spatial distribution;
- To analyze the spatial distribution of the HS community in El-Zaraniq Protected Area, North Sinai, Egypt; and
- To provide a combination of models those best reflect the observed structures.

1.6 Thesis structure and organization

This thesis resulted in some innovative methodologies for monitoring and assessing the desertification development. Each chapter represents one article and the sequences of these articles are organized following the outline, as shown in Figure 1.7 . Monitoring and evaluating desertification development are discussed in this thesis over various case studies, going from regional to small spatial scale. A brief description of every chapter is given below.

After providing the basic understanding of the global allure of desertification, the state-of-art for monitoring technology, and the main objectives of this thesis in **Chapter 1**. Egypt will be described in term of the geo and bio-physical characteristics in **Chapter 2**, in order to show the varieties in landforms, vegetation types, and climatic condition of the case study. **Chapter 3** assesses the spatio-temporal changes of the vegetation cover via the Soil-Adjusted Vegetation Index (SAVI), which is used as an indicator to monitor the desertification change in Egypt. In **Chapter 4**, a new satellite-based algorithm is proposed to monitor the desertification disturbance dynamics over the years 2002, 2005, 2008, and 2011 in Sinai Peninsula of Egypt. **Chapter 5** monitors LULC of El-Arish using multi-temporal Landsat satellite data. In **Chapter 6**, a spatial distribution analysis of HS is modeled using a high resolution Google Earth image of El-Zaraniq Protected Area in North Sinai, which is improved via using different digital image processing operators. Finally, the general conclusions and recommendations are presented in **Chapter 7**.

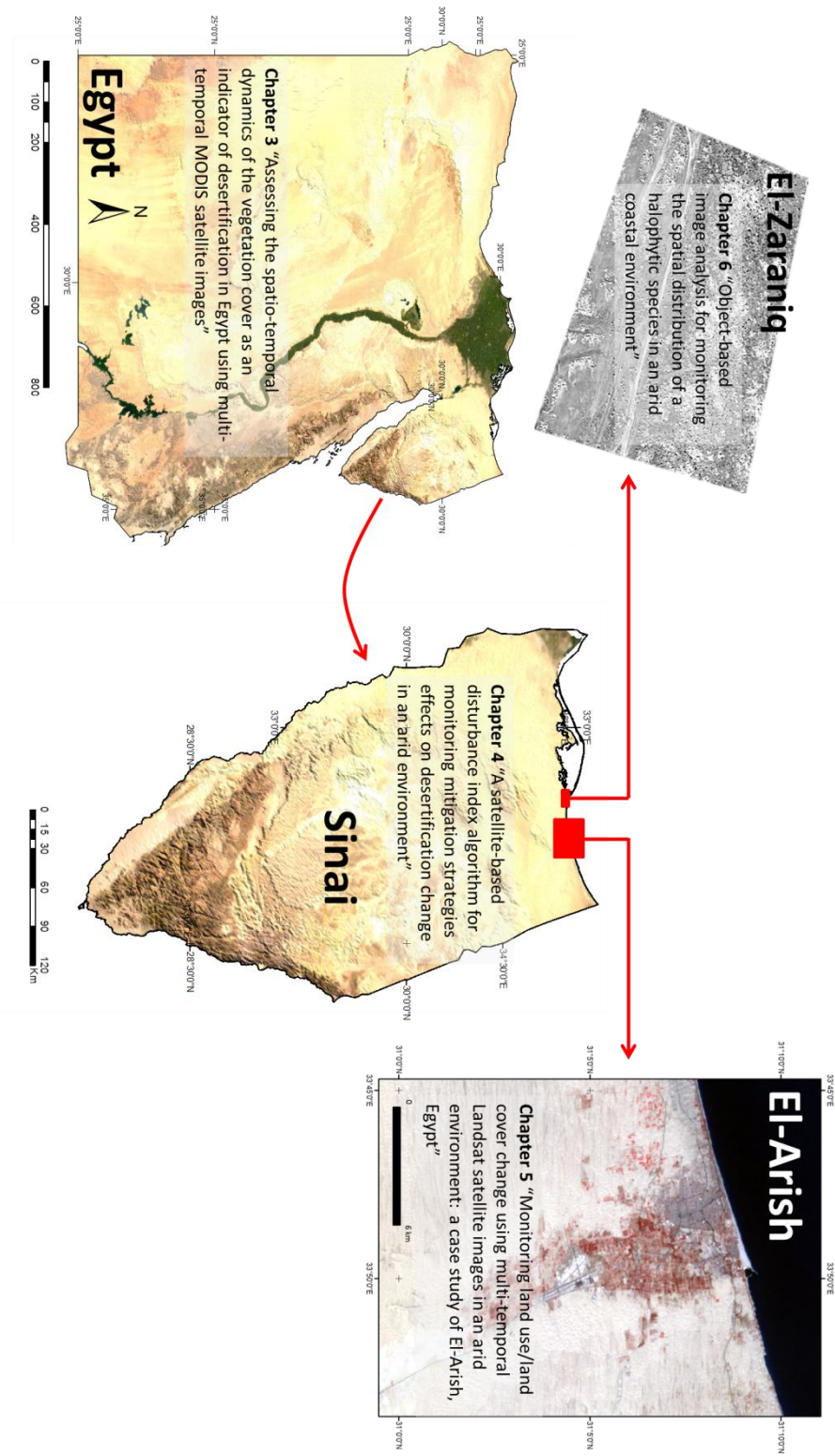


Figure 1.7 The multi-spatial scale of different case studies in the thesis

1.7 References

- Aboelghar M, Ali A-R, Arafat S (2012) Spectral wheat yield prediction modeling using SPOT satellite imagery and leaf area index. *Arabian Journal of Geosciences*. doi: 10.1007/s12517-012-0772-6
- Adamo SB, Crews-Meyer K a. (2006) Aridity and desertification: Exploring environmental hazards in Jáchal, Argentina. *Applied Geography* 26:61–85.
- Adiat K a. N, Nawawi MNM, Abdullah K (2012) Assessing the accuracy of GIS-based elementary multi criteria decision analysis as a spatial prediction tool – A case of predicting potential zones of sustainable groundwater resources. *Journal of Hydrology* 440–441:75–89.
- AghaKouchak A, Nakhjiri N (2012) A near real-time satellite-based global drought climate data record. *Environmental Research Letters* 7:044037. doi: 10.1088/1748-9326/7/4/044037
- Al-Adamat RAN, Foster IDL, Baban SMJ (2003) Groundwater vulnerability and risk mapping for the Basaltic aquifer of the Azraq basin of Jordan using GIS, Remote sensing and (DRASTIC). *Applied Geography* 23:303–324.
- Baartman JEM, Lynden GWJ van, Reed MS, et al. (2007) Desertification and land degradation : origins , processes and solutions. ISRIC. Netherlands. p 104.
- Bannari A, Morin D, Bonn F, Huete AR (1995) A review of vegetation indices. *Remote Sensing Reviews* 13:95–120.
- Bastawesy M a., Khalaf FI, Arafat SM (2008) The use of remote sensing and GIS for the estimation of water loss from Tushka lakes, southwestern desert, Egypt. *Journal of African Earth Sciences* 52:73–80.
- Batty M, Xie Y (1994) Research Article. Modelling inside GIS: Part 1. Model structures, exploratory spatial data analysis and aggregation. *International journal of geographical information systems* 8:291–307.
- Bregt AK, Skidmore AK, Nieuwenhuis G (2002) Environmental modelling : issues and discussion. In: Skidmore A (ed) *Environmental Modelling with GIS and Remote Sensing*. Taylor & Francis, New York, USA, pp 251–259.
- Brooker RW, Matesanz S, Valladares F, Klotz S (2012) Long-term spatial pattern change in a semi-arid plant community: The role of climate and composition. *Acta Oecologica* 45:8–15.
- Brown DG, Riolo R, Robinson DT, et al. (2005) Spatial process and data models: Toward integration of agent-based models and GIS. *Journal of Geographical Systems* 7:25–47.
- Buchanan S (2007) Salinity Hazard Mapping And Risk Assessment In The Bourke Irrigation District. University of New South Wales. p 469.
- Chavez PS (1988) An improved dark-object subtraction technique for atmospheric scattering correction of multispectral data. *Remote Sensing of Environment* 24:459–479.
- Chen J, Zhu X, Vogelmann JE, et al. (2011) A simple and effective method for filling gaps in Landsat ETM+ SLC-off images. *Remote Sensing of Environment* 115:1053–1064.
- Chen Y, Xia J, Liang S, et al. (2014) Comparison of satellite-based evapotranspiration models over terrestrial ecosystems in China. *Remote Sensing of Environment* 140:279–293.
- Choi J-K, Oh H-J, Koo BJ, et al. (2011) Crustacean habitat potential mapping in a tidal flat using remote sensing and GIS. *Ecological Modelling* 222:1522–1533.
- Chowdary VM, Chandran RV, Neeti N, et al. (2008) Assessment of surface and sub-surface waterlogged areas in irrigation command areas of Bihar state using remote sensing and GIS. *Agricultural Water Management* 95:754–766.
- D’Odorico P, Bhattachan A, Davis KF, et al. (2013) Global desertification: Drivers and feedbacks. *Advances in Water Resources* 51:326–344.
- D’Odorico P, Caylor K, Okin GS, Scanlon TM (2007) On soil moisture–vegetation feedbacks and their possible effects on the dynamics of dryland ecosystems. *Journal of Geophysical Research* 112:G04010.
- Dale, M. R. T. (1999). *Spatial Pattern Analysis in Plant Ecology*. Cambridge, UK: Cambridge University Press. pp. 337.
- De Longe M, D’Odorico P, Lawrence D (2007) Feedbacks between phosphorus deposition and canopy cover: The emergence of multiple stable states in tropical dry forests. *Global Change Biology* 14:154–160.
- De Freitas DM, Tagliani PR a (2009) The use of GIS for the integration of traditional and scientific knowledge in supporting artisanal fisheries management in southern Brazil. *Journal of environmental management* 90:2071–80.
- Ehlers M (2007) Integration taxonomy and uncertainty. In: Mesev V (ed) *Integration of GIS and Remote Sensing*, Wiley. West Sussex, England, pp 17–42
- Foody GM (2002) Status of land cover classification accuracy assessment. *Remote Sensing of Environment* 80:185–201.

- Foody GM (2010) Assessing the accuracy of land cover change with imperfect ground reference data. *Remote Sensing of Environment* 114:2271–2285.
- Fortin M-J, Dale MRT (2005) *Spatial Analysis: A Guide for Ecologists*. 380.
- Forzieri G, Battistini A, Catani F (2012) ES4LUCC: A GIS-tool for remotely monitoring landscape dynamics. *Computers & Geosciences* 49:72–80.
- Ganapuram S, Kumar GTV, Krishna IVM, et al. (2009) Mapping of groundwater potential zones in the Musi basin using remote sensing data and GIS. *Advances in Engineering Software* 40:506–518.
- Gao J (2002) Integration of GPS with Remote Sensing and GIS: Reality and Prospect. *Photogrammetric Engineering and Remote Sensing* 68:447–453.
- Gemitzi A, Tolikas D (2007) (HYDRA) model: Simulation of salt intrusion in coastal aquifers using Visual Basic and (GIS). *Environmental Modelling & Software* 22:924–936.
- Getzin S, Dean C, He F, et al. (2006) Spatial patterns and competition of tree species in a Douglas-fir chronosequence on Vancouver Island. *Ecography* 29:671–682.
- Ghoneim E, Benedetti M, El-Baz F (2012) An integrated remote sensing and GIS analysis of the Kufrah Paleoriver, Eastern Sahara. *Geomorphology* 139–140:242–257.
- Gilabert M.A., J. G-P, F.J. G-H, J. M (2002) A generalized soil-adjusted vegetation index. *Remote Sensing of Environment* 82:8.
- Gratani L, Varone L, Ricotta C, Catoni R (2012) Mediterranean shrublands carbon sequestration: environmental and economic benefits. *Mitigation and Adaptation Strategies for Global Change*. doi: 10.1007/s11027-012-9415-1.
- Gunderson LH (2000) Ecological resilience - in theory and application. *Annual Review of Ecology and Systematics* 31:425–439.
- Haq M, Akhtar M, Muhammad S, et al. (2012) Techniques of Remote Sensing and GIS for flood monitoring and damage assessment: A case study of Sindh province, Pakistan. *The Egyptian Journal of Remote Sensing and Space Science* 15:135–141.
- Honnay O, Piessens K, Van Landuyt W, et al. (2003) Satellite based land use and landscape complexity indices as predictors for regional plant species diversity. *Landscape and Urban Planning* 63:241–250.
- Haining R (2004) *Spatial Data Analysis: Theory and Practice*. Cambridge University Press. Cambridge, UK. p454.
- Huete A. (1988) A soil-adjusted vegetation index (SAVI). *Remote Sensing of Environment* 25:295–309.
- Ichoku C, Kahn R, Chin M (2012) Satellite contributions to the quantitative characterization of biomass burning for climate modeling. *Atmospheric Research* 111:1–28.
- Irons JR, Dwyer JL, Barsi JA (2012) The next Landsat satellite: The Landsat Data Continuity Mission. *Remote Sensing of Environment* 122:11–21.
- Jiménez C, Prigent C, Aires F (2009) Toward an estimation of global land surface heat fluxes from multisatellite observations. *Journal of Geophysical Research* 114:D06305.
- Jongman B, Ward PJ, Aerts JCJH (2012) Global exposure to river and coastal flooding: Long term trends and changes. *Global Environmental Change* 22:823–835.
- Joshi PN, Maurya DM, Chamyal LS (2013) Morphotectonic segmentation and spatial variability of neotectonic activity along the Narmada–Son Fault, Western India: Remote sensing and GIS analysis. *Geomorphology* 180–181:292–306.
- Kassas M (1977) Arid and semi-arid lands: problems and prospects. *Agro-Ecosystems* 3:185–204.
- Kassas M (1995) Desertification: a general review. *Journal of Arid Environments* 30:115–128.
- Khalifa IH, Arnous MO (2010) Assessment of hazardous mine waste transport in west central Sinai, using remote sensing and GIS approaches: a case study of Um Bogma area, Egypt. *Arabian Journal of Geosciences* 5:407–420.
- Kim Y (2013) Drought and elevation effects on MODIS vegetation indices in northern Arizona ecosystems. *International Journal of Remote Sensing* 34:4889–4899.
- Laity J (2008) *Deserts and desert environments*. John Wiley & Sons, Inc., Chichester . p 357.
- Langer M, Westermann S, Heikenfeld M, et al. (2013) Satellite-based modeling of permafrost temperatures in a tundra lowland landscape. *Remote Sensing of Environment* 135:12–24.
- Le Hégarat-Masclé S, Ottlé C, Guérin C (2005) Land cover change detection at coarse spatial scales based on iterative estimation and previous state information. *Remote Sensing of Environment* 95:464–479.
- Le Houerou HN (1977) Biological recovery vs desertization. *Economic Geography* 53:413–420.
- Le Houerou HN (1996) Climate change, drought and desertification. *Journal of Arid Environments* 34:133–185.
- Le Houerou HN (1986) Salt-tolerant plants of economic value in the Mediterranean Basin. *Reclamation and Revegetation Research* 5:319–341.
- Linstädter A, Baumann G (2012) Abiotic and biotic recovery pathways of arid rangelands: Lessons from the High Atlas Mountains, Morocco. *CATENA*. doi: 10.1016/j.catena.2012.02.002
- Liu JG, Mason PJ (2009) *Essential Image Processing and GIS for Remote Sensing*. John Wiley & Sons, Ltd., Chichester, UK. p 462.

- López RP, Larrea-Alcázar D, Zenteno-Ruiz F (2010) Spatial pattern analysis of dominant species in the Prepuna: Gaining insight into community dynamics in the semi-arid, subtropical Andes. *Journal of Arid Environments* 74:1534–1539.
- Los SO, Tucker CJ, Anyamba A, et al. (2002) The biosphere: a global perspective. In: Skidmore A (ed) *Environmental Modelling with GIS and Remote Sensing*. Taylor & Francis Group, London, UK, pp 70–96
- Lyon JG, Yuan D, Lunetta RS, Elvidge C (1998) A change detection experiment using vegetation indices. *PHOTOGRAMMETRIC ENGINEERING AND REMOTE SENSING* 64:143–150.
- Magesh NS, Chandrasekar N, Soundranayagam JP (2012) Delineation of groundwater potential zones in Theni district, Tamil Nadu, using remote sensing, GIS and MIF techniques. *Geoscience Frontiers* 3:189–196.
- Martin R V (2008) Satellite remote sensing of surface air quality. *Atmospheric Environment* 42:7823–7843.
- Martinez Beltran J, Licona Manzur C (2005) Overview of salinity problems in the world and FAO strategies to address the problem. *International salinity forum managing saline soils and water*. Riverside Convention Center, Riverside, California, USA, pp 311–314.
- Melesse AM, Weng Q, Thenkabail PS, Senay GB (2007) Remote Sensing Sensors and Applications in Environmental Resources Mapping and Modelling. *Sensors* 7:3209–3241.
- Mildrexler DJ, Zhao M, Heinsch FA, Running SW (2007) A new satellite-based methodology for continental-scale disturbance detection. *Ecological applications: a publication of the Ecological Society of America* 17:235–50.
- Mildrexler DJ, Zhao M, Running SW (2009) Testing a MODIS Global Disturbance Index across North America. *Remote Sensing of Environment* 113:2103–2117.
- Millennium Ecosystem Assessment (2005) *Ecosystems and human well-being: desertification synthesis*. 36.
- Nagendra H, Lucas R, Honrado JP, et al. (2012) Remote sensing for conservation monitoring: Assessing protected areas, habitat extent, habitat condition, species diversity, and threats. *Ecological Indicators* 33:45–59.
- Nagler PL, Glenn EP, Hinojosa-Huerta O (2009) Synthesis of ground and remote sensing data for monitoring ecosystem functions in the Colorado River Delta, Mexico. *Remote Sensing of Environment* 113:1473–1485.
- Nakayama Y, Yanagi T, Yamaguchi S, et al. (2007) Monitoring of environmental change in Dzongar Basin by the analysis of multi-temporal satellite data sets. *Advances in Space Research* 39:52–59.
- Natural Resources Conservation Service (NRCS) (1999) *Soil Taxonomy: A Basic System of Soil Classification for Making and Interpreting Soil Surveys*, 2nd ed. United States Department of Agriculture (USDA), Washington, p 871.
- Okin GS, D'Odorico P, Archer SR (2009a) Impact of feedbacks on Chihuahuan desert grasslands: Transience and metastability. *Journal of Geophysical Research* 114:G01004.
- Okin GS, Parsons AJ, Wainwright J, et al. (2009b) Do Changes in Connectivity Explain Desertification? *BioScience* 59:237–244.
- Ozkan K, Mert A (2011) Ecological Land Classification and Mapping of Yazili Canyon Nature Park in the Mediterranean Region, TURKEY. *Journal of Environmental Engineering and Landscape Management* 19:296–303.
- Pahlevan N, Schott JR (2012) Characterizing the relative calibration of Landsat-7 (ETM+) visible bands with Terra (MODIS) over clear waters: The implications for monitoring water resources. *Remote Sensing of Environment* 125:167–180.
- Perotto-Baldovieso HL, Ben Wu X, Peterson MJ, et al. (2011) Flooding-induced landscape changes along dendritic stream networks and implications for wildlife habitat. *Landscape and Urban Planning* 99:115–122.
- Petrou M, Bosdogianni P (1999) *Image Processing: The Fundamentals*. John Wiley & Sons, Ltd., Chichester, UK. pp 347.
- Pradhan S (2001) Crop area estimation using GIS, remote sensing and area frame sampling. *International Journal of Applied Earth Observation and Geoinformation* 3:86–92.
- Pueyo Y, Alados CL (2007) Abiotic factors determining vegetation patterns in a semi-arid Mediterranean landscape: Different responses on gypsum and non-gypsum substrates. *Journal of Arid Environments* 69:490–505.
- Rapport DJ, Whitford WG (1999) How ecosystems respond to stress: Common properties of arid and aquatic systems. *BioScience* 49:193–203.
- Reed BC, Brown JF, Loveland TR (2002) Geographic data for environmental modelling and assessment. In: Skidmore A (ed) *Environmental Modelling with GIS and Remote Sensing*. Taylor & Francis, New York, USA, pp 52–69.
- Rengasamy P, Chittleborough D, Helyar K (2003) Root-zone constraints and plant-based solutions for dryland salinity. *Plant and Soil* 257:249–260.

- Reynolds JF, Smith DMS, Lambin EF, et al. (2007) Global desertification: building a science for dryland development. *Science* (New York, NY) 316:847–51.
- Reynolds JF, Stafford-smith DM, Lambin E (2003) Do humans cause deserts? An old problem through the lens of a new framework: the Dahlem desertification paradigm. In: Allsopp N, Palmer AR, Milton SJ, et al. (eds) the VIIth International Rangelands Congress. Durban, South Africa, pp 2042–2048.
- Rhodes SL (1991) Rethinking desertification: What do we know and what have we learned? *World Development* 19:1137–1143.
- Richards JA (2013) *Remote Sensing Digital Image Analysis: An Introduction*, 5th ed. Springer-Verlag, Berlin, Heidelberg, pp494.
- Ripley BD (1981) *Spatial Statistics*. John Wiley & Sons, Inc. Hoboken, NJ, USA. pp260.
- Rozema J, Flowers T (2008) Crops for a salinized world. *Science* 322:1478–1480.
- Santini M, Caccamo G, Laurenti A, et al. (2010) A multi-component GIS framework for desertification risk assessment by an integrated index. *Applied Geography* 30:394–415.
- Santos C, Lorite IJ, Tasumi M, et al. (2007) Integrating satellite-based evapotranspiration with simulation models for irrigation management at the scheme level. *Irrigation Science* 26:277–288.
- Schepanski K, Tegen I, Macke A (2012) Comparison of satellite based observations of Saharan dust source areas. *Remote Sensing of Environment* 123:90–97.
- Schowengerdt RA (2007) *Remote sensing: models and methods for image processing*, 3rd edn. Elsevier, Amsterdam, pp 558
- Siart C, Bubenzer O, Eitel B (2009) Combining digital elevation data (SRTM/ASTER), high resolution satellite imagery (Quickbird) and GIS for geomorphological mapping: A multi-component case study on Mediterranean karst in Central Crete. *Geomorphology* 112:106–121.
- Silva RM, Montenegro SMGL, Santos CAG (2012) Integration of GIS and remote sensing for estimation of soil loss and prioritization of critical sub-catchments: a case study of Tapacurá catchment. *Natural Hazards* 62:953–970.
- Singh RB, Kumar D (2012) Remote sensing and GIS for land use/cover mapping and integrated land management: case from the middle Ganga plain. *Frontiers of Earth Science* 6:167–176.
- Sjöström M, Ardö J, Eklundh L, et al. (2009) Evaluation of satellite based indices for gross primary production estimates in a sparse savanna in the Sudan. *Biogeosciences* 6:129–138.
- Sun Q, Wu Z, Tan J (2011a) The relationship between land surface temperature and land use/land cover in Guangzhou, China. *Environmental Earth Sciences* 65:1687–1694.
- Sun Z, Guo H, Li X, et al. (2011b) Estimating urban impervious surfaces from Landsat-5 TM imagery using multilayer perceptron neural network and support vector machine. *Journal of Applied Remote Sensing* 5:053501.
- Sutcu EC (2012) Use of GIS to discover potential coalfields in Yatagan–Milas area in Turkey. *International Journal of Coal Geology* 98:95–109.
- Thenkabail PS, Enclona EA, Ashton MS, et al. (2004) Hyperion, IKONOS, ALI, and ETM+ sensors in the study of African rainforests. *Remote Sensing of Environment* 90:23–43.
- Thomas DSG (2011) *Arid Environments: Their Nature and Extent*. Arid Zone Geomorphology. John Wiley & Sons, Ltd, pp 1–16
- Thomson CN, Hardin P (2000) Remote sensing/GIS integration to identify potential low-income housing sites. *Cities* 17:97–109.
- UNEP (1992) *World Atlas of Desertification*. Nairobi: UNEP, and London: Edward Arnold. p69.
- United Nations (1994) United Nations convention to combat desertification in countries experiencing serious drought and/or desertification, particularly in Africa. New York, USA, pp 241.
- United Nations (2011) *Global Drylands: a UN system-wide response*. United Nations Environment Management Group. New York, USA. pp132.
- United Nations Convention to Combat Desertification (UNCCD) (2012) Background Information on Desertification and Land Degradation for World Day to Combat Desertification - 17 June. World Day to Combat Desertification.
- Van der Meer FD, van der Werff HM a., van Ruitenbeek FJ a., et al. (2012) Multi- and hyperspectral geologic remote sensing: A review. *International Journal of Applied Earth Observation and Geoinformation* 14:112–128.
- Van Westen CJ (2002) Remote sensing and geographic information systems for natural disaster management. In: Skidmore A (ed) *Environmental Modelling with GIS and Remote Sensing*. Taylor & Francis Group, London, pp 200–226
- Verón SR, Paruelo JM, Oesterheld M (2006) Assessing desertification. *Journal of Arid Environments* 66:751–763.
- Vogt J V., Safriel U, Von Maltitz G, et al. (2011) Monitoring and assessment of land degradation and desertification: Towards new conceptual and integrated approaches. *Land Degradation & Development* 22:150–165.

- Walker B, Salt D (2006) *Resilience Thinking: Sustaining Ecosystems and People in a Changing World*. 192.
- Wasige JE, Groen T a., Smaling E, Jetten V (2013) Monitoring basin-scale land cover changes in Kagera Basin of Lake Victoria using ancillary data and remote sensing. *International Journal of Applied Earth Observation and Geoinformation* 21:32–42.
- Weickert J, Ishikawa S, Imiya A (1999) Linear Scale-Space has First been Proposed in Japan. *Journal of Mathematical Imaging and Vision* 10:237–252.
- Weng Q (2010) *Remote Sensing and GIS Integration Theories, Methods, and Applications*. The McGraw-Hill, NY. pp433.
- Weng Q (2008) *Remote Sensing of Impervious Surfaces*. CRC Press. New York. pp496.
- Wessels K., Prince S., Frost P., van Zyl D (2004) Assessing the effects of human-induced land degradation in the former homelands of northern South Africa with a 1 km AVHRR NDVI time-series. *Remote Sensing of Environment* 91:47–67.
- Woodcock CE, Macomber SA, Kumar L (2002) Vegetation mapping and monitoring. In: Skidmore A (ed) *Environmental Modelling with GIS and Remote Sensing*. Taylor & Francis Group, London, UK, pp 97–120
- Wu Q, Li H, Wang R, et al. (2006) Monitoring and predicting land use change in Beijing using remote sensing and GIS. *Landscape and Urban Planning* 78:322–333.
- Yang J, Weisberg PJ, Bristow N a. (2012a) Landsat remote sensing approaches for monitoring long-term tree cover dynamics in semi-arid woodlands: Comparison of vegetation indices and spectral mixture analysis. *Remote Sensing of Environment* 119:62–71.
- Yang X, Jiang G-M, Luo X, Zheng Z (2012b) Preliminary mapping of high-resolution rural population distribution based on imagery from Google Earth: A case study in the Lake Tai basin, eastern China. *Applied Geography* 32:221–227.
- Yang X, Zhang K, Jia B, Ci L (2005) Desertification assessment in China: An overview. *Journal of Arid Environments* 63:517–531.
- Yiran G a. B, Kusimi JM, Kufogbe SK (2012) A synthesis of remote sensing and local knowledge approaches in land degradation assessment in the Bawku East District, Ghana. *International Journal of Applied Earth Observation and Geoinformation* 14:204–213.
- Yousif M, Bubenzer O (2013) Integrated remote sensing and GIS for surface water development. Case study: Ras El Hekma area, northwestern coast of Egypt. *Arabian Journal of Geosciences* 6:1295–1306.
- Zhou W, Troy A, Grove M (2008) Object-based Land Cover Classification and Change Analysis in the Baltimore Metropolitan Area Using Multitemporal High Resolution Remote Sensing Data. *Sensors* 8:1613–1636.
- Zinck JA, López J, Metternicht GI, et al. (2001) Mapping and modelling mass movements and gullies in mountainous areas using remote sensing and GIS techniques. *International Journal of Applied Earth Observation and Geoinformation* 3:43–53.
- Zucca C, Peruta R Della, Salvia R, et al. (2012) Towards a World Desertification Atlas. Relating and selecting indicators and data sets to represent complex issues. *Ecological Indicators* 15:157–170.

Chapter 2

Egypt dry lands: A general description^{*}

^{}The specific study area description will be presented with the relevant details in every chapter of this thesis*

2.1 Overview

The land of Egypt occupies the northeastern part of the African continent. It is roughly quadrangular, extending about 1073 km from north to south and about 1229 km from east to west (Said 1962). Thus, the total area of Egypt is a little more than one million square kilometers (1,019,600 km²), occupying nearly 3% of the total area of Africa (Abu-Al-lzz 1971; Ball 1939). Egypt is bordered on the north by the Mediterranean Sea, on the south by the Republic of Sudan, on the west by Libya and on the east by the Gulf of Aqaba and the Red Sea (Figure 2.1). Egypt extends over about 10 degrees of latitude, being bounded by Lat. 22 °N and 32 °N, i.e. lies mostly within the temperate zone, less than a quarter being south of the Tropic of Cancer. The whole country forms part of the great desert belt that stretches from the Atlantic across the whole of North Africa through Arabia. Abd El-Kawy et al. (2011) reported that is about 95% of Egypt's are deserts and extremely arid, Egypt comprises four main geographical units (Said 1962): 1) the Nile Valley and the Delta, 2) the Western Desert, 3) the Eastern Desert, and 4) the Sinai Peninsula.

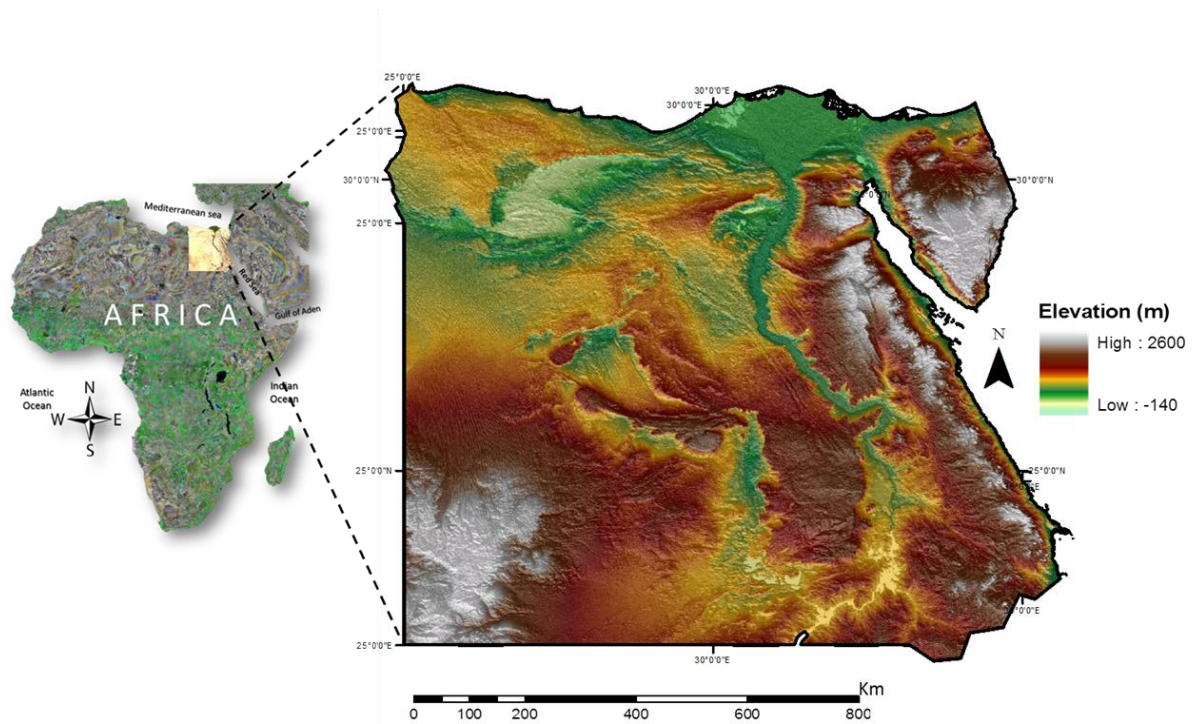


Figure 2.1. The geographical location of Egypt

2.2 Geological characteristics

The Archean is covering about 93,000 km² (10%) of Egypt's area. The formations of the Carboniferous period cover about 1,200 km² and found in western Sinai, Wadi Araba in the North Eastern Desert and El-Oweinat Mountain. The Triassic deposits cover 50 km² in small area of northeastern Sinai and the Khashm El-Galala area along the Gulf of Suez. Jurassic formations are found in small patches in Gebel El-Maghara and the El-Tih Plateau in Sinai as well as the Galala El-Bahariya Plateau along the Gulf of Suez, which is cover about 450 km². 40% of Egypt is covered by the Cretaceous exposures and it is also extend under more recent formations in about 90% of the country. the Eocene rocks found in the central and northern parts of the Al-Ugma and Tih Plateaus in Sinai desert (Said 1962), and it has a thickness of 700 m and reach 1000 m in Sinai, also it consists of limestone, marl and clay and contain in most parts marine fossil, Egyptian Eocene limestone are termed "nummulitic limestone" because of the presence of these fossils (El-Shahat 1993). The Oligocene formations are found in some isolated sites of the Western Desert between the Fayium and Bahariya Depressions, this formation covered about 1.5% of Egypt. Miocene formations cover about less than 20% of Egypt's area, extending west of Cairo in a triangular shape with the apex to the northwest of Cairo and base along the Egyptian-Libyan border (Albritton et al. 1990). Pliocene formations occupy not more than 700 km² and present in the Western Desert, the Gulf of Suez, Sinai and wadis of the Eastern Desert.

2.3 Geographical Characteristics

The Nile is more than 6650 km long from its source near Lake Tanganyika to the Mediterranean Sea, and only about 1530 km lies in Egypt (Hurst 1952). Before the construction of Aswan High Dam, the fertile land in Egypt was depending on the carried silt by the Nile water from Ethiopia through the Blue Nile (Kassas 1971; Mohamed et al. 2012). The total area of the Nile Valley is about 12,000 km². The Nile delta appears as a triangle shape, occupy about 22,000 km² and consist about 63% of Egypt's fertile soil (FAO 2005), Said (1962) reported that seven major branches of the Nile delta were mentioned by various historical literature, and five of these branches silted up in the course of time, these branches are: Bolbitinic branch, Sebennitic branch, Mendisy branch, Tanitic branch, the Pelusiatic branch, Fatmetic branch (the present Damietta branch; about 245 km long), Canopic branch (the present Rosetta branch; about 239 km long).

The Western Desert extended from Libya border to the Nile Valley, and occupies about 681,000 km², 60% of Egypt's area. Land surface is composed of bare rocky plateau and sandy plains. Mountains are found in the far southwestern side, where Gebel El-Oweinat is about 1907 m elevation (Figure 2.2). And the great depressions and most of the oases are found in the northern and central parts of the Western Desert. The arid conditions in the Western Desert encourage the driven sand

particles by wind motion and build up massive sand dunes, which become the most geographical feature (Abdel Kawy and Abou El-Magd 2012). Another distinctive feature is the nature and distribution of the water sources in the Western Desert, which are mostly depending on wells and cisterns that fed by local rainfall (Said 1962; Zahran and Willis 2009). The oases such as Siwa, Bahariya, Kharga and Dakhla are located in great depressions where the ground water supplies can rise to the surface, but the vast intervening areas of high plateau are waterless (Laity 2008; Masoud and Koike 2006).

The Eastern Desert occupies 223,000 km² which extends eastwards from the Nile Valley to the Red Sea. It consists essentially of a great backbone of high mountains more or less parallel to the Red Sea. These mountains are igneous and limestone (Said 1962). The igneous mountains extend southward from about Lat. 28°N to beyond the Sudan and Egypt border, Gebel Shayeb El-Banat is the highest mountain, about 2184 m elevation. In the north of the igneous mountains are the extensive and lofty limestone mountains of South Galala (1464 m), North Galala (1274 m) and Gebel Ataqa (871 m) which separated by broad valleys “wadis”, about 25% of the total area of the Eastern Desert covered by the Nubian sandstone. The dissection of the Eastern Desert by dense networks of wadis indicates that although the present time is a dry period.

The Sinai Peninsula is about 61,000 km², which is separated from the Eastern Desert by the Gulf of Suez. Geomorphologically, the Sinai Peninsula region divided into three sub-regions (southern, central and northern). The western coastal plain, known as El-Qaa and it borders with the Gulf of Suez, which has a length of about 400 km and a depth of 100 m, also it is a subject to flooding with water and in the dry season these areas become covered with a thin mantle of white salts (Greenwood 1997), the eastern coastal plain extends about 235 km from Aqaba southwards to Ras Muhammed. The mountains which form the igneous core of the Sinai Peninsula rise to considerably greater heights than any of those of the African part of Egypt (Said 1962). The highest peak is Gebel St Katherine, about 2641 m elevation, and many other conspicuous peaks and crests rise above the 2000 m elevation, which are Gebel Umm Shomer (2586 m), Gebel Al-Thabt (2439 m), Gebel Musa (2285 m) and Gebel Sebal Pile (2070 m). Because of its high altitude, the southern section of Sinai receives ample rainfall which has produced wadis and most of these wadis run in long hollows and appear as valleys, Some these wadis flow to the Gulf of Aqaba, such as Wadis Ghayib, Nasb and Watir which are the most steep valleys, wide and relatively rich vegetation (Zahran and Willis 2009). The higher part of the limestone plateau which flanks the igneous core to the north is called El-Tih, Ugma Plateau is about 1620 m elevation, and it covered by sandy marls and gypsum, covered in some parts with gravels (Said 1962). The northern part of Sinai “Mediterranean Foreshore” has an average relief of approximately 56 meters (Mahmoud et al. 2005), the highest point is about 229 meters above sea level, and the lowest points are in the El Tina Plain and at the eastern edge of Lake Bardawil, where the elevation is slightly below sea level (El-Bana et al. 2002). There are two

landform classes of sand dunes in the north of Sinai, 1) stabilized dunes occur on the eastern side and 2) The active sand dunes can be divided into two geomorphic types (Barchan and Seif dunes)(Greenwood 1997). Coastal wetlands and marshes (in the El Tina Plain area), sand bars and extensive beaches along the Mediterranean Sea coast, sabkhas such as Lake Bardawil and Lake Malaha (El-Bana et al. 2002; Zahran 1982).

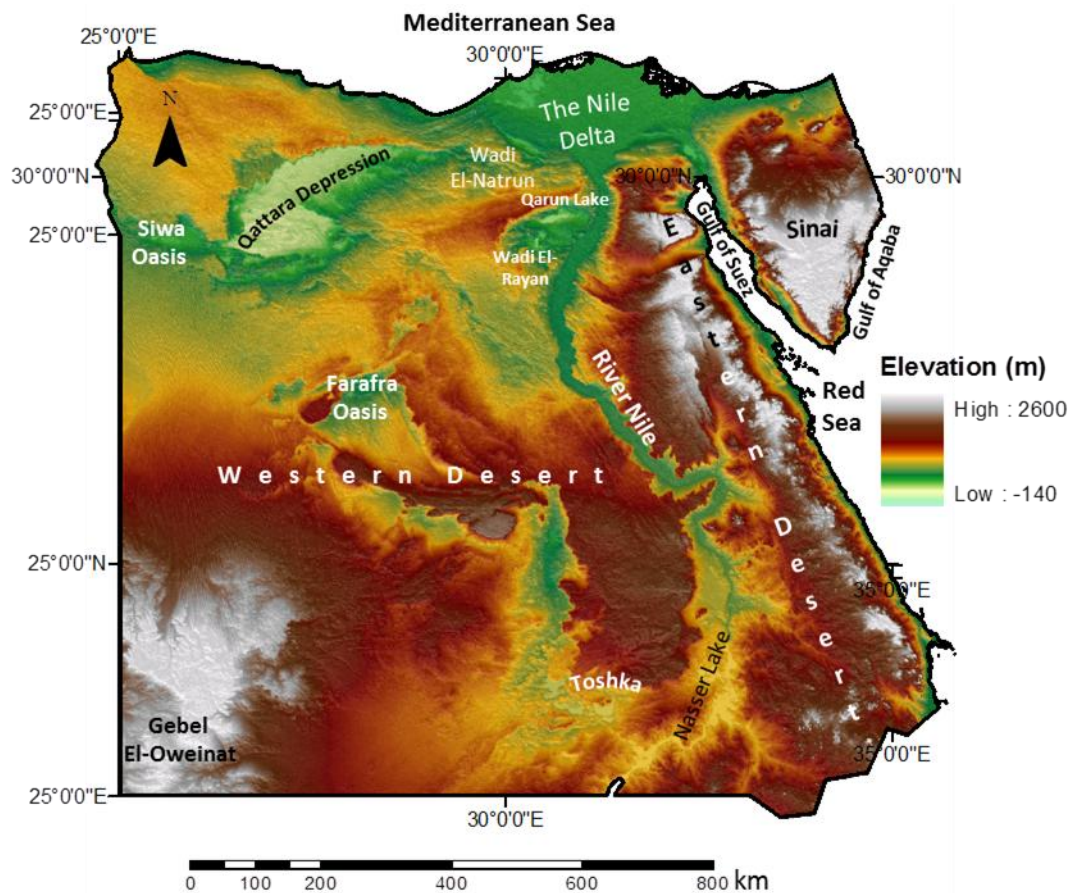


Figure 2.2. The geomorphology of Egypt.

2.4 Soil-Vegetation Relationships

The soils in Egypt fall into two main orders, Entisols: alluvial soils and soils of sandy and stony deserts) and Aridisols: essentially desert soils, (Natural Resources Conservation Service (NRCS) 1999). Entisols is the most common soil order in arid regions, little or not developed pedogenic horizons are due to recent deposition of material, or the former surface has been lost by erosion (Greenwood 1997), this order found in Qattara Depression and North Sinai (Dregne 1976; Pueyo and Alados 2007). (Natural Resources Conservation Service, NRCS (1999) defined Aridisols as the soil

type which is confined to arid regions, the main characteristics of this order is that the mineral soils distinguished by the presence of horizons showing accumulations, e.g. carbonates, soluble salts, and the soil horizons have been formed under recent conditions of climate or those of earlier pluvial periods. The horizon at the surface (the epipedon) of this soil type is light-coloured and more probably salic (salty) horizon near to the surface or an argillic (clayey) horizon. These saline soils are well represented in the coastal plain of the Red Sea, and around El-Bardawil Lake

Vegetation in Egypt varies with the degree of aridity condition. The role of vegetation distribution is insignificantly correlated to the soil development. Two factors are attributed to form the relationship between landforms and the vegetation cover in Egypt, (1) it is controlling water availability; and (2) the landform is responsible for human and natural habitats accessible for grazing and interference (Zahran and Willis 2009). Water resources is the most important factor for controlling the vegetation distribution in arid environments, the vegetation in the northern Mediterranean coastal belt in Egypt is denser as a result of rainfall (Kassas 1953).

Wadis are the main ecosystems of the Egypt's dry lands, which has the great merit of being a drainage system collecting water from an extensive catchment area. The soils of the wadi beds are usually composed of rock waste varying in texture from fine particles to gravel and boulders (Kassas and Imam 1954), and the beds are often covered with layers of eroded fine materials. The soil depth is the most vital factor that controls the type of vegetation in Egypt's dryland, the thinner soil will be dried faster by the approach of dry season, where the ephemeral vegetation appears, deeper soil profile storage more water, which will provide a continuous supply of moisture for the deeply seated roots of herbaceous perennials, undershrubs, shrubs and trees (Reynolds et al. 2007). The wadis environment is characterized by rock surfaces, erosion pavements, gravel deserts, slopes and cliffs, and each has its unique vegetation type (Said 1962). The rocky surfaces provide little opportunity for vegetation growth and extreme aridity condition. During rainfall events a shallow depressions store water by ephemeral vegetation cover, which appear in the late winter and early spring. Chasmophytes, which can extend their roots into the rock crevices, e.g. *Erodium glaucophyllum*, *Fagonia mollis*, *Helianthemum kahiricum*, *Iphiona mucronata*, *Reaumuria hirtella* and *Stachys aegyptiaca*.

Erosion pavement and gravel desert are a flat or undulating landform that formed mainly from transported material, where the runoff water is collected by the formed drainage systems, and the beds of these water-ways are covered with layers of eroded soft materials which have the potential of holding more water (Said 1962; Zahran and Willis 2009). In these water-ways the vegetation find suitable conditions, ephemerals, e.g. *Anastatica hierochuntica*, *Diplotaxis acris* and *Pteranthus dichotomus*, or of perennials which acquire a summer-deciduous growth-form, e.g. *Asteriscus graveolens*, *Farsetia aegyptia* and *Iphiona mucronata*. The flat land surface of the gravel desert is a subject to the deposition and accumulation of wind-borne materials which produce sand sheet

where ephemeral plants can grow and acquire more permanent appearance (Zahran and Willis 2009). As the sheet becomes deeper more species find the habitat favourable and the vegetation acquires a more permanent appearance, e.g. *Hammada elegans*, *Panicum turgidum* and *Zilla spinosa*.

In the slopes which represented on the plateau edges, wadi sides and mountain and hillsides, are always little sites among the surface fragments where some soil accumulates permit the growth of vegetation (Zahran and Willis 2009). The vegetation cover show zonation in relation to altitude, the lower levels of the slopes receive more water and are less exposed than higher level, and the south-facing side of the mountains nearly always barren. The species that found in the mountains of the Red Sea coastal land and those of the Sinai Peninsula and in this particular condition are *Diploaxis harra*, *Fagonia kahirina*, *Gymnocarpos decander*, *Limonium pruinsum*, *Reaumuria hirtella* and *Salsola volkensis* (Zahran and Willis 2009).

The vegetation that found on sand dunes such as psammophytes are growing in the path of air currents, usually form mounds of accumulated wind-borne material around them but they may be overwhelmed by extensive deposition of sand, these plants are good sand collectors and binders, producing phytogenic mounds, hillocks or dunes. Such species include *Ammophila arenaria*, *Anabasis articulata*, *Atriplex farinosa*, *Cornulaca monacantha*, *Halopyrum mucronatum*, *Hammada elegans*, *Nitraria retusa*, *Panicum turgidum*, *Stipagrostis scoparia* and *Tamarix* spp. (El-Bana et al. 2010; El-Bana et al. 2002).

The aridity condition increase rate of evaporation and as rainfall is low, and cause more accumulation of salts, which form surface salt crust. the total amounts of soluble salts are generally high in the salt marshes of Egypt but the amounts are greater in the inland and Red Sea salt marshes than in the Mediterranean ones (Zahran 1982). There are two types of salt marshes in Egypt (littoral and inland), the littoral salt marshes occur along the coasts of the Mediterranean Sea, Red Sea, Gulfs of Aqaba and Suez and around the northern lakes (Mariut, Idku, Burullus, Manzala and Bardawil). The inland salt marshes are far from the maritime influences. These marshes are represented by the sabkhas and playas of the oases and depressions of the inland drylands. Being lower in level than the surrounding territories, the inland salt marshes are characterized by a shallow underground water-table. In certain localities the water is exposed, forming lakes of brackish or saline nature. *Arthrocnemum macrostachyum* found in Red Sea coast, where the surface layer contains 60.5% of soluble slats, and *Typha elephantina* in the Wadi El-Natron Depression are found in 0.4% soluble salts.

2.5 Climate

Kottek et al. (2006) and Peel et al. (2007) updated the climate classification of Köppen-Geiger, and mainly Egypt was classified as (Bwh) arid-desert-hot climate. The southern part of Egypt is more dry and arid than the northern part. Egypt is an arid country, and this aridity can be divided into provinces hyperarid and arid, described as follow:

2.5.1 Hyperarid provinces

In the southwestern part of the Western Desert the mean temperature of the coldest month between 10 °C and 20 °C and the mean temperature of the hottest month more than 30°C. The Eastern Desert and the northeastern part of the Western Desert and Gebel El-Oweinat area have a mild winter (mean temperature between 10° and 20 °C) and a hot summer (mean temperature of the hottest month 20–30 °C) (Harris 2003).

2.5.2 Arid provinces

In the Mediterranean coast and the Gulf of Suez are under the maritime influence of the Mediterranean, with a shorter dry period, mild winter and a hot summer. The northern section of inland province, Accentuated longer dry period and an annual rainfall of 20–100 mm. this province also characterized by a mild winter and a hot summer. Also, a mild winter and a very hot summer, with annual rainfall is about < 50 mm in Gebel Elba area of the Red Sea coast of Egypt.

2.6 References

- Abd El-Kawy OR, Rød JK, Ismail H a., Suliman a. S (2011) Land use and land cover change detection in the western Nile delta of Egypt using remote sensing data. *Applied Geography* 31:483–494.
- Abdel Kawy WAM, Abou El-Magd IH (2012) Use of satellite data and GIS for assessing the agricultural potentiality of the soils South Farafra Oasis, Western Desert, Egypt. *Arabian Journal of Geosciences*. doi: 10.1007/s12517-012-0518-5
- Abu-Al-lzz MS (1971) Landforms of Egypt. The American University in Cairo Press. Cairo, Egypt. p281.
- Albritton CC, Brooks JE, Issawi B, Swedan A (1990) Origin of the Qattara Depression, Egypt. *Geological Society of America Bulletin* 102:952–960.
- Ball J (1939) Water economy of desert plants in Wadi Hof. Cairo University, Egypt
- Dregne HE (1976) Soils of Arid Regions. Elsevier. Amsterdam, NL. pp237.
- El-Bana M, Khedr A, Hecke P Van, Bogaert J (2002) Vegetation composition of a threatened hypersaline lake (Lake Bardawil), North Sinai. *Plant Ecology* 63–75.
- El-Bana M, Shaltout K, Khalafallah A, Mosallam H (2010) Ecological status of the Mediterranean *Juniperus phoenicea* L. Relicts in the desert mountains of North Sinai, Egypt. *Flora - Morphology, Distribution, Functional Ecology of Plants* 205:171–178.
- El-Shahat A (1993) Middle Miocene carbonates from the Northern Plateau of the Western Desert (Egypt): Petrography and geochemistry. *Facies* 28:67–76.
- FAO (2005) Fertilizer use by crop in Egypt, Land and Plant Nutrition Management Service Land and Water Development Division. p62.
- Greenwood NH (1997) The Sinai: a physical geography. University of Texas Press, Austin, p148.
- Harris N (2003) Atlas of the world's deserts. Taylor and Francis. New York, USA. p 359.
- Hurst HE (1952) The Nile. Constable. London, UK. p 326.
- Kassas M (1971) The River Nile Ecological System : A Study Towards an International Programme. *Biological Conservation* 4:19–25
- Kassas M (1953) Landforms and plant cover in the Egyptian Desert. *Bulletin de la Société de Géographie d'Égypte* 26:193–205.
- Kassas M, Imam M (1954) Habitat and plant communities in the Egyptian desert. III. The wadi bed ecosystem. *Journal of Ecology* 42:424–441.
- Kottek M, Grieser J, Beck C, et al. (2006) World Map of the Köppen-Geiger climate classification updated. *Meteorologische Zeitschrift* 15:259–263.
- Laity J (2008) Deserts and desert environments. John Wiley & Sons, Inc. Chichester, UK, pp 357.
- Masoud A.A and Koike K (2006) Arid land salinization detected by remotely-sensed landcover changes: A case study in the Siwa region, NW Egypt. *Journal of Arid Environments* 66:151–167.
- Mohamed ES, Belal A, Saleh A (2012) Assessment of land degradation east of the Nile Delta, Egypt using remote sensing and GIS techniques. *Arabian Journal of Geosciences*. doi: 10.1007/s12517-012-0553-2
- Natural Resources Conservation Service (NRCS) (1999) Soil Taxonomy: A Basic System of Soil Classification for Making and Interpreting Soil Surveys, 2nd ed. United States Department of Agriculture (USDA), Washington , p 871.
- Peel MC, Finlayson BL, McMahon TA (2007) Updated world map of the Köppen-Geiger climate classification. *Hydrology and Earth System Sciences* 11:1633–1644.
- Pueyo Y, Alados CL (2007) Abiotic factors determining vegetation patterns in a semi-arid Mediterranean landscape: Different responses on gypsum and non-gypsum substrates. *Journal of Arid Environments* 69:490–505.
- Reynolds JF, Smith DMS, Lambin EF, et al. (2007) Global desertification: building a science for dryland development. *Science (New York, NY)* 316:847–51.
- Said R (1962) The Geology of Egypt. Elsevier, Amsterdam, NL, pp377.
- Zahrán MA (1982) Ecology of the halophytic vegetation of Egypt. In: Sen DN, Rajpurohit KS (eds) Part I. In Contributions to the Ecology of Halophytes, Tasks for Vegetation Science. The Hague, pp 3–20
- Zahrán MA, Willis AJ (2009) The Vegetation of Egypt, 2nd ed. Springer, Heidelberg, pp 451.

Chapter 3

Assessing the spatio-temporal dynamics of vegetation cover as an indicator of desertification in Egypt using multi-temporal MODIS satellite images

This chapter is modified from:

Nasem Badreldin, Amaury Frankl and Rudi Goossens (2013) Assessing the spatio-temporal dynamics of the vegetation cover as an indicator of desertification in Egypt using multi-temporal MODIS satellite images. *Arabian Journal of Geosciences*. DOI: 10.1007/s12517-013-1142-8

3.1 Introduction

Desertification is the process whereby the productivity of land is reduced, essentially by the loss of topsoil and the decrease in vegetation cover (Kassas 1977). It is often the result of complex interactions between biophysical and anthropological factors, like poor agricultural practices, land surface temperature anomalies and drought. It is among the most threatening environmental hazards, responsible for the rapid deterioration of dry land regions (Diouf and Lambin 2001). As reported by (Dregne 1977; Dregne and Chou 1992; Reynolds et al. 2003), desertification is responsible for depleting the soil resources of the land, which is globally happening in an alarming rate, and directly affecting one-fifth of the world population (Adamo and Crews-Meyer 2006; G.Kepner et al. 2006).

Remote sensing is a powerful tool for quantifying vegetation cover dynamics, which provides multi- temporal data necessary for understanding patterns and processes of desertification in arid environments (Badreldin and Goossens 2013a; Bannari et al. 1995; Grainger et al. 2000; Hall et al. 1995; Herrmann et al. 2005; Richards 2013; Wang et al. 2008; Weng 2002). While no consensus exist on adequate methods to monitor and quantify these developments (Geist and Lambin 2004; Salinas and Mendieta 2012; Verón et al. 2006), monitoring the vegetation cover change from remote sensing data is acknowledged as a powerful indicator for dryland regions (Armah et al. 2010; Dawelbait and Morari 2012). Field measurement on their hand are often too time consumptive, expensive or difficult to organize in areas with limited accessibility (Yang et al. 2012).

Most of the remote sensing applications for monitoring vegetation cover dynamics in dry land regions have either used vegetation indices such as the normalized difference vegetation index (NDVI), or a soil-adjusted vegetation index (SAVI) (Abd El-Kawy et al. 2011; Du et al. 2010; Herrmann et al. 2005; Schnur et al. 2010; Yeganeh et al. 2012). Huang and Siegert (2006) and Schowengerdt (2007) found that the SAVI vegetation index is especially useful for low cover environments, able to detect sparse vegetation cover in exposed areas that is normally categorized as arid land like Egypt. However, little research has been done to monitor spatio-temporal desertification dynamics using SAVI in arid ecosystems (e.g., Epiphanyo and Huete 1992; Gilabert M.A. et al. 2002; Huete et al. 1992; Mildrexler et al. 2007; Qi et al. 1994; Rondeaux et al. 1996). In addition, remotely sensed land-surface temperatures (LST) have been used for monitoring land-cover change and drought (Wan et al. 2002), which is considered as one of the key factors that provide a clear explanation about desertification developments (Feizizadeh et al. 2012; Feizizadeh and Blaschke 2013; Feizizadeh and Blaschke 2012).

It is important to understand the relationship between the vegetation cover change and LST and the relation with climatic data at regional and global scales (Dousset and Gourmelon 2003).

This study will investigate dynamics in spatial and temporal vegetation cover change of Egypt, as a direct indicator of desertification development. Therefore, trends of vegetation cover change are being established for the period 2002-2011. Furthermore, this study will monitor the vegetated and desertified locations, as a result of the bi-stable ecosystem dynamics over periods 2002-2005, 2005-2008 and 2008-2011 at three different sites (Kom Ombo, El-Oweinat and Nile Delta) in Egypt; and finally, assessing the relationship between the vegetation cover distribution along with precipitation, LST and elevation at these chosen locations.

3.2 Study area description

The total area of Egypt is about one million square kilometers (A.Bard and Shubert 1999) , latitudes 22° and 32°N and longitudes 24° and 36°E (Figure 3.1). In the year 2013 the population was about 85 million with a population growth rate of 1.92% (CIA 2013). Approximately 95% of population lives on only 4% of the land (Bakr et al. 2010).

The Nile River flows from the south to the north and enrich the valley soils with fertile deposits. The south of Egypt is called “Upper Egypt” and the northern part including Cairo and the Delta is called “Lower Egypt”. The river Nile in Egypt is surrounded by two huge deserts in west and east. The lowest point is about -133 m which is found in the west of Nile Delta called “the Qattara Depression”. Sinai Peninsula is located in the eastern north part of Egypt; the highest elevation is the Mount of Catherine about 2,641 m, located in the southern part of Sinai Peninsula. Within the Western Deserts there are many oases formed by springs such as, Siwa, Farafra, Bahariya, Dakhla and Kharga. The Red Sea Hills occupy the Eastern Desert from the south to the north. Most of the agricultural activities are located around the Nile River, where the soils are silt-clay mixtures of good quality, which was deposited during thousands of years of Nile flooding. As shown in Table 3.1, four agro-ecological zones for Egypt were identified, where the total cropped area in 2005 was approximately 58000 km² with a cropping intensity of 180 percent, and most of the newly reclaimed desert areas use modern irrigation practices such as drip and sprinkler systems (FAO 2005).

Table 3.1. The agro-ecological zones of Egypt, adopted from (FAO, 2005)

Agro-ecological zones	Region	Area (km ²)	Soil characteristics	Water resources
Old land	Nile Valley and Delta	22,500	alluvial soils (clay to loamy)	The Nile is the main source of water for irrigation
New land	East and west sides of the Delta and scattered over various areas in the country	10,500	Mainly formed by Aeolian deposits (sandy to loamy)	Nile water is the main source of irrigation water but in some desert areas underground water is the only source of irrigation water. Sprinkler and drip irrigation regimes are practiced
Oases	Western Desert	400	alluvial, sandy and calcareous soils	Underground water is the main source for irrigation
Rainfed areas	north coastal areas	1700	Traditional soil fertility management leads to environmental contamination through the over-application of fertilizers	rainfall fluctuates between 100 and 200 mm annually

Kottek et al. (2006) and Peel et al. (2007) updated the climate classification of Köppen-Geiger, and mainly Egypt was classified as (Bwh) arid-desert-hot climat. The southern part of Egypt is more dry and arid than the north. The south receives less rain in the winter at < 5 mm a year and the air temperature is between (10 – 20°C) in the winter and (30 – 40°C) in the summer. The north is less dry; rainfall is < 150 mm and (5 – 20°C) in winter and (20 – 35°C) in the summer of air temperature (World Bank 2013).

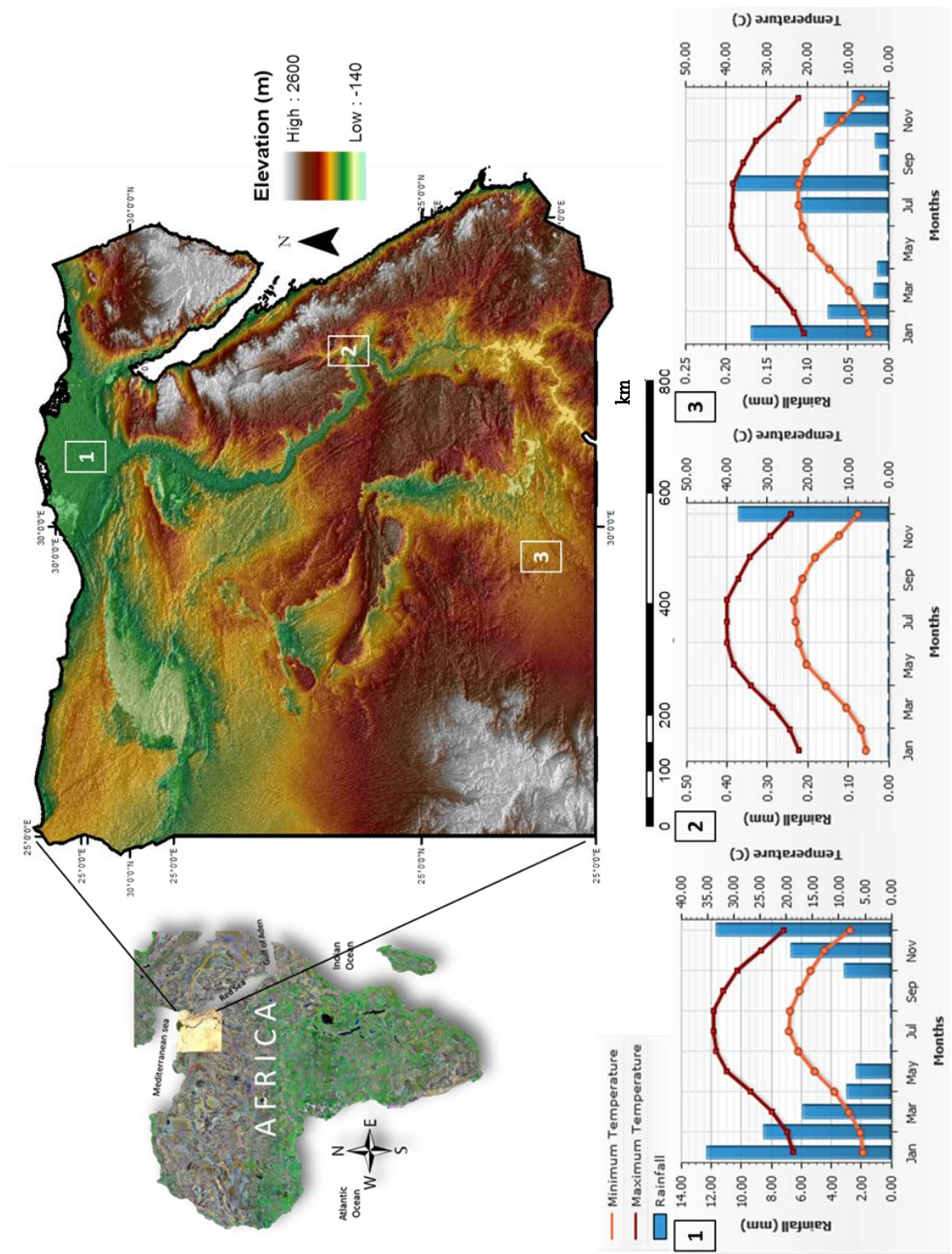


Figure 3.1 The geographical location and geomorphology of Egypt. Climatic information (lower section), presenting the mean rainfall and air temperature of period (1980: 2012) for different locations over the case study, rainfall (blue columns), maximum air temperature (red lines) and minimum air temperature (orange lines).

3.3 Materials and methods

3.3.1 Remote sensing and meteorological datasets

This study used MODerate resolution Imaging Spectroradiometer (MODIS) satellite images, which were obtained from the U.S. Geological Survey (USGS) Earth Resources Observation and Science (EROS) Center. Satellite data for the months January, March, June, September and December in the years 2002, 2005, 2008 and 2011 were acquired over Egypt in a clear atmospheric condition. The MODIS Re-projection Tool (MRT) software version 4.1 was used in order to re-project MODIS images into a known map projection system and extension. MOD13A3 satellite is the MODIS Terra, vegetation indices (VI) were provided monthly at 1 kilometer spatial resolution and used for estimating SAVI. VI were computed from atmospherically corrected bi-directional surface reflectance's that were masked for water, clouds, heavy aerosols, and cloud shadows (U.S. Geological Survey 2011a). MOD09Q1 satellite is the MODIS Terra, LST was provided every 8 days of data at 250 meters spatial resolution, the data were validated via a widely distributed dataset of locations and time periods via several ground-truth and ready for use in scientific publications (U.S. Geological Survey 2011b). Global Multi-resolution Terrain Elevation Data 2010 (GMTED2010) provides a new level of detail in global topographic data. The accuracy was measured by a global set of control points. Root Mean Square Error (RMSE) of the products that were used for this study was between (26 – 30 meters) at 7.5 arc-seconds (U.S. Geological Survey 2011c). Meteorological data were obtained from 33 weather stations over Egypt which was provided via the National Oceanic and Atmospheric Administration (NOAA) and the National Climatic Data Center (NCDC), as shown in Figure 3.2. Precipitation data for over all Egypt data was used.

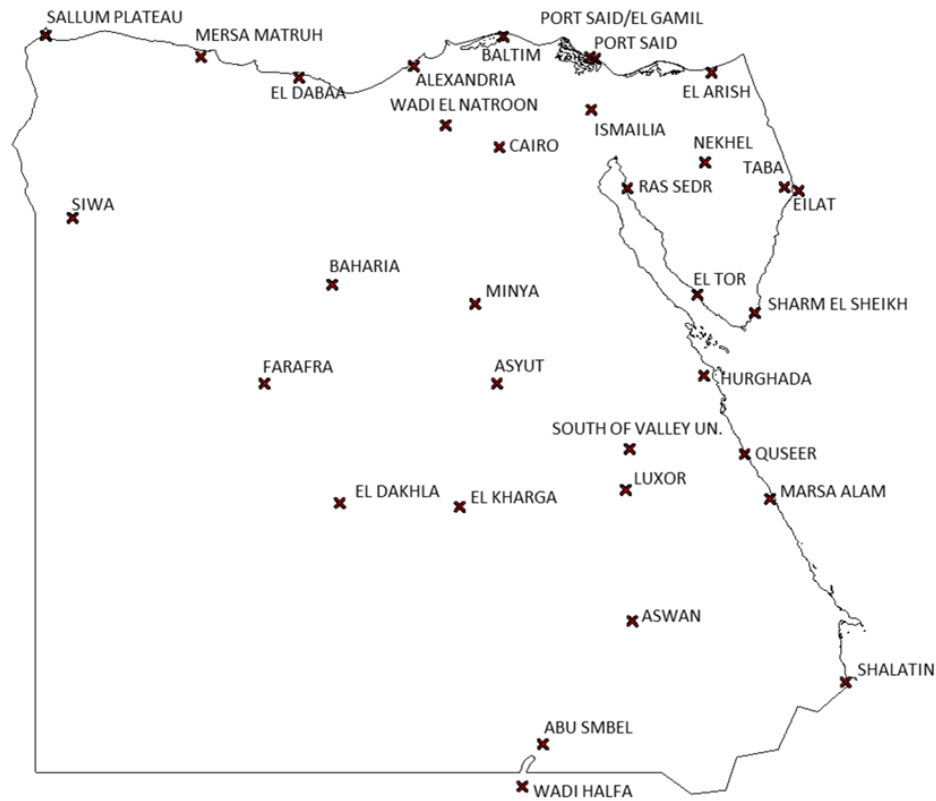


Figure 3.2 The distribution of the weather stations over the case study, Egypt

3.3.2 Field survey

Six study sites in Sinai Peninsula were chosen to represent the variety of the land covers of Egypt; a field survey was conducted to observe land cover types in different arid environmental conditions. Also, anthropological activities were different in terms of agricultural management and urbanization growth, which were influencing the agro-ecosystem distribution (Badreldin and Goossens 2013b), as shown in Table 3.2. The field survey will be used as supportive information for interpreting the reasons of the vegetation cover change and the possible associated land degradation.

Table 3.2. Description of soil properties and filed survey observations for six chosen study sites in Sinai Peninsula, Egypt.

Location	Latitude	Longitude	Description
El-Tina Plain,	31° 00' 00.09"	32° 26' 11.25"	Soil contains fine particles size, elevation < 50 m, waterlogging and salinization is the major land degradation. Cultivation is the main agricultural activity, plant cultivars are mostly salt tolerant
Arish&Rafaa	31° 09' 35.72"	34° 02' 11.83"	Soil contains coarse to moderate particle sizes, elevation < 150 m, wind erosion in the major land degradation, cultivation and natural plant are the major characteristic of vegetation cover.
Qantara Shark	30° 26' 31.58"	32° 24' 23.19"	Soil contains coarse particle sizes, elevation < 100 m, wind erosion and sandstorms are the major land degradation, intensive agricultural production and various plant cultivars.
Zaraniq	31° 06' 07.77"	33° 28' 57.82"	Soil contains coarse particle sizes, elevation < 50m, wind erosion and salinization are the major land degradation, natural halophyte plant species.
South-Sinai	28° 27' 38.70"	34° 04' 15.03"	Soil contains coarse particle sizes, elevation > 2000 m, water erosion is the major land degradation, drought tolerant natural plants species.
El-Wasat	29° 52' 08.36"	33° 47' 21.85"	Soil contains moderate to fine particle sizes, elevation < 1500 m, water erosion is the major land degradation, drought tolerant natural plants species and rare cultivation activity.

3.3.3 Data analysis

Data analysis was conducted according to the framework in (Figure 3.3). In this investigation, the atmospheric and geometric corrections were operated for the satellite images, which were based on truth information, RMSE was less than 0.6 (Kelarestaghi and Jafarian Jeloudar 2009; Yeganeh et al. 2012).

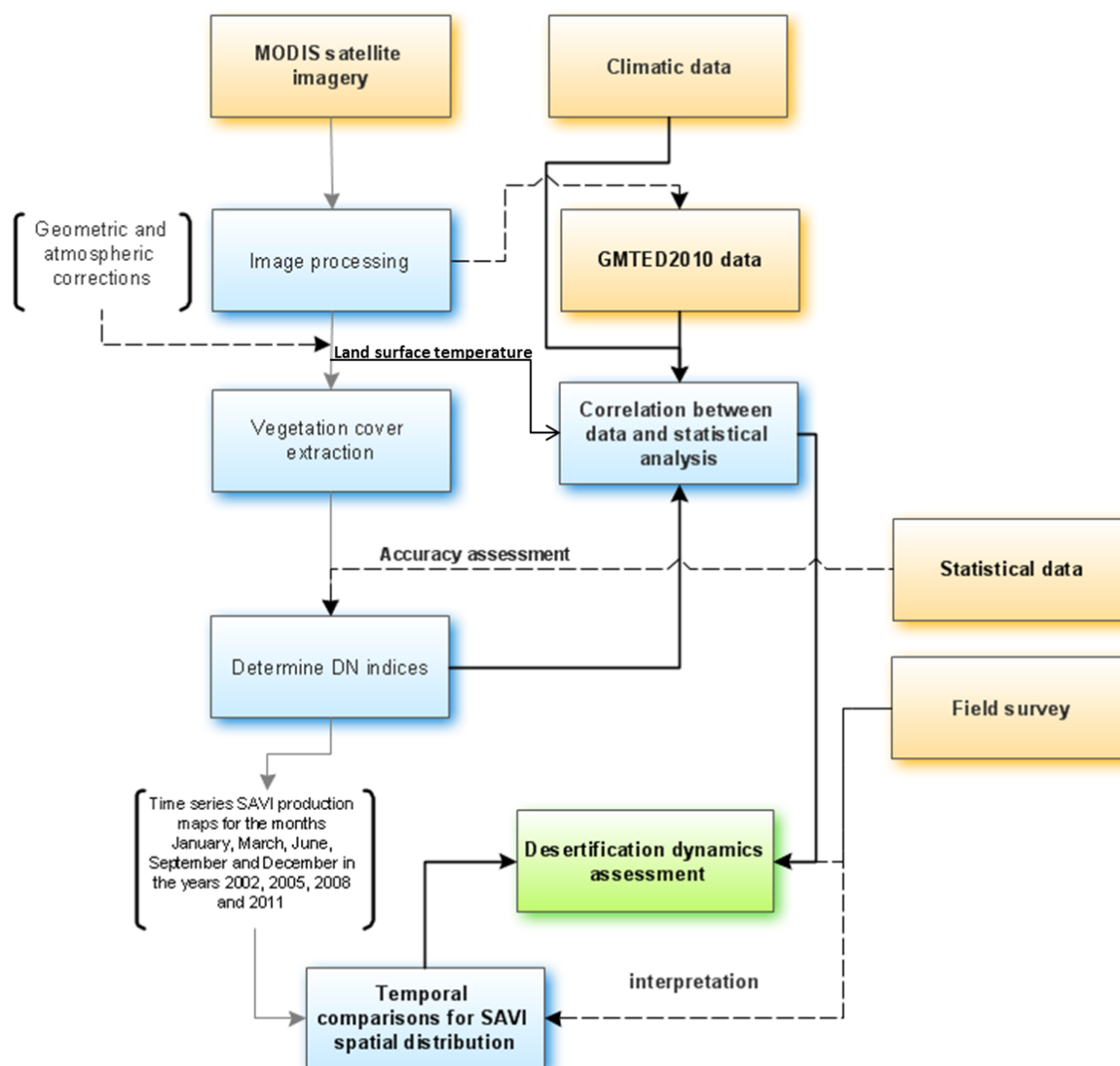


Figure 3.3 The stepwise process of data analysis used for assessing desertification change.

One of the primary sources of information for observing the Earth's vegetative cover were vegetation indices which were derived from satellite data (Gilbert M.A. et al. 2002). The vegetation index values in this particular investigation were affected by the reflectance of light in the red and near-infrared spectra, where the vegetative cover was lower than 40% and the soil surface was exposed, typical for arid regions (Yang et al. 2012). In order to correct the influence of the soil brightness when vegetative cover was low, the NDVI was replaced by SAVI (Bannari et al. 1995; Huete 1988).

$$SAVI = \left(\frac{\rho_{NIR} - \rho_{RED}}{\rho_{NIR} + \rho_{RED} + L} \right) \times (1 + L) \quad (3.1)$$

Where ρ_{NIR} is the reflectance value of the near infrared band, ρ_{RED} is the reflectance of the red band, and L is the soil brightness correction factor. $L=0.5$ was successfully minimizing the effect of soil variations in green vegetation compared to NDVI (Aboelghar et al. 2012). The average values of SAVI were used to evaluate changes in the vegetation cover over the studied years and periods. Change detection analysis was based on two multi-temporal images, and the changes were extracted via direct comparisons in order to detect vegetation cover change.

LST was estimated using the generalized split window technique of (Wan et al. 1996), which represents the 8-day average of cloud free daily MOD09Q1 data. Version-5 MODIS/Terra Surface Reflectance products were validated stage 2, meaning that accuracy was assessed over a widely distributed set of locations and time periods, and via several ground-truth and validation efforts. (U.S. Geological Survey 2011b), LST was estimated in various land cover types with accuracy to within 1 °C (Wan et al. 2002). The cloudy data was avoided, which is potentially could contaminate observations, we only used LST data with quality control flags set to 00 (highest quality) (Hashimoto et al. 2008). The products were thus ready to use in scientific publications (Son et al. 2012; Vermote et al. 2011; Zhang et al. 2003).

The spatial pixel-based scale of the data was considered in the analysis in order to monitor the temporal changes for the vegetation cover in Egypt, while the polygons correspond to the territorial disparities in the vegetation cover along the environmental variables. Average SAVI values for the months January, March, June, September and December in the years 2002, 2005, 2008 and 2011 were computed, in order to estimate the seasonal change in SAVI, LST, precipitation (P) and elevation. The temporal change analysis of the vegetation cover distribution was carried out along with the elevation, Classes' calculations and intersections were obtained by using the spatial analysis tools which are provided by ArcGIS software. The trends of change over the periods 2002-2005, 2005-2008 and 2008-2011, were quantified separately at two temporal seasons where the maximum vegetated season (March) and the minimum vegetated season (September) in Egypt.

A linear Regression model was calculated for estimating the relationship between the spatial distribution of temporal average score of SAVI and environmental variables (LST, P and elevation) for each three chosen locations in Egypt (Kom Ombo, Shark El-Oweinat and Nile Delta), where the environmental conditions and vegetation cover distribution are different (Zahran and Willis 2009).

$$y = \alpha + \beta (x) + e \quad (3.2)$$

Where y is SAVI, x is the environmental variable, α and β are the regression coefficients, and e is the regression error. Regressions were estimated for the average of years 2002, 2005, 2008 and 2011; significant regressions were checked via a t-test at ($\alpha=0.01$).

3.3.4 Accuracy assessment of SAVI distributions

The vegetation cover data for the years 2002, 2005, 2008 and 2011 were validated against statistical data of Egypt (El-Nahrawy 2011; World Bank 2012). Validation was carried out by comparing four regional statistical data of (Nile Delta, North Sinai, Western Desert and south on Nile Valley) to the average SAVI data of the same location. As shown in Figure 3.4. the results showed a strong relationships between the reference data “statistical data” and estimated values “SAVI” (Nile Delta, $r^2=0.84$; North Sinai, $r^2=0.88$; Western Desert, $r^2=0.93$; South of Nile valley, $r^2=0.87$; $P<0.01$), which approved using the SAVI for monitoring the vegetation cover change in Egypt.

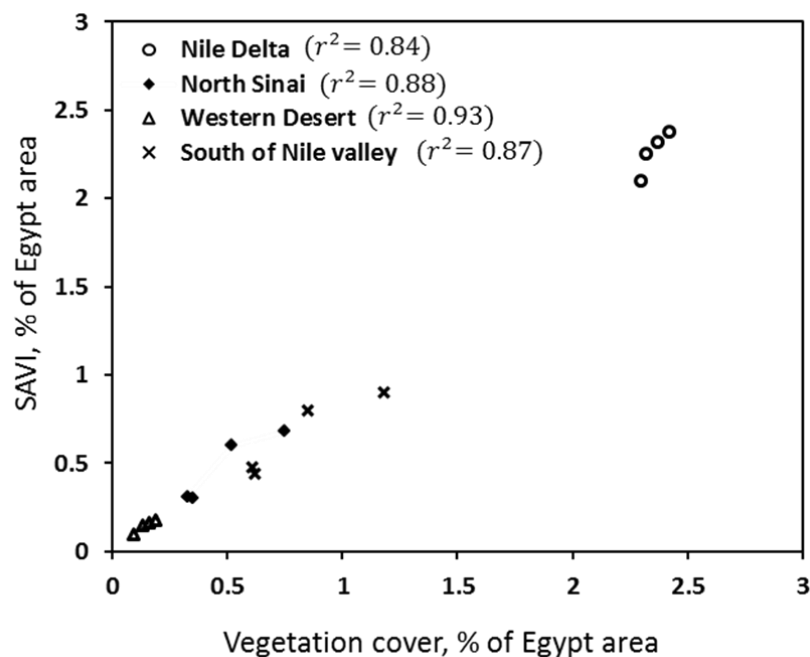


Figure 3.4. Vegetation cover, % of Egypt area “statistical data” and the SAVI, % of Egypt area “estimated data” relationship; four chosen locations (Nile Delta, North Sinai, Western desert, and South of Nile valley) for the years 2002, 2005, 2008 and 2011.

3.3.5 The vegetation covers feedbacks as desertification indicator

The development of desertification observed in many regions in Egypt is associated with a transition between the two stable states, vegetated and desertified in bistable ecosystem dynamics. Both of vegetated and desertified states would be stable configurations of the system (D’Odorico et

al. 2013). The bi-stable ecosystem dynamics, as shown in Figure 3.5, can explain the desertification development in Egypt as a result of interactions between the positive and negative feedbacks. The disturbance causes a transition to the stable states, where the resilience of the bi-stable system depends on the disturbance strength, furthermore the system will move forward to the other stable state, and it will be difficult to revert back to the initial state (Gunderson 2000).

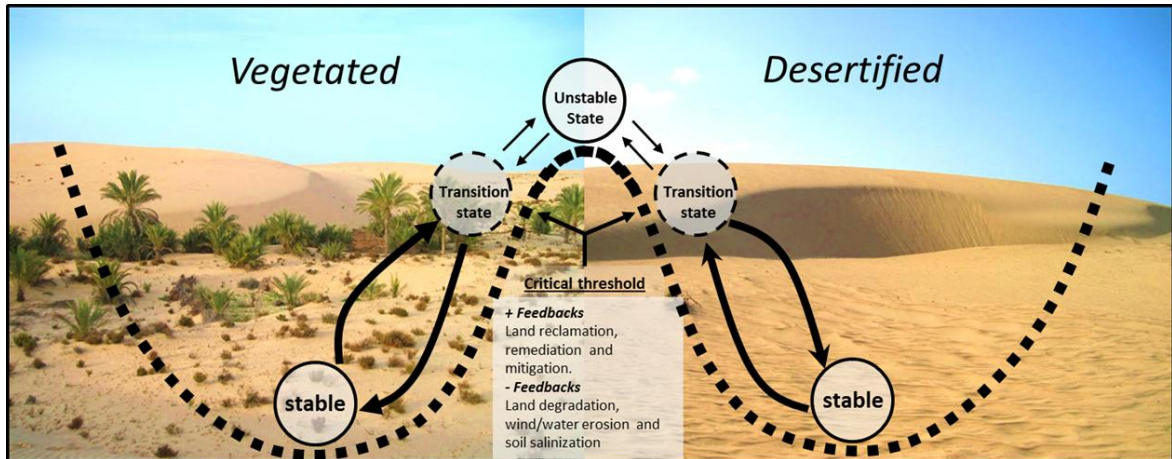


Figure 3.5 Illustration draws of the bi-stable ecosystem balance for an arid environment, both sections (vegetated and desertified) are hosting the transition and stable states, the critical threshold containing (positive and negative) environmental feedbacks. Positive feedbacks are the drivers that influence the system positively to move to the vegetated section, where the negative feedbacks are the drivers that cause more land degradation and orient the system to move to the desertified section.

3.4 Results and discussion

3.4.1 Spatio-temporal patterns in vegetation cover spatial distribution along with elevation

Vegetation cover is facing changes through seasons and the results show that the changes are both positive by gaining, and negative by losing vegetation. The period January – March showed that vegetation cover dynamics were in a symmetric window of change ± 0.2 . The suitable climatic

conditions were responsible for the recovery in this particular period, beside the positive contribution of the intensive agricultural activities that dominated the lands that found below 100 m elevation. March – June was the period where vegetation cover is decreasing dramatically. There are two annual agriculture seasons in Egypt (winter and summer), and during the period of June – September was the summer season of crop cultivation, which occurred mainly in the Nile Delta. Also, vegetation cover keeps increasing in the period September – December. The vegetation found above 250 meter of elevation was mostly natural flora, which has tolerant characteristics to the abiotic environmental conditions, as shown in Figure 3.6.

Spatial representation of the vegetation cover change provided useful information about the most sensitive locations to seasonal change and environmental variability. The Nile Delta and Valley hosted the most land cover dynamics. Remote areas such as Marsa Matroh and El Arish were more sensitive to any environmental change, which indicated that these locations were having limited natural resources and less environmental conservation (FAO 2005). Wadi Natroon and 6th October in the western side of the Nile Delta were the opposite story, more resistance to any environmental change, which were the results of precision agriculture and modern irrigation management (El-Nahrawy 2011), as shown in Figure 3.6.

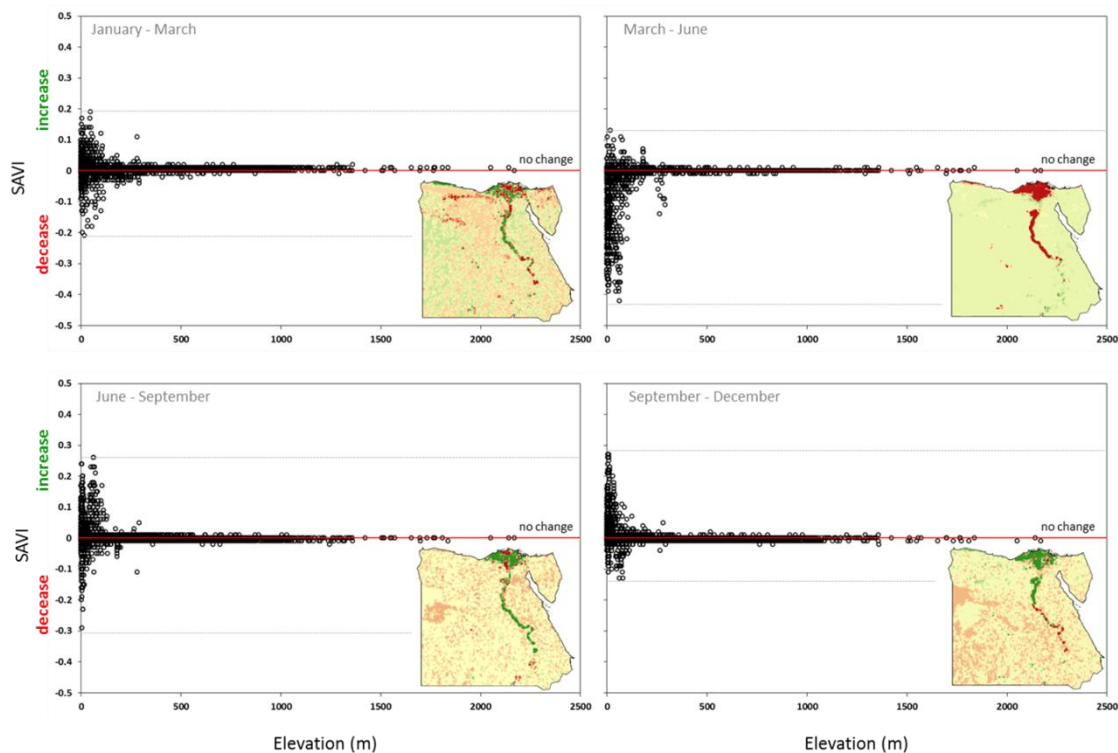


Figure 3.6 Multi-temporal changes of the vegetation cover (SAVI) along with the elevation (m) over Egypt for the periods (January – March), (March – June), (June – September), and (September – December).

3.4.2 Vegetation covers distribution along with elevation at two significant seasons

Two seasons were chosen to investigate the difference in vegetation intensity and spatial distribution over various elevation ranges over Egypt. March represented seasons of the maximum vegetation cover and September was the lowest recorded month of vegetation. The highest SAVI values were mainly found in elevation of ≤ 100 m, 0.68 and 0.51 in March and September respectively. The concentration of SAVI in a certain elevation limits gave an indication of the suitability of these locations for agriculture and vegetation production, which were the high soil fertility and water availability (FAO 2005). With the increase of elevation up to 2200 m, the intensity of vegetation cover started to decrease with $\text{SAVI} < 0.2$. As shown in Figure 3.7, *i* is the location of moderate elevation about 250 m, which produced vegetation cover with an intensity of approximately 0.25 in March, and < 0.2 in September. These locations were mainly found in oases of the Western Desert and the new reclamation areas of the New Valley governorate.

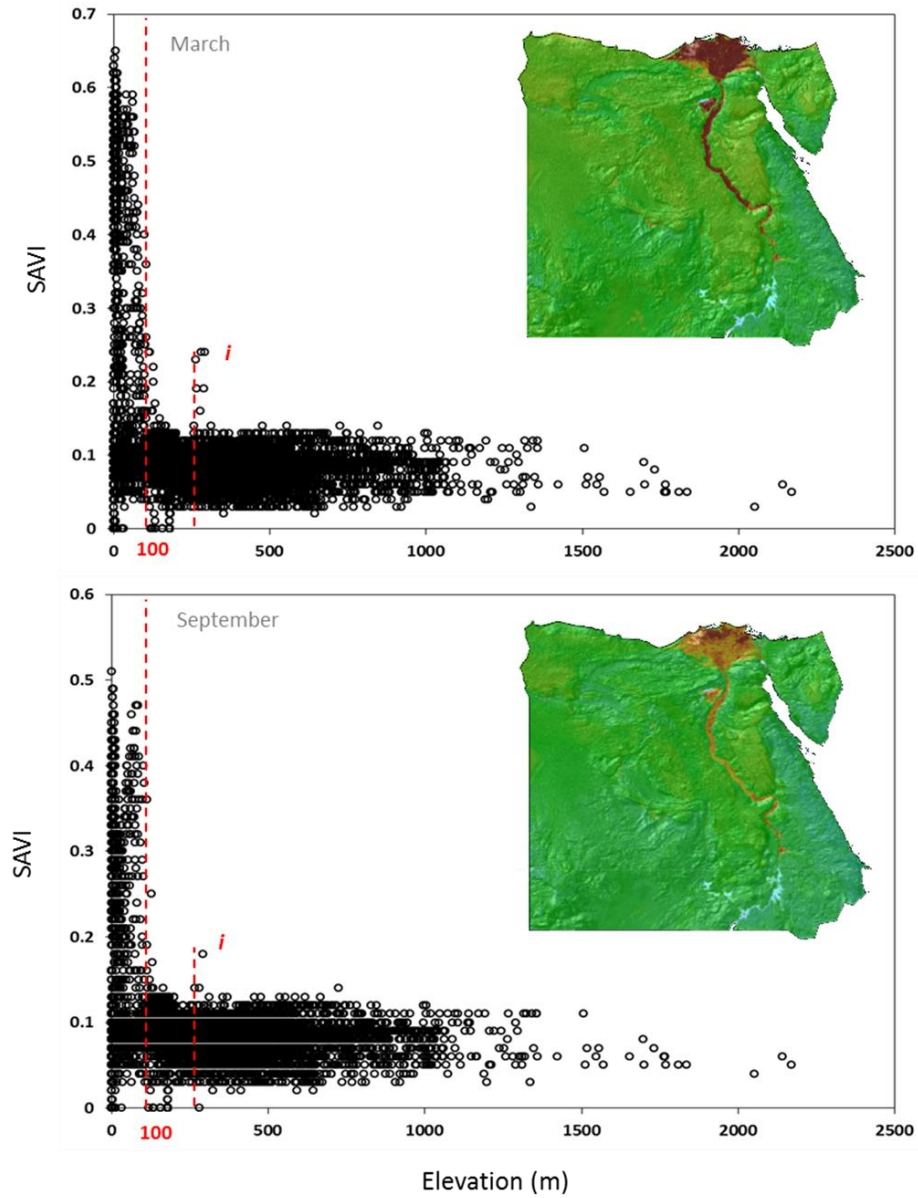


Figure 3.7 The spatial distribution of the vegetation cover (SAVI) along with elevation (m) over Egypt at two significant months, March “maximum” and September “minimum”; the boundary of vegetation intensity at 100 m elevation “dash line”, found over Nile Delta and Valley; *i* is the locations of 250 m, found over the oases of the Western Desert and the new reclamation areas of the New Valley governorate

3.4.3 Spatio-temporal patterns in vegetation cover spatial distribution along with climatic condition (LST and P)

The vegetation cover in Egypt showed a similar pattern of change in period January – March, as a response to the LST increase and P decrease, as shown in Figure 4.8a, b. With the continues LST increase and major P decrease, the vegetation cover shrank more, which indicated that the desertification process started to take place in this particular season March – June, the increase of LST in arid regions usually associated with strong evaporation, which encouraged water logging process that carried the soluble salts up to the soil surface, and cause a permanent land degradation, so called soil salinization (Ci and Yang 2009), the salt accumulation on soil surface affected agricultural production and ecosystems stability (Nawar et al. 2011; Rengasamy 2006). Agricultural activities in Egypt have made some improvement in vegetation cover distribution in period June – September, as a result of positive the human impact (Badreldin and Goossens 2013b; Othman et al. 2012), which has vital potential to decrease desertification in arid regions. With the association of more suitable climatic conditions, such as P with (100-200mm), the vegetation cover found better condition to increase, as shown in period (September – December), see Figure 3.8a,b.

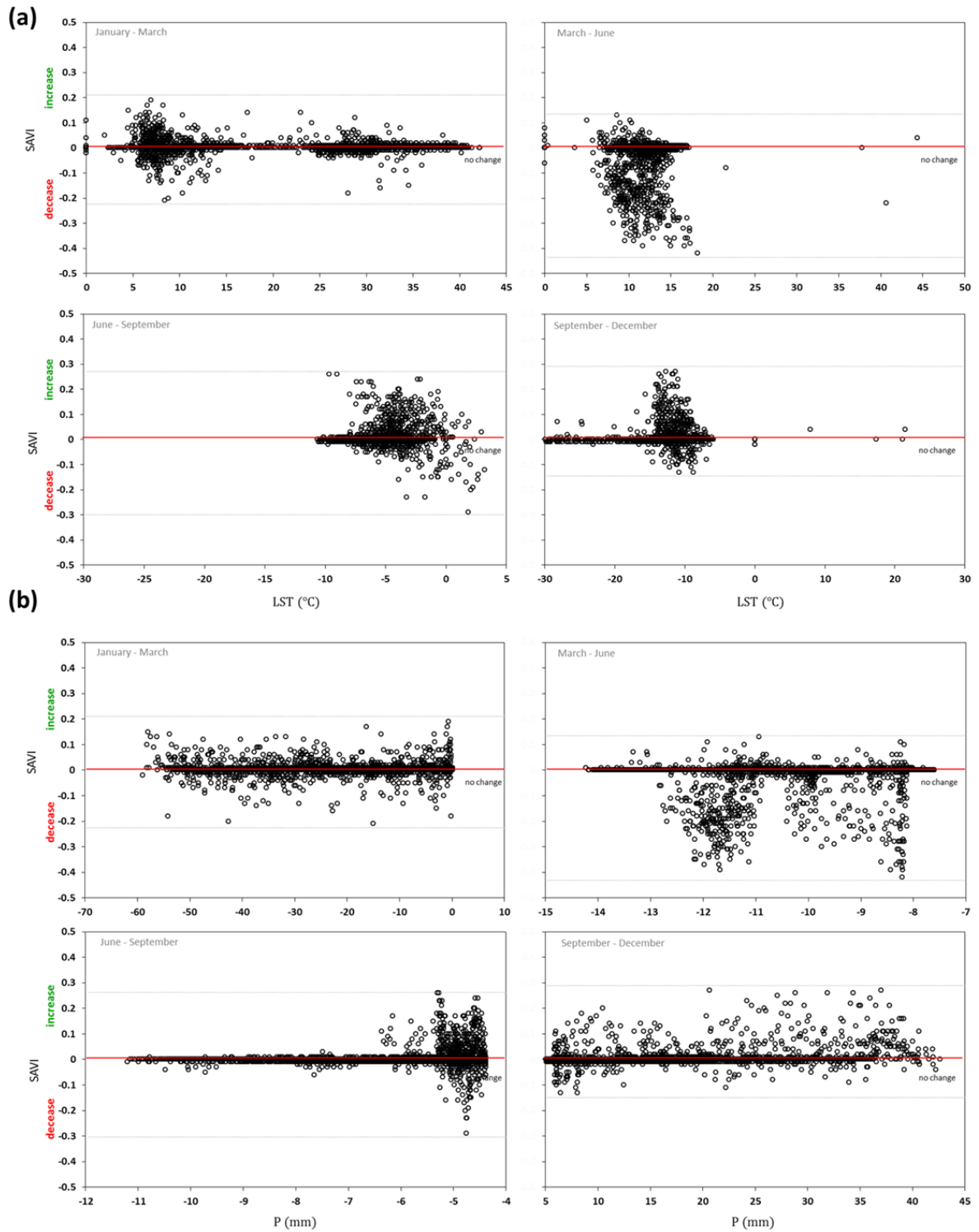


Figure 3.8 Multi-temporal changes of the vegetation cover (SAVI) over Egypt for the periods (January – March), (March – June), (June – September), and (September – December); **a)** the response of SAVI along with LST change; and **b)** the response of SAVI along with P (mm) change over the studied periods.

3.4.4 Trends of the vegetation cover in Egypt (2002-2011)

Table 3.3 shows the trends in the area of vegetation cover with SAVI values above 0.5 in periods 2002-2005, 2005-2008 and 2008-2011 at ≤ 100 and > 100 meters of elevation. The total area lower than 100 meters is 279,150 km² which is occupying about 28% of Egypt. Most of these areas were found in the Nile Delta (22,000 km²), Nile Valley (12,000 km²), North Sinai (30,000 km²) and the northern oases in the northern western part of the Western Desert like Siwa. The vegetation cover with SAVI values below 0.15 were found above 100 meters elevation. Most of these areas were found in the upper of Egypt, the Eastern Desert, the south of Western Desert and south Sinai. The total vegetated area in March for the years 2002, 2005, 2008 and 2011 are 54881.5, 58304.6, 52877.3 and 54280.3 km², respectively and in September for the years 2002, 2005, 2008 and 2011 are 35516.4, 35667.4, 35073.2 and 36346.4 km², respectively.

In the period of 2002-2005 two national mega-projects (Toshka Project and El-Salam Canal) were established for agricultural improvement, and creating new valleys in order to provide more job opportunities and to release the pressure on the Nile delta, where 40% of Egypt's populations are living. The Toshka Project was the Southern Egypt Development project in the Western Desert, the goals of this project were to increase the agricultural lands to 8400 km², establishment of agro-industrial complexes based on the agricultural raw materials available in the area, establishment of new communities expected to attract work force to solve the problem of overpopulation in the Nile Valley and the promotion of touristic activities (Zahran and Willis 2009). El-Salam Canal project was considered as a unique project bringing the Nile water to the deserts of North Sinai. This canal was planned to provide water for cultivating 1500 km² in North Sinai out of the total targeted area of 2480 km² (Othman et al. 2012). These projects produced a rearrangement in the vegetation distribution along the bare lands (desertified areas) in Egypt. The major increase occurred in March, where the climate conditions support the cultivation and natural plants, see Table 3.3. This increase was particularly a clear evident to the advantages of the integration between Biophysical feedbacks and socio-economical activities.

During the period 2005-2008, it became obvious that the former Egyptian government did not work hard to make its costly mega-projects work, while a minor percentage of the cultivated area was held back for smallholders and young graduates (Warner 2012). Several peri-urban regions in remote locations expand with the association to the climate aridity, low vegetation cover. Poor soil quality became more degraded (Salvati and Zitti 2012), which affected negatively the change of the vegetation cover in Egypt, and causes a dramatic decrease, as shown in Table 3.3. Comparing the trend of vegetation cover change and the average population growth rate (+1.82%) in period 2008-2011 was giving clear information about the huge gap in food security. One of the major threats in the most vegetated area (Nile Delta) was the sea level rising which salinized the ground water and

increased the process of the soil salinization and salty-waterlogging. The Egyptian revolution at 25th January, 2011 might slow down the agricultural development as socio-economic impact.

Table 3.3. The vegetation cover changes over Egypt at the periods of (2002-2005, 2005-2008 and 2008-2011)

	Vegetation cover (km²)	2002-2005	2005-2008	2008-2011
Maximum	March \leq 100 m	1126.86	258.21	-142.06
	March > 100 m	2296.34	-5685.60	1545.07
Total vegetation cover in March (km ²)		3423.20	-5427.39	1403.01
Minimum	September \leq 100 m	212.73	-486.88	893.97
	September > 100 m	-61.69	-107.39	379.27
Total vegetation cover in September (km ²)		151.04	-594.27	1273.24

3.4.5 Bi-stable system for assessing desertification dynamics

The bi-stable system was capable to provide meaningful information in order to assess the evolution of land degradation and desertification in arid regions. Analyzing the impacts of the environmental factors (LST, P and elevation) on SAVI distribution at three sites (Kom Ombo, El-Oweinat and Nile Delta), which were chosen to monitor the desertification development in Egypt. These sites were representing unique patterns of vegetation cover distribution under different environmental variables, as shown in Table 3.4


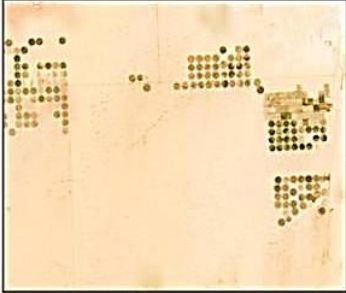

The ecosystem in Egypt was characterized by spatial and temporal variations in rainfall, temperature and land morphology. The desertification dynamics in Egypt was a result of long-term historical processes from the interaction between socio-economic, political and environmental factors (FAO 2005)

The vegetation distribution pattern over time in Kom Ombo was followed by land degradation development, which was a result of low level of precision farming (Figure 3.9a). The usage of the limited available land resources regardless to the sustainability caused more damage to soil. The erratic precipitation was responsible for the erratic changes in the spatio-temporal distribution of the vegetation cover in Kom Omboin, which has the strongest positive relationship with the vegetation cover ($r^2 = 0.83$, $P < 0.01$), as shown in Figure 3.10. Zahran and Willis (2009) reported that the differences in rainfall were seen in the growth of ephemerals and the appearance of seedlings of perennials in the wet season which may or may not continue to grow, depending on the volume of water resources.

Shark El-Oweinat was the site where the agriculture sustainability depends on the precision farming system of using groundwater for irrigation and cultivating plant species, these species were tolerant to dry and hyperarid environments (Governorate 2011). In the period of 2008-2011 vegetation cover increased dramatically in both seasons (March and September) with the presence of desertification such as wind erosion and drought (Figure 3.9b). The vegetation cover respond positively with the increase of elevation ($r^2 = 0.63$, $P < 0.01$). The lower the elevation the more chances to be buried by sand saltation as a result of the wind erosion effects, see Figure 3.10.

The loss of vegetation cover in the Nile Delta was increased as a result of desertification over periods 2002-2005 and 2005-2008, as shown in Figure 3.9c, and this became dominant in the period of 2008-2011 especially in September. As shown in Figure 3.10, the vegetation in the Nile Delta showed a significant negative relationship response to the LST ($r^2 = 0.67$, $P < 0.01$) as a result of water logging and soil salinization feedbacks, which were the major degradation effects in the Nile Delta (Frihy and El-Sayed 2012; Mohamed et al. 2012), the salt accumulation decreasing the agricultural and ecosystem productivity, and thus leaves the soil in a more permanently degraded status (Rengasamy 2006).

Table 3.4. Short description of the three chosen case studies in Egypt.

Kom Ombo	Shark El-Oweinat	Nile Delta
		
24°28'36.60"N 32°56'37.88"E	22°34'58.05"N 28°29'35.29"E	30°51'49.28"N 31°00'57.70"E
Ephemeral and perennial vegetation communities. Cultivation is depending on Nile river water, natural plants depending on rainfall. The area is made up of an eastern basement complex section and a western Nubian sandstone section (Zahran & Willis, 2009).	Newly reclaimed for cultivating crops and fruits. The ground water is the only source of irrigation and can be used for 100 year. The major soil texture type is sandy to sandy loam. (Governorate, 2011)	Agricultural region with main cultivation activities, vegetables, fruits and crops production. Nile river is the source of water supply and fresh water irrigation. It comprises about 63% of Egypt's fertile land (FAO, 2005).

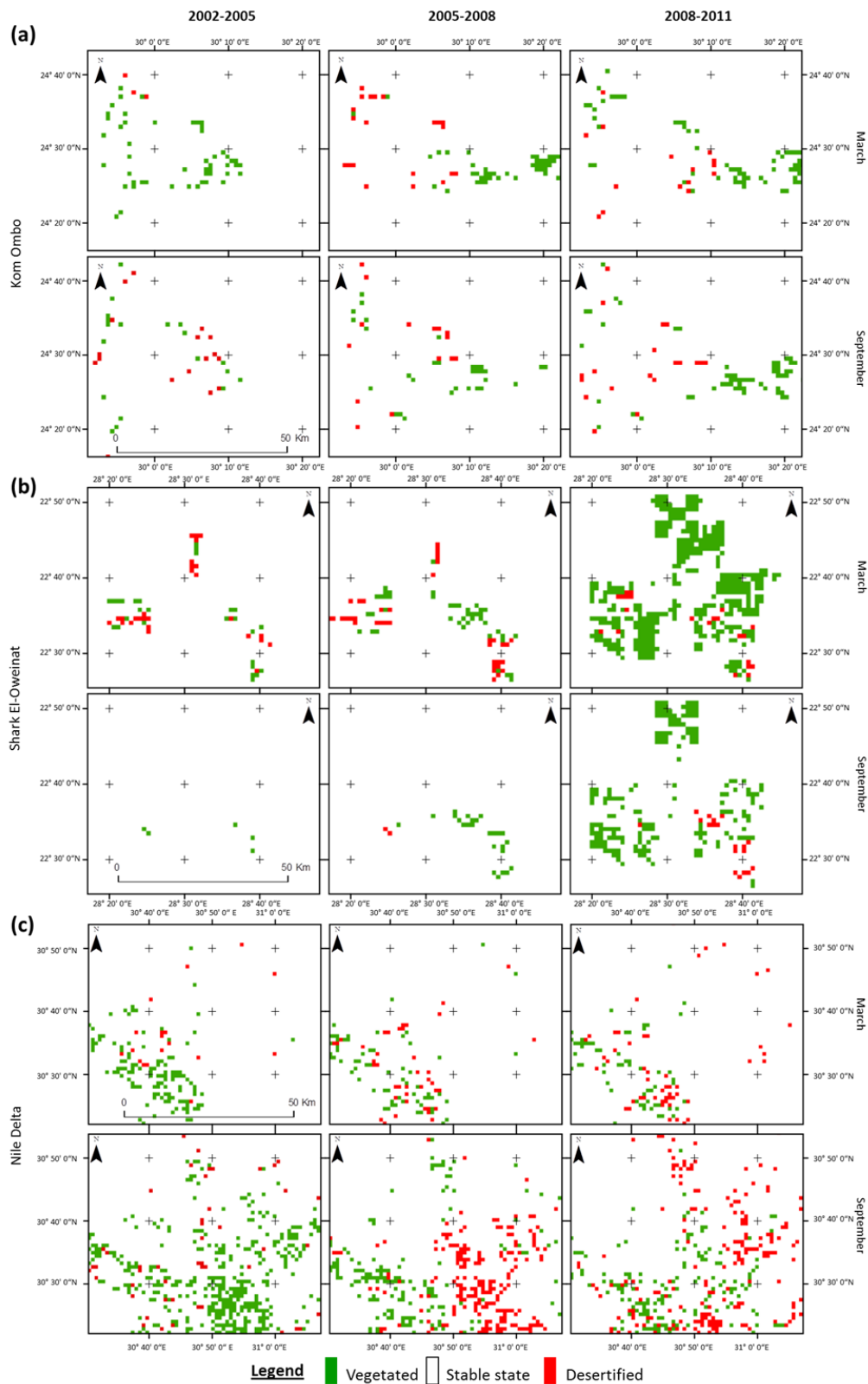


Figure 3.9. Desertification development over the periods (2002-2005, 2005-2008 and 2008-2011) at three case studies **a)** Kom Ombo, $24^{\circ}28'36.60''\text{N}$, $32^{\circ}56'37.88''\text{E}$; **b)** Shark El-Oweinat, $22^{\circ}34'58.05''\text{N}$, $28^{\circ}29'35.29''\text{E}$ and **c)** Nile Delta, $30^{\circ}51'49.28''\text{N}$, $31^{\circ}00'57.70''\text{E}$; each case study represent the desertification change at two significant months, March “maximum” and September “minimum”.

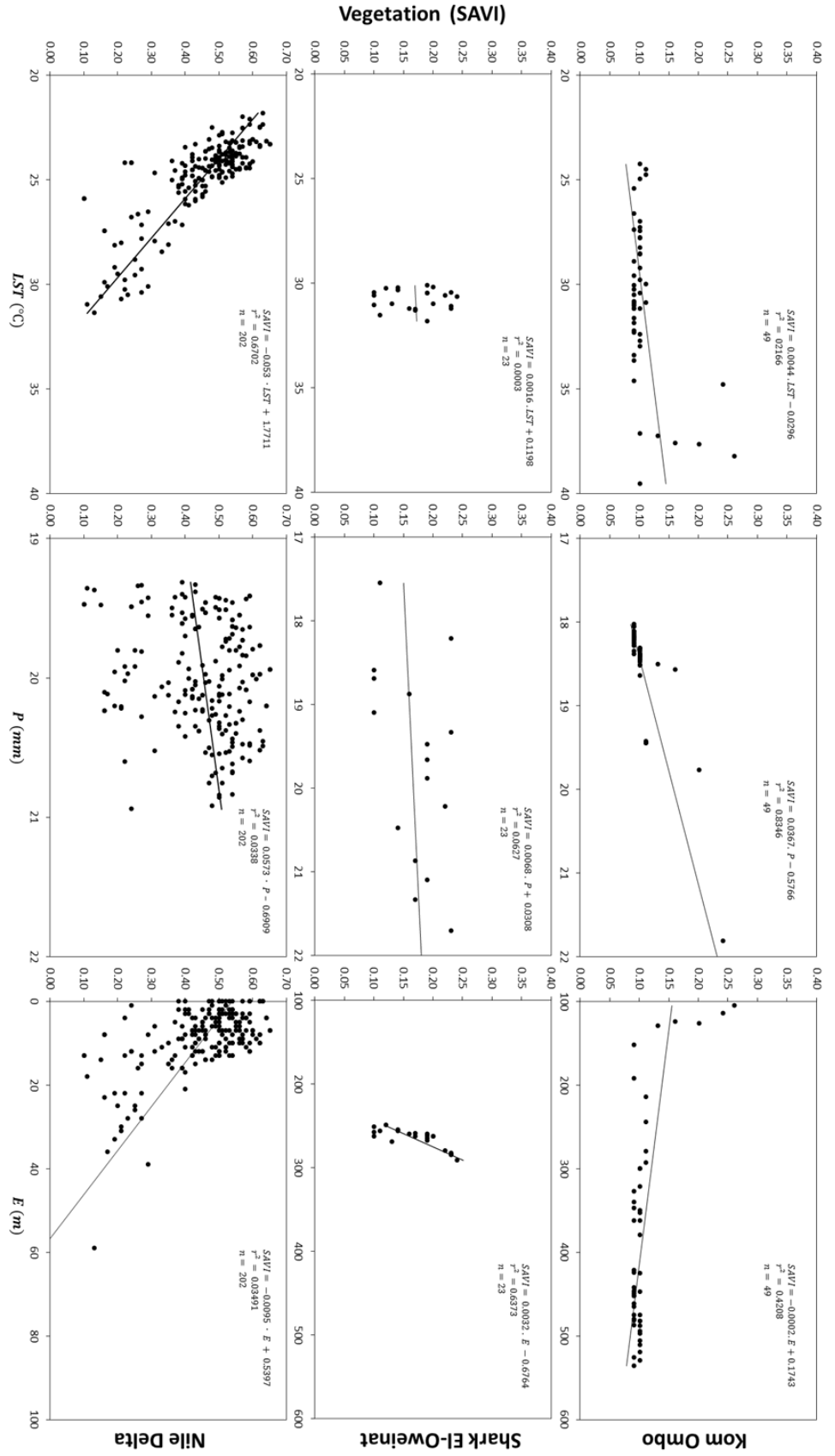


Figure 3.10. The relationship between vegetation cover (SAVI) over (Kom Ombo, Shark El-Oweinat, and Nile Delta) and LST ($^{\circ}\text{C}$), P (mm) and E (m) at $P < 0.01$

3.5 Conclusions and perspectives

MODIS satellite data provide researchers with a straightforward way to assess the degree of desertification through monitoring the vegetation cover distribution in arid regions like Egypt. The resilience of the bi-stable ecosystem dynamics depends on the disturbance strength like land degradation or remediation in order to reach the stable state of the system like desertified or vegetated. Seasonal changes in SAVI allow us to demonstrate the extent of vegetation cover in Egypt. We observed a balanceable change between (January – March) in the Nile Valley and Delta, unlike the period of (March – June) which was the harvesting season in most of the agricultural locations. The increase started again in (June – September) which was the annual period of cultivating the summer crops. The vegetation intensity and distribution varied along with the elevation, the highly SAVI are found in elevation ≤ 100 meter (0.68 and 0.51) in March and September, respectively. Above 100 meters the vegetation cover decreased to < 0.15 SAVI. Socio-economic impact was responsible for the increase vegetation cover of Egypt (+0.18%) in period (2002-2005) and directly after initiating two national mega-projects (Toshka Project and El-Salam Canal). Irreversible pattern of desertification was monitored in Kom Ombo where the vegetated areas turned to be desertified. Combating desertification development in Shark El-Oweinat was a complex combination of agriculture sustainability treatments, which appeared in maintaining and increasing the vegetated areas. The vegetation cover in the Nile Delta decreased dramatically and the desertified areas increased more in September.

Selecting the most significant variables as an indicator was an efficient way to monitor the desertification at different sites in Egypt, but it may be advisable to integrate more environmental and socio-economic drivers for better understanding desertification development. Vogt et al. (2011) Suggested that the long-term and continuous monitoring investigation will help to yield a systematic and meaningful assessment of desertification and land degradation at local to regional scales. Prioritizing sites that have risk of degradation was an important and continuing challenge for those charged with anti-desertification intervention (Amiraslani and Dragovich 2011; Salinas and Mendieta 2012). The challenges that faces Egypt now are, how to compact the land degradation?, how to mitigate and control the desertification?.

3.6 References

- A.Bard K, Shubert SB (1999) Encyclopedia of the Archaeology of Ancient Egypt. Routledge, New York, p 1280.
- Abd El-Kawy OR, Rød JK, Ismail H a., Suliman a. S (2011) Land use and land cover change detection in the western Nile delta of Egypt using remote sensing data. *Applied Geography* 31:483–494.
- Aboelghar M, Ali A-R, Arafat S (2012) Spectral wheat yield prediction modeling using SPOT satellite imagery and leaf area index. *Arabian Journal of Geosciences*. doi: 10.1007/s12517-012-0772-6
- Adamo SB, Crews-Meyer K a. (2006) Aridity and desertification: Exploring environmental hazards in Jáchal, Argentina. *Applied Geography* 26:61–85.
- Amiraslani F, Dragovich D (2011) Combating desertification in Iran over the last 50 years: an overview of changing approaches. *Journal of environmental management* 92:1–13.
- Armah F a., Odoi JO, Yengoh GT, et al. (2010) Food security and climate change in drought-sensitive savanna zones of Ghana. *Mitigation and Adaptation Strategies for Global Change* 16:291–306.
- Badreldin N, Goossens R (2013a) Monitoring land use/land cover change using multi-temporal Landsat satellite images in an arid environment: a case study of El-Arish, Egypt. *Arabian Journal of Geosciences*. doi: 10.1007/s12517-013-0916-3
- Badreldin N, Goossens R (2013b) A satellite-based disturbance index algorithm for monitoring mitigation strategies effects on desertification change in an arid environment. *Mitigation and Adaptation Strategies for Global Change*. doi: 10.1007/s11027-013-9490-y
- Bakr N, Weindorf DC, Bahnassy MH, et al. (2010) Monitoring land cover changes in a newly reclaimed area of Egypt using multi-temporal Landsat data. *Applied Geography* 30:592–605.
- Bannari A, Morin D, Bonn F, Huete AR (1995) A review of vegetation indices. *Remote Sensing Reviews* 13:95–120.
- Ci L, Yang X (2009) Desertification and Its Control in China. Higher Education Press and Springer, Beijing and Dordrecht, p 533.
- CIA (2013) The world factbook. Washington, DC: Central Intelligence Agency.URL. <https://www.cia.gov/library/publications/the-world-factbook/geos/eg.html>.
- D’Odorico P, Bhattachan A, Davis KF, et al. (2013) Global desertification: Drivers and feedbacks. *Advances in Water Resources* 51:326–344.
- Dawelbait M, Morari F (2012) Monitoring desertification in a Savannah region in Sudan using Landsat images and spectral mixture analysis. *Journal of Arid Environments* 80:45–55.
- Diouf a., Lambin EF (2001) Monitoring land-cover changes in semi-arid regions: remote sensing data and field observations in the Ferlo, Senegal. *Journal of Arid Environments* 48:129–148.
- Dousset B, Gourmelon F (2003) Satellite multi-sensor data analysis of urban surface temperatures and landcover. *ISPRS Journal of Photogrammetry and Remote Sensing* 58:43–54.
- Dregne HE (1977) Desertification of arid lands. *Economic Geography* 53:322–331.
- Dregne HE, Chou N-T (1992) Global desertification dimensions and costs. 249–282.
- Du P, Li X, Cao W, et al. (2010) Monitoring urban land cover and vegetation change by multi-temporal remote sensing information. *Mining Science and Technology (China)* 20:922–932.
- El-Nahrawy MA (2011) Country pasture / forage resource profiles: Egypt, FAO, Rome, p 44.
- Epiphany JCN, Huete AR (1992) Dependence of NDVI and SAVI on Sun / Sensor Geometry and Its Effect on fAPAR Relationships in Alfalfa. *Remote Sensing of Environment* 51:351–360.
- FAO (2005) Fertilizer use by crop in Egypt, Land and Plant Nutrition Management Service Land and Water Development Division, Rome, p 62.
- Feizizadeh B, Blaschke T (2013) Examining Urban Heat Island Relations to Land Use and Air Pollution: Multiple Endmember Spectral Mixture Analysis for Thermal Remote Sensing. *IEEE Journal of Selected Topics in Applied Earth Observations and Remote Sensing* 6:1749–1756.
- Feizizadeh B, Blaschke T (2012) Thermal remote sensing for examining the relationship between urban Land surface Temperature and land use/cover in Tabriz city, Iran. *Geoscience and Remote Sensing Symposium (IGARSS), 2012 IEEE International. Ieee, Munich*, pp 2229–2232
- Feizizadeh B, Blaschke T, Nazmfar H, et al. (2012) Monitoring land surface temperature relationship to land use/land cover from satellite imagery in Maragheh County, Iran. *Journal of Environmental Planning and Management* 1–26. doi: 10.1080/09640568.2012.717888
- Frihy OE, El-Sayed MK (2012) Vulnerability risk assessment and adaptation to climate change induced sea level rise along the Mediterranean coast of Egypt. *Mitigation and Adaptation Strategies for Global Change*. doi: 10.1007/s11027-012-9418-y

- G.Kepner W, Rubio JL, Mouat DA, Pedrazzini F (2006) Desertification in the Mediterranean Region. A Security Issue. Proceedings of the NATO Mediterranean Dialogue Workshop on Desertification in the Mediterranean Region. A Security Issue. Springer, Dordrecht, NL, p 606
- Geist HJ, Lambin EF (2004) Dynamic Causal Patterns of Desertification. *BioScience* 54:817–829.
- Gilbert M.A., J. G-P, F.J. G-H, J. M (2002) A generalized soil-adjusted vegetation index. *Remote Sensing of Environment* 82:8.
- Governorate NV (2011) Shark El-Oweinat (arabic). Agriculture in the New Valley p 5.
- Grainger A, Smith MS, Squires VR, Glenn EP (2000) Desertification and climate change: the case for greater convergence. *Mitigation and Adaptation Strategies for Global Change* 5:361–377.
- Gunderson LH (2000) Ecological resilience - in theory and application. *Annual Review of Ecology and Systematics* 31:425–439.
- Hall FG, Townshend JR, Engman ET (1995) Status of remote sensing algorithms for estimation of land surface state parameters. *Remote Sensing of Environment* 51:138–156.
- Hashimoto H, Dungan J, White M, et al. (2008) Satellite-based estimation of surface vapor pressure deficits using MODIS land surface temperature data. *Remote Sensing of Environment* 112:142–155.
- Herrmann SM, Anyamba A, Tucker CJ (2005) Recent trends in vegetation dynamics in the African Sahel and their relationship to climate. *Global Environmental Change* 15:394–404.
- Huang S, Siegert F (2006) Land cover classification optimized to detect areas at risk of desertification in North China based on SPOT VEGETATION imagery. *Journal of Arid Environments* 67:308–327.
- Huete A. (1988) A soil-adjusted vegetation index (SAVI). *Remote Sensing of Environment* 25:295–309.
- Huete AR, G. Hua JQ, Leeuwen AC, Van WJD (1992) Normalization of Multidirectional Red and NIR Reflectances with the SAVI. *Remote Sensing of Environment* 41:143–154.
- Kassas M (1977) Arid and semi-arid lands: problems and prospects. *Agro-Ecosystems* 3:185–204.
- Kelarestaghi A, Jafarian Jeloudar Z (2009) Land use/cover change and driving force analyses in parts of northern Iran using RS and GIS techniques. *Arabian Journal of Geosciences* 4:401–411.
- Kottek M, Grieser J, Beck C, et al. (2006) World Map of the Köppen-Geiger climate classification updated. *Meteorologische Zeitschrift* 15:259–263.
- Mildrexler DJ, Zhao M, Heinsch FA, Running SW (2007) A new satellite-based methodology for continental-scale disturbance detection. *Ecological applications*: a publication of the Ecological Society of America 17:235–50.
- Mohamed ES, Belal A, Saleh A (2012) Assessment of land degradation east of the Nile Delta, Egypt using remote sensing and GIS techniques. *Arabian Journal of Geosciences*. doi: 10.1007/s12517-012-0553-2
- Nawar S, Reda M, Farag F, El-nahry A (2011) Mapping Soil Salinity in El-Tina Plain in Egypt Using Geostatistical Approach. *Geoinformatics Forum*. Salzburg, Austria, pp 81–90
- Othman A a., Rabeh S a., Fayez M, et al. (2012) El-Salam canal is a potential project reusing the Nile Delta drainage water for Sinai desert agriculture: Microbial and chemical water quality. *Journal of Advanced Research* 3:99–108.
- Peel MC, Finlayson BL, McMahon TA (2007) Updated world map of the Köppen-Geiger climate classification. *Hydrology and Earth System Sciences* 11:1633–1644. doi: 10.5194/hess-11-1633-2007, 2007
- Qi J, Chehbouni A, Huete AR, et al. (1994) A Modified Soil Adjusted Vegetation Index. *Remote Sensing of Environment* 48:119–126.
- Rengasamy P (2006) World salinization with emphasis on Australia. *Journal of experimental botany* 57:1017–23.
- Reynolds JF, Stafford-smith DM, Lambin E (2003) Do humans cause deserts? An old problem through the lens of a new framework: the Dahlem desertification paradigm. In: Allsopp N, Palmer AR, Milton SJ, et al. (eds) the VIIth International Rangelands Congress. Durban, South Africa, pp 2042–2048
- Richards JA (2013) *Remote Sensing Digital Image Analysis: An Introduction*, 5th edn. Springer, Heidelberg, pp 494.
- Rondeaux G, Steven M, Baret F (1996) Optimization of Soil-Adjusted Vegetation Indices. *Remote Sensing of Environment* 55:95–107.
- Salinas CX, Mendieta J (2012) Mitigation and adaptation investments for desertification and climate change: an assessment of the socioeconomic return. *Mitigation and Adaptation Strategies for Global Change*. doi: 10.1007/s11027-012-9380-8
- Salvati L, Zitti M (2012) Monitoring vegetation and land use quality along the rural–urban gradient in a Mediterranean region. *Applied Geography* 32:896–903.
- Schnur MT, Xie H, Wang X (2010) Estimating root zone soil moisture at distant sites using MODIS NDVI and EVI in a semi-arid region of southwestern USA. *Ecological Informatics* 5:400–409.
- Schowengerdt RA (2007) *Remote sensing: models and methods for image processing*, 3rd edn. Elsevier, Amsterdam, p 558.

- Son NT, Chen CF, Chen CR, et al. (2012) Monitoring agricultural drought in the Lower Mekong Basin using MODIS NDVI and land surface temperature data. *International Journal of Applied Earth Observation and Geoinformation* 18:417–427.
- U.S. Geological Survey (2011a) Vegetation Indices Monthly L3 Global 1km. URL. https://lpdaac.usgs.gov/products/modis_products_table/mod13a3.
- U.S. Geological Survey (2011b) Surface Reflectance 8-Day L3 Global 250m. URL. https://lpdaac.usgs.gov/products/modis_products_table/mod09Q1.
- U.S. Geological Survey (2011c) Global Multi-resolution Terrain Elevation Data 2010 (GMTED2010). URL. http://eros.usgs.gov/#/Find_Data/Products_and_Data_Available/GMTED2010.
- Vermote EF, Kotchenova SY, Ray JP (2011) MODIS Surface Reflectance User 's Guide. 1–40.
- Verón SR, Paruelo JM, Oesterheld M (2006) Assessing desertification. *Journal of Arid Environments* 66:751–763.
- Vogt J V., Safriel U, Von Maltitz G, et al. (2011) Monitoring and assessment of land degradation and desertification: Towards new conceptual and integrated approaches. *Land Degradation & Development* 22:150–165.
- Wan Z, Dozier J, Member A (1996) A Generalized Split- Window Algorithm for Retrieving Land-Surface Temperature from Space. *IEEE Transactions on Geoscience and Remote Sensing* 34:892–905.
- Wan Z, Zhang Y, Zhang Q, Li Z (2002) Validation of the land-surface temperature products retrieved from Terra Moderate Resolution Imaging Spectroradiometer data. *Remote Sensing of Environment* 83:163–180.
- Wang XD, Zhong XH, Liu SZ, et al. (2008) Regional assessment of environmental vulnerability in the Tibetan Plateau: Development and application of a new method. *Journal of Arid Environments* 72:1929–1939.
- Warner J (2012) The Toshka mirage in the Egyptian desert – River diversion as political diversion. *Environmental Science & Policy* 1–11.
- Weng Q (2002) Land use change analysis in the Zhujiang Delta of China using satellite remote sensing, GIS and stochastic modelling. *Journal of Environmental Management* 64:273–284.
- World Bank (2013) Climate baseline. Egypt dashboard. URL. http://sdwebx.worldbank.org/climateportal/index.cfm?page=country_historical_climate&ThisRegion=Africa&ThisCCode=EGY.
- World Bank (2012) Agricultural areas statistics. Egypt, Arab Rep Data. URL. http://data.worldbank.org/country/egypt-arab-republic#cp_cc.
- Yang J, Weisberg PJ, Bristow N a. (2012) Landsat remote sensing approaches for monitoring long-term tree cover dynamics in semi-arid woodlands: Comparison of vegetation indices and spectral mixture analysis. *Remote Sensing of Environment* 119:62–71.
- Yeganeh H, Khajedein S jamale, Amiri F, Shariff ARBM (2012) Monitoring rangeland ground cover vegetation using multitemporal MODIS data. *Arabian Journal of Geosciences*. doi: 10.1007/s12517-012-0733-0
- Zahrán MA, Willis AJ (2009) *The Vegetation of Egypt*, 2nd edn. Springer, Heidelberg, p 451.
- Zhang X, Friedl M a., Schaaf CB, et al. (2003) Monitoring vegetation phenology using MODIS. *Remote Sensing of Environment* 84:471–475.

Chapter 4

A satellite-based disturbance index algorithm for monitoring mitigation strategies effects on desertification change in an arid environment

This chapter is modified from:

Nasem Badreldin and Rudi Goossens (2013) A satellite-based disturbance index algorithm for monitoring mitigation strategies effects on desertification change in an arid environment. *Mitigation and Adaptation Strategies for Global Change*. DOI: 10.1007/s11027-013-9490-y.

4.1 Introduction

Deserts around the world share common characteristics in terms of their edaphic environments, climate, geomorphology, hydrology, and soils (Laity 2008). The wild life adapted their morphology formation and metabolism to conserve moisture and avoid effects of aridity (Harris 2003). Deserts have become the new home and hope for agriculture and business for 900 million people (Thomas 2011), resulting in a need for smart and innovative desert management solutions. Such solutions will require the monitoring of hazards and natural resources.

Desertification is one the hazard that face arid environments, which is the process whereby the productivity of land was reduced, this land deterioration involves changes in vegetation cover by reduction, replacement, and destruction (Kassas 1977). Desertification plays a vital role in land cover distribution in arid regions. While incidents of drought prevail in all climate zones of the world, the impacts of drought are deeply felt in drier lands (Diouf and Lambin 2001; Grainger et al. 2000; Kassas 1995; Stiles 1984), Desertification directly affects about one-fifth of the world population in over 110 usually developing countries (Adamo and Crews-Meyer 2006; Armah et al. 2010; G.Kepner et al. 2006). Regarding to the fuzzy interpretation of the United Nations Convention to Combat Desertification (UNCCD) definition of desertification, estimating environmental disturbance can be used as an indicator to determine desertification change (Dawelbait and Morari 2012; Salinas and Mendieta 2012b). Disturbance has been defined as any factor that brings significant changes to the ecosystem over more than one year, and that occurs over large spatial scales (Pickett and White 1987; Tilman 1985).

Climate change increases the desertification threat (Salinas and Mendieta 2012c). Agricultural activity is highly related to the interaction between the socioeconomic and environmental situations. The efficient use of natural resources in arid environment is a vital strategy to combat the climate change and desertification effects (Misra 2013; Salinas and Mendieta 2012a). Monitoring disturbances in arid eco-systems is essential, especially in agro-ecosystems affected by desertification, in order to manage food security by improving agriculture and promoting sustainable mitigation strategies as anti-desertification act (Armah et al. 2010).

Remotely sensed data provide multi-temporal information that reflects environmental changes in the earth's surface (Bannari et al., 1995; Hall et al., 1995; Herrmann et al., 2005; Richards, 2013; Wang et al., 2008). Integration with geographic information systems (GIS) offers a wide range of facilities for better data analysis and interpretation (Weng 2002).

In this investigation, we will propose a new satellite-based disturbance index algorithm for monitoring agro-ecosystem changes in arid environmental conditions in the years 2002, 2005, 2008 and 2011. We will also assess the relationship between the land surface temperature and vegetation cover at different sites in the Sinai Peninsula, thereby providing useful information about biophysical feedback.

4.2 Materials and methods

4.2.1 Study area description and field survey

The total area of the Sinai Peninsula is 61,000 km², and it occupied about 6% of the total area in Egypt as shown in Figure 4.1. The population is almost 500,000, and the majority found in the North of Sinai. WFP (2006) reported that Sinai remain food-insecure and has the highest levels of poverty in Egypt. The main limitation of natural resources in Sinai is water, and there is only marginal capacity for expansion (FAO 2005).

A general overview of Sinai's land use is categorized in five physiographic regions (Dames and Moore 1981). The Mediterranean foreshore is the most inhabited area in the Sinai Peninsula, highly developed in agriculture production, especially El Arish and Raffa, see Table 4.1. The greatest environmental threats in North Sinai are shifting sand dunes and soil salinity; fishing provides a major form of nourishment along the coast and El-Bardawil Lake. The regions of Mobile and Stable platform are sparsely inhabited, agriculture activity is restricted to rain-fed patches in the wadi beds, and urbanization growth is stunted because of the considerable distance from markets and shipping. Suez Rift Province, on the western coastline, is relatively well populated, the growth of agriculture is gradual because of the lack of a reliable source of fresh water, industrial capacity is substantial, based on the potential for extracting mineral and petroleum resources; it also has a strong potential for development of tourism. Southern Mountains Province is extremely sparsely inhabited, agriculture is always near oases, and there is poor grazing. The future land use in the Southern Mountains Province will almost entirely be limited to tourism.

Based on the classification system (soil taxonomy) that was developed by the United States Soil Conservation Services (USSCS), the major soil groups that have been found in Sinai are Entisols and Aridisols (Greenwood 1997). Natural Resources Conservation Service, NRCS (1999) described the soils that are found in the Entisols order as having little or no development of pedogenic horizons, and some of these soils are on a site that is actively eroding or are found in additional deposits (alluvium, in the wadis or aeolian, forming sand dunes). Original soils in this category, which occupy most of

North Sinai, consist mainly of quartz or other minerals that are resistant to the weathering needed to develop diagnostic horizons. The Aridisols order represents the soils that developed in a stable arid environment setting, where water has not been available to mesophytic plants for a long time, this order was found in the middle and south of Sinai, in places such as El-Tih Plateau, where it was classified to the Orthid suborder and soil group of Typic Calciorthids, which contain calcic horizons with accumulation of ≥ 15 % calcium carbonate.

The climate classification of Köppen-Geiger has been updated (Kottek et al. 2006; Peel et al. 2007), and Sinai was classified as (Bwh) arid-desert-hot climate, where the southern part of Sinai is more dry and more arid than the north, the south received less rain in the winter <5 mm a year and air temperature is between 10– 20°C in the winter and 30–40°C in the summer. The north is less dry, rainfall is <200 mm and 5–20°C in winter and air temperature 20–35°C (World Bank 2013).

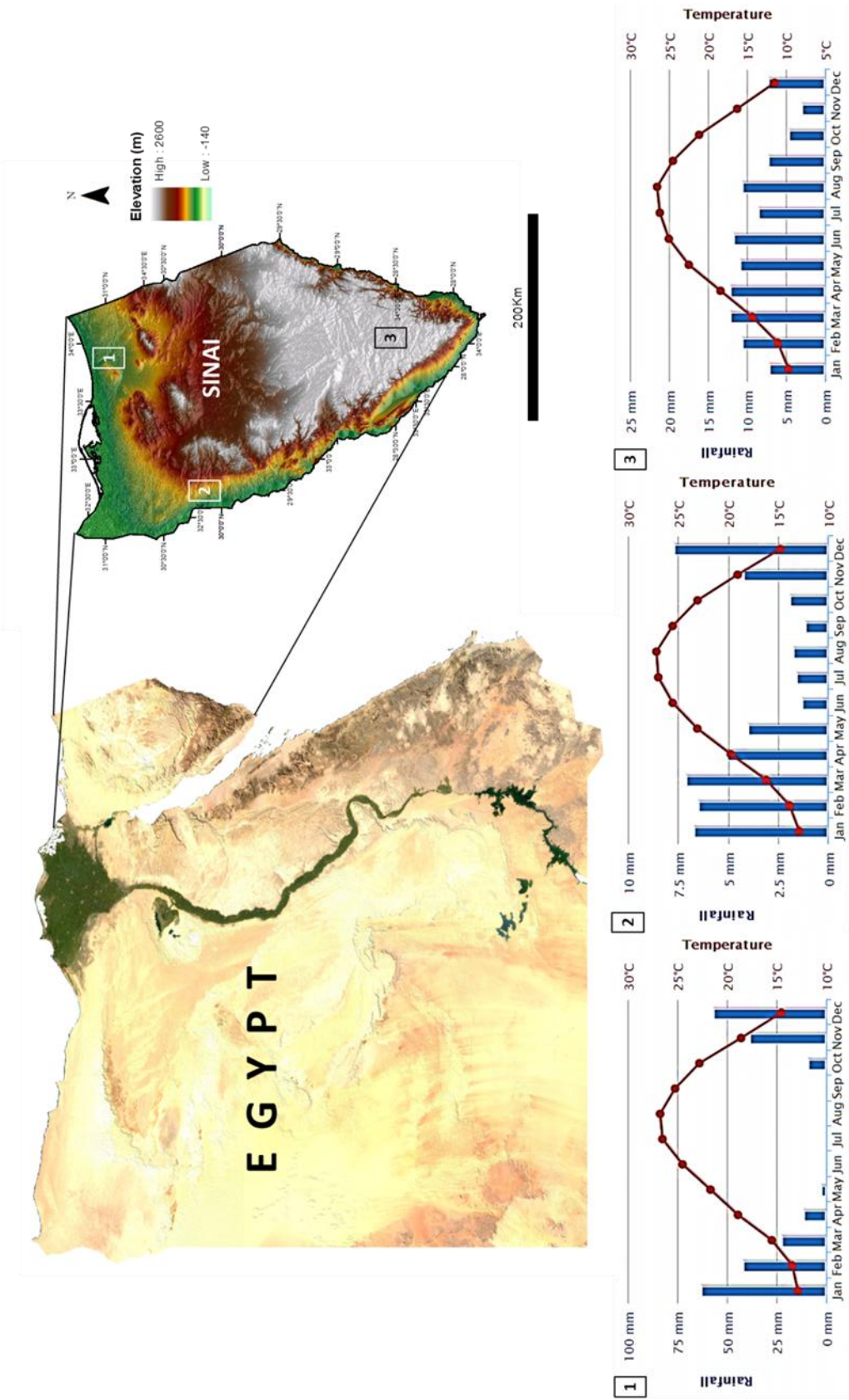


Figure 4.1. The geographical location and geomorphology of Sinai Peninsula. Climatic information (lower section), presenting the mean rainfall and air temperature of period (1980: 2012) for different locations over the case study, rainfall (blue columns) and air temperature (red lines).

Table 4.1. The most common vegetation types (crops and flora) in Sinai Peninsula, based on field survey and statistical data of (North Sinai Governorate, 2011).

Vegetation category	Types
Irrigated crops	Olives (<i>Olea europaea</i>), Pomegranates (<i>Punica granatum</i>), Almonds (<i>Prunus amygdalus</i>), Oranges (<i>Citrus sinensis</i>), Lemons (<i>Citrus limon</i>), and Figs (<i>Ficus carica</i>) Tomatoes (<i>Solanum lycopersicum</i>), Cucumbers (<i>Cucumis sativus</i>), Bell pepper (<i>Capsicum annuum</i>), Eggplant (<i>Solanum melongena</i>), Watermelon (<i>Citrullus lanatus</i>), and Okra (<i>Abelmoschus esculentus</i>)
Non-irrigated crops	Barley (<i>Hordeum vulgare</i>), wheat (<i>Triticum aestivum</i>) and Date Palm (<i>Phoenix dactylifera</i>)
Natural plants	Glaucous Glasswort (<i>Arthrocnemum glaucum</i>), Somerset Rush (<i>Juncus subulatus</i>), White Bean-Caper (<i>Zygophyllum album</i>), and Athel tree (<i>Tamarix aphylla</i>)

Six study sites were chosen to represent the variety of the land cover of the Sinai Peninsula; a field survey was conducted to observe land cover types in different arid environmental conditions. Also, anthropological activities were different in terms of agricultural management and urbanization growth, which were influencing the agro-ecosystem distribution. Ten soil samples were collected based on a random sampling design (unbiasedness) and representativeness for each study site in order to analyze physical soil properties along with the field observations as shown in Table 4.2.

Table 4.2. Description of soil properties and filed survey observations for six chosen study sites in Sinai Peninsula.

Location	Latitude	Longitude	Description
El-Tina Plain,	31° 00' 00.09"	32° 26' 11.25"	Soil contains fine particles size, elevation < 50 m, waterlogging and salinization is the major land degradation. Cultivation is the main agricultural activity, plant cultivars are mostly salt tolerant.
Arish&Rafaa	31° 09' 35.72"	34° 02' 11.83"	Soil contains coarse to moderate particle sizes, elevation < 150 m, wind erosion in the major land degradation, cultivation and natural plant are the major characteristic of vegetation cover.
Qantara Shark	30° 26' 31.58"	32° 24' 23.19"	Soil contains coarse particle sizes, elevation < 100 m, wind erosion and sandstorms are the major land degradation, intensive agricultural production and various plant cultivars.
Zaraniq	31° 06' 07.77"	33° 28' 57.82"	Soil contains coarse particle sizes, elevation < 50m, wind erosion and salinization are the major land degradation, natural halophyte plant species.
South-Sinai	28° 27' 38.70"	34° 04' 15.03"	Soil contains coarse particle sizes, elevation > 2000 m, water erosion is the major land degradation, drought tolerant natural plants species.
El-Wasat	29° 52' 08.36"	33° 47' 21.85"	Soil contains moderate to fine particle sizes, elevation < 1500 m, water erosion is the major land degradation, drought tolerant natural plants species and rare cultivation activity.

4.2.2 Statistical analysis

The spatial pixel-based scale of the data was considered in the analysis; the polygons correspond to the territorial disparities in the vegetation cover along the land surface temperature. The relationship between maximum land surface temperature (LST) and maximum soil-adjusted vegetation index (SAVI) across different sites in the study area was estimated using land cover types that were explored during field work in 2011. The mean-maximum LST and SAVI were calculated as the sum of the highest values at each location for the studied periods within the observed land cover types. To assess the significance of the relationship between SAVI and LST on the regional

scale, Pearson's correlation analysis (r) was used, and the confidence limits surrounding r were calculated (Zahran and Willis 2009; Zar 2010).

4.2.3 Remote sensing data

This study was based on MODerate resolution Imaging Spectroradiometer (MODIS) satellite images, which were obtained from the Earth Resources Observation and Science (EROS) Center. Monthly data in the years 2002, 2005, 2008 and 2011 in clear atmospheric conditions were acquired for this study. MODIS Re-projection Tool (MRT) software version 4.1 was used to reproject MODIS images into a known map projection system and extension. The MOD13A3 satellite is the MODIS Terra, vegetation indices (VI) were provided monthly at 1 kilometer spatial resolution and used for estimating SAVI, VI were computed from atmospherically corrected bi-directional surface reflectance's that were masked for water, clouds, heavy aerosols, and cloud shadows (U.S. Geological Survey 2011a). The MOD09Q1 satellite is the MODIS Terra, LST was provided every eight days of data at 250 meters spatial resolution, the data were validated via a widely distributed dataset of locations and time periods via several ground-truths and were ready for use in scientific publications (U.S. Geological Survey 2011b). Global Multi-resolution Terrain Elevation Data 2010 (GMTED2010) provided a new level of detail in global topographic data, the accuracy was measured by a global set of control points, root mean square error (RMSE) of the products that were used for this study was between 26–30 meters at 7.5 arc-seconds (U.S. Geological Survey 2011c).

4.2.4 MBDI improvement for monitoring desertification change

The MODIS-based disturbance index (MBDI) is the ratio of annual maximum composite LST and SAVI. Based on a multi-temporal datasets, it is designed to capture long-term variations on a pixel-by-pixel basis, and to detect significant inter-annual changes in surface energy, which is responsible for the natural variability of instantaneous and non-instantaneous desertification symptoms (e.g., erosion, overgrazing, climate change and drought) (Mildrexler et al. 2007).

$$MBDI_i = \frac{\frac{LST_{i \max}}{SAVI_{i \max}}}{\sum_{i=1}^{LST_{\max}} \left(\frac{LST_{\max}}{SAVI_{\max}} \right)} \quad (4.1)$$

Where $MBDI_i$ is the MBDI value for year i , $LST_{i \max}$ is the annual maximum eight-day composite LST for year i , $SAVI_{i \max}$ is the annual maximum 16-day SAVI for year i , LST_{\max} is the multiyear LST_{\max} but, not including the analysis year ($i-1$) and $SAVI_{\max}$ is the multiyear mean of $SAVI_{\max}$ but not including the analysis year ($i-1$).

VI values were affected by the reflectance of light in the red and near-infrared spectra, where the vegetative cover was lower than 40%, and the soil surface was exposed, which is a typical environment in arid regions (Yang et al. 2012). In order to correct the influence of the ground brightness when vegetative cover is low, the NDVI was modified through SAVI (Bannari et al. 1995; Huete 1988).

$$SAVI = \left(\frac{\rho_{NIR} - \rho_{RED}}{\rho_{NIR} + \rho_{RED} + L} \right) \times (1 + L) \quad (4.2)$$

Where ρ_{NIR} is the reflectance value of the near infrared band, ρ_{RED} is the reflectance of the red band, and L is the soil brightness correction factor. L=0.5 was successfully minimizing the impact of soil variations in green vegetation compared to NDVI (Aboelghar et al. 2012).

According to Coops et al. (2009) and Mildrexler et al. (2007) the success of this algorithm was dependent on two factors: (1) sufficiently strong and frequent signals to detect disturbance and (2) having signals greater than the natural variability. The disturbance in Sinai occurred as a result of vegetation demise, which will lead to an increase in LST.

The natural variability was defined for each individual pixel that falls within \pm standard deviation for the long-term mean LST/SAVI ratio. Instantaneous disturbance such as water erosion and floods cause an immediate increase in MBDI from the natural variability range, whereas non-instantaneous disturbance such as drought and soil salinization, will incrementally shift the MBDI from the natural variability range, and may be recovered in the long or short term, depending on mitigation and remediation programs and methods, see Figure 4.2.

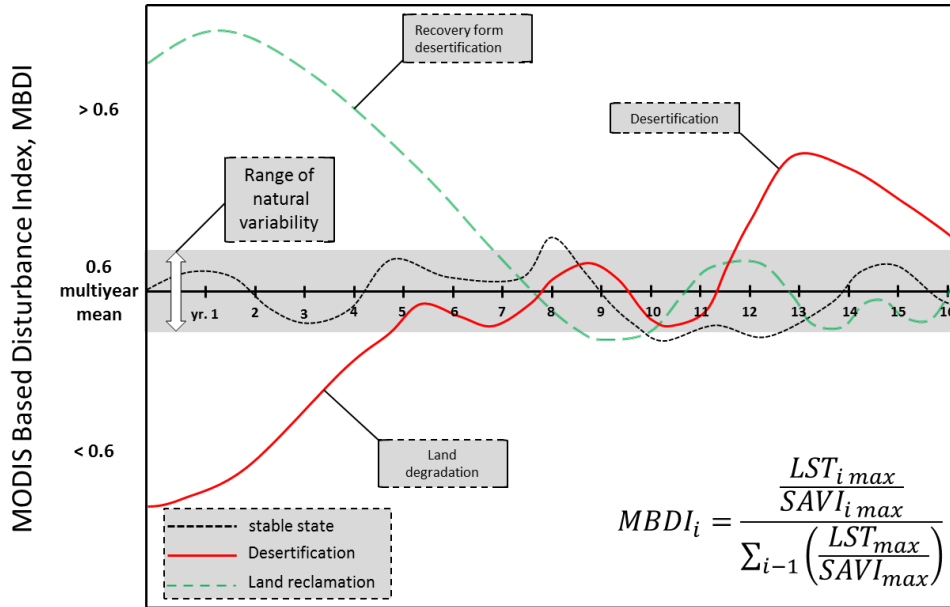


Figure 4.2. The MODIS Based Disturbance Index (MBDI) algorithm with a bi-directional aspect, for tracking the disturbance that caused by desertification in an arid environment. The normal environmental condition exist in the range of the natural variability (gray zone), when the studied year LST_{max} and $SAVI_{max}$ have the mean of 0.6. In cases of desertification the LST_{max} increases and the $SAVI_{max}$ decreases (red solid line). The recovery state found when the LST_{max} decreases and the $SAVI_{max}$ increases (green dashed line).

The development of desertification was observed in many regions in Sinai, the bi-stable ecosystem dynamics, as shown in Figure 4.3, can explain the desertification development in the case study. Both vegetated and desertified states are the stable configurations of the system (D’Odorico et al. 2013). A disturbance can cause a transition to the stable states, and the resilience to change of the bi-stable system depends on the disturbance strength per duration; if the system makes a transition to the other stable state it will be difficult to revert to the initial state (Gunderson 2000).

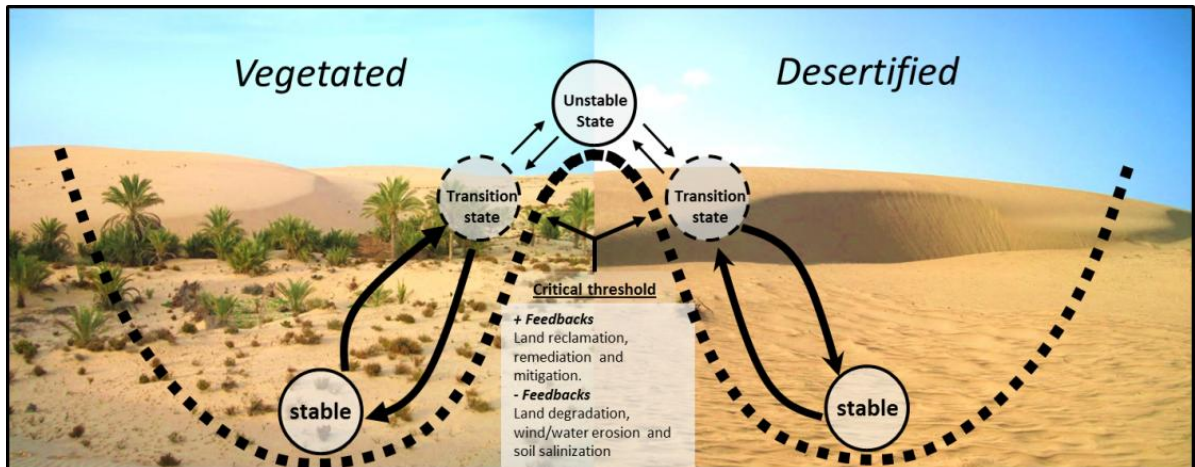


Figure 4.3. Illustration draws of the bi-stable ecosystem balance for an arid environment, both sections (vegetated and desertified) are hosting the transition and stable states, the critical threshold containing (positive and negative) environmental feedbacks. Positive feedbacks are the drivers that influence the system positively to move to the vegetated section, where the negative feedbacks are the drivers that cause more land degradation and orient the system to move to the desertified section.

4.2.5 Assessing the MBDI algorithm

Many disturbance agents such as sand dunes shifting, flash flood, and over grazing were attributed to MBDI change in the case study, but the soil salinity was considered the greatest land degradation in Sinai (Nawar et al. 2011). The salt accumulation occurred as a result of evaporation to the salty waterlogging, which formed salt crust on the soil surface (Carrow and Duncan 2012). The soil salinity in the case study was classified into five groups as shown in Table 4.3. And 44 soil samples were collected from different spots in North Sinai for analyzing soil salinity using the saturated paste extraction method (U.S. Salinity Laboratory 1954). The obtained data from the field were compared with the number of MBDI pixels, that were disturbed over the same temporal-frame of the year 2011 and spatial location, as shown in Figure 4.4. The results showed a strong relationship between the measured data (soil samples) and the estimated values of disturbance (MBDI) ($r = 0.79$; $p < 0.001$), which approved using the algorithm for monitoring the desertification in the case study.

Table 4.3. The classification of soil salinity and field observation for each class, based on the soil salinity classification and EC ranges, (Carrow and Duncan, 2012).

Soil salinity type	EC range (dS/m)	Field observation
Non-saline	<2	<ul style="list-style-type: none"> No salt crust or affected vegetation by soil salinity. Intensive agricultural activities and fruit production. No observations of waterlogging areas or saline soils "Sabkhas".
Slightly-saline	2-4	<ul style="list-style-type: none"> Salt tolerant species found in healthy condition. Land cultivation and drip irrigation system. No observations of surface salt crystals.
Moderately-saline	4-8	<ul style="list-style-type: none"> Domination of salt tolerant natural plants community. No cultivation areas and more land reclamation activities. Present of small bare areas and salt with salt crusts.
Highly-saline	8-16	<ul style="list-style-type: none"> Domination of salt tolerant natural plants community. No cultivation areas and more land reclamation activities. Large bare saline areas and wetlands as a result of the uprising waterlogging.
Extremely-saline	>16	<ul style="list-style-type: none"> Domination of the halophyte species and dead natural plants. Salt mining activities for industrial production. Large white land surface as a result of salt crust accumulation.

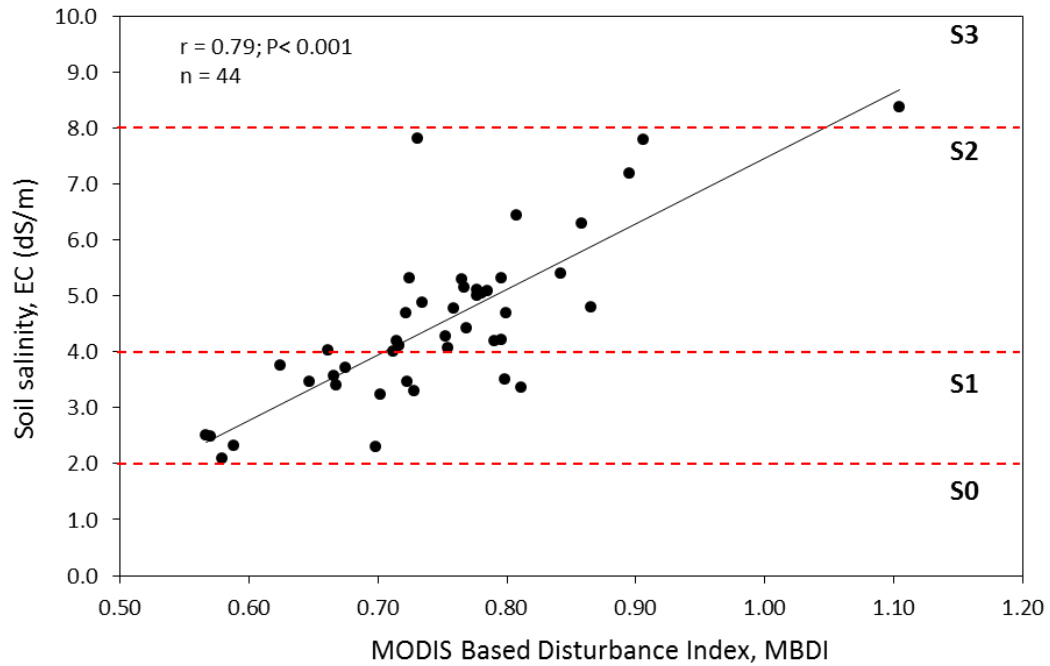


Figure 4.4. Soil salinity, EC (dS/m) and the MODIS-Based Disturbance Index, MBDI relationship; $n=44$ soil samples were obtained during field survey in 2011, the soil salinity classified into four major groups, see table 4. S0: Non-saline (< 2 dS/m); S1: Slightly-saline (2-4 dS/m); S2: Moderately-saline (4-8 dS/m); S3: Highly-saline (8-16 dS/m).

4.3 Results and discussions

4.3.1 Mean-maximum LST and SAVI relationship

The mean-maximum SAVI and mean-maximum LST over Sinai for 2011 were strongly negatively correlated ($r=-0.88$; $P < 0.001$) after the dry season in the case study (September), see Figure 5.5. The land cover types in the case study were observed during field work, and connected to the modified energy balance curve in Figure 4.5 according to the hypothesized groups by (Mildrexler et al. 2007; Nemani and Running 1997). In the water-limited section, plant communities grow in drier weather or poor soil conditions, also the high fraction of the exposed soil increases the LST as a result of inadequate water supply. The predominant land cover types for this section were barren lands and desert flora (Figure 4.6a, b), where LST was high and SAVI low. In the energy-limited section, wetlands and open water fall into this category, the water adequacy is responsible for low LST and Bowen ratios, the dominant land cover types that were found in this section were wetlands “Sabkhas” and halophyte species, which were tolerant to salty water conditions (Figure 4.6c). the atmospherically decoupled section has a distinctive vegetation cover type different to the ecological optimality as a result of agricultural activity, which provided fertilization and appropriate irrigation

systems for a dry environment, such as sprinkler and drip irrigation regimes for maximum vegetation production in high LST. Crops were the dominant land cover type found during the field work, as shown in Figure 4.6d. The climate and soil properties controlled the vegetation density in the atmospherically coupled section, trees with deep-root systems tend to dissipate more energy by transpiration through much of the growing season, this land cover type has high vegetation cover and low exposed ground, which was responsible for the low radiometric temperature, Figure 5.6e.

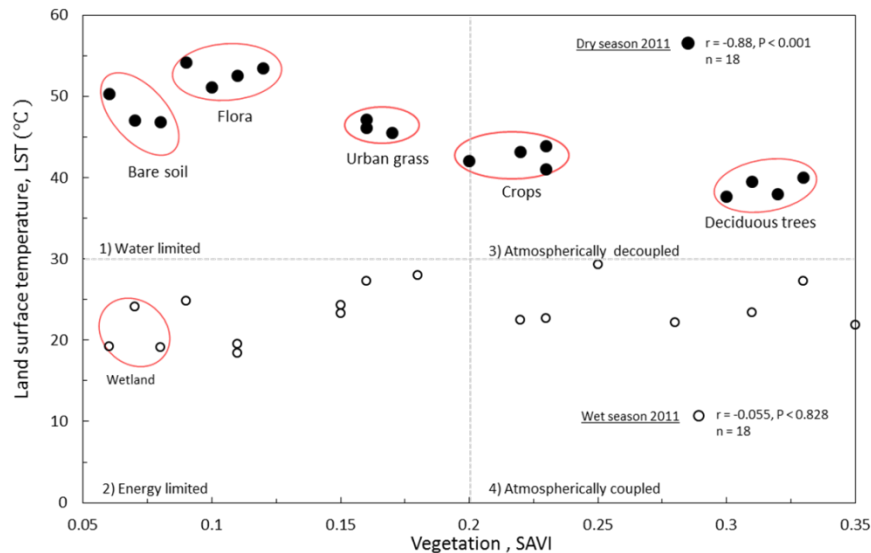


Figure 4.5. The distribution of land cover types in Sinai Peninsula based on the energy balance relationship, over four environmental categories, which are conceptualized by (Nemani & Running, 1997)

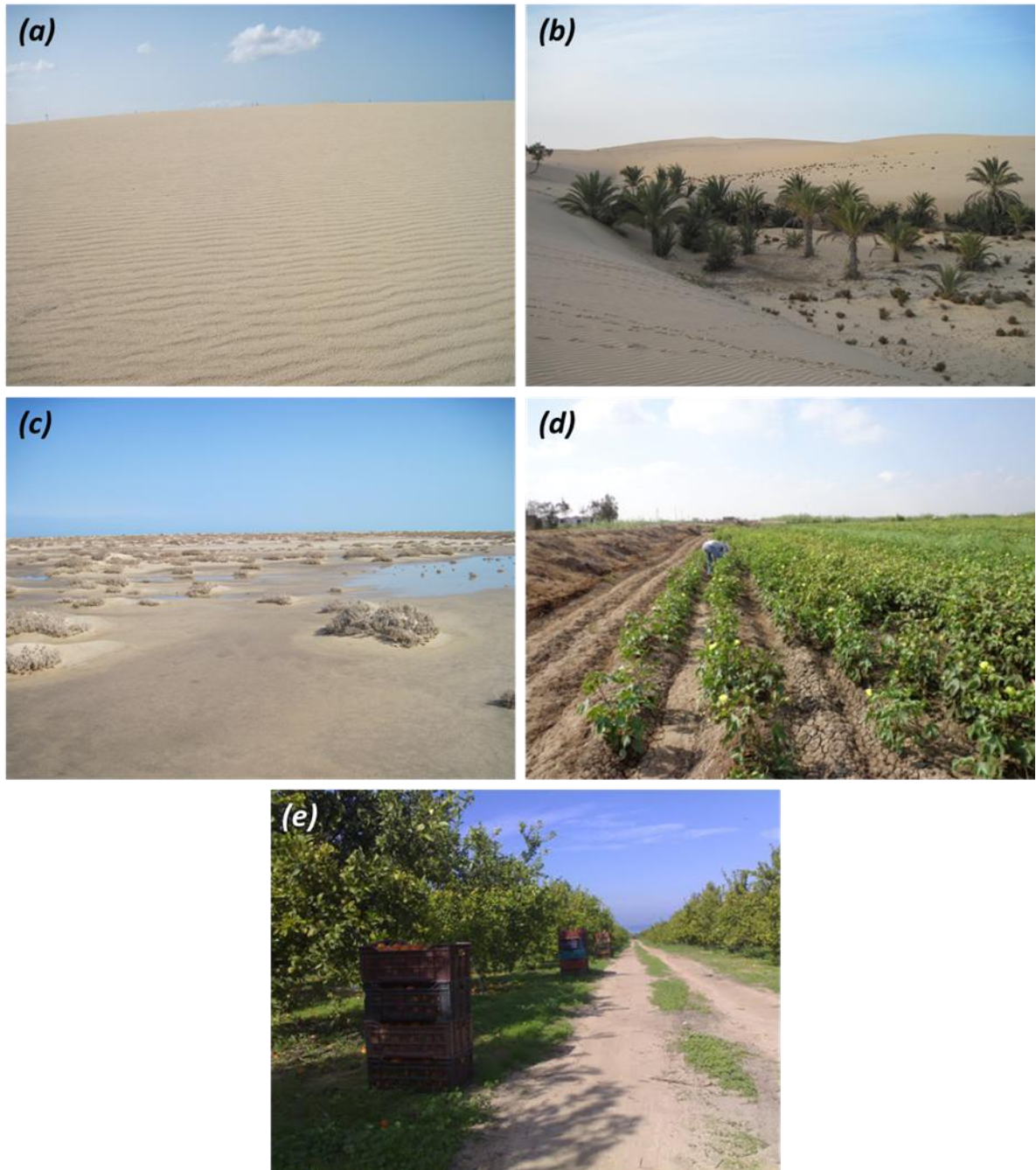


Figure 4.6. Different examples of land cover classes in Sinai Peninsula; **a)** barren lands ; **b)** natural plants; **c)** wetlands “sabkhas”; **d)** crops, taken by Said Nawar; **e)** deciduous trees, taken by Abo Al-Amer.

The relationship between mean-maximum LST and maximum SAVI across the Sinai Peninsula at each pixel for the years 2002, 2005, 2008 and 2011 provided useful information to determine the spatial variation of disturbance. Six sites were chosen with different characteristics, in order to represent the whole Sinai Peninsula. This relationship across Sinai provided an initial assessment of the vegetation cover variation over the studied years, as shown in Figure 4.7. Arish&Rafaa and Qantara Shark sites, dominated by agriculture (Badreldin and Goossens 2013), and after the year 2002 El-Tina Plain became a zone for crop production as a result of El-Salam Canal project for land

reclamation and agricultural production (Othman et al. 2012). As shown in Figure 4.7a, b and c. Zaraniq, South-Sinai and El-Wasat have constant low SAVI over different LSTs, which varied from 50°C in the summer seasons such as June and September, to approximately 15 °C in January and December. As shown in Figure 4.7d, e and f, these sites were dominated by natural plants that have tolerance to arid environmental conditions.

In general, the increase in LST in the case study was associated with strong evaporation and water logging that carried the soluble salts up to the soil surface (Ci and Yang 2009), salt accumulates on soil surface as a salt crust and affects agricultural production and ecosystems stability, and permanently degrades soil productivity (Rengasamy 2006).

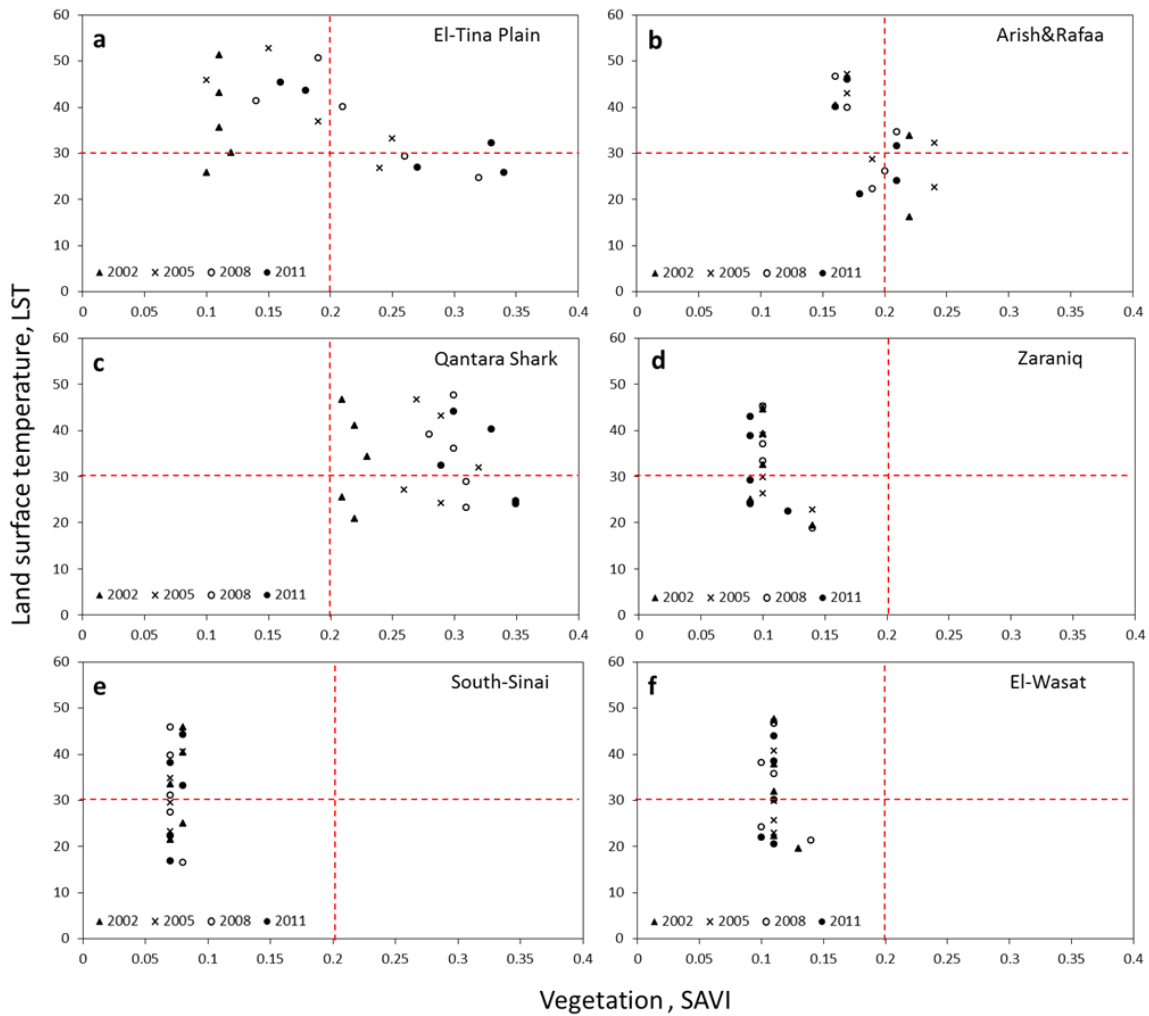


Figure 4.7. The mean-maximum LST and SAVI relationship over years 2002, 2005, 2008 and 2011; **a)** El-Tina Plain, Lat. 31° 00' 00.09", Long. 32° 26' 11.25"; **b)** Arish&Rafaa, Lat. 31° 09' 35.72" Long. 34° 02' 11.83"; **c)** Qantara Shark, Lat. 30° 26' 31.58", Long. 32° 24' 23.19"; **d)** Zaraniq, Lat. 31° 06' 07.77", Long. 33° 28' 57.82"; **e)** South Sinai, Lat. 28° 27' 38.70", Long. 34° 04' 15.03"; **f)** El-Wasat, Lat. 29° 52' 08.36", Long. 33° 47' 21.85".

4.3.2 MBDI application for desertification recovery detection

We applied the MBDI algorithm to the MODIS data for the years 2002, 2005, 2008 and 2011 across the Sinai Peninsula. The mean MBDI value for the entire study area was 0.6. The MBDI range was extended from <0.5 to >1.2 . The natural variability range was defined as the values that found within one standard deviation ± 0.1 of the mean 0.6. The natural variability range $0.7 - 0.5$ was mapped in yellow, moderate disturbance $0.7 - 1.2$ was mapped in orange, extreme disturbance values >1.2 in red, and <0.5 for the recovery was mapped in gray. The MBDI algorithm detected a recovery from desertification at sites in El-Tina plain and Qanatra Shark, through the studied years 2002, 2005, 2008 and 2011.

The soil properties in the El-Tina Plain area are a combination of alluvium deposits, originating from ancient Nile branches, and lacustrine sand deposits (Hassan 2002), which covered the north-western corner of Sinai. Nawar et al. (2011) classified the salt-affected soils in the El-Tina plain as very strong saline soils $> 32 \text{ dS.m}^{-1}$, strongly saline soils $16-32 \text{ dS.m}^{-1}$, moderately saline soils $8-16 \text{ dS.m}^{-1}$, slightly saline soils $4-8 \text{ dS.m}^{-1}$, and very slightly saline $2-4 \text{ dS.m}^{-1}$. The southern part of the El-Tina plain recovered from desertification over the years 2002, 2005, 2008 and 2011, as shown in Figure 4.8a, as a result of extensive agricultural development, Kaiser (2009) found that the cultivated land areas increased significantly while wetlands decreased over the years.

Wind erosion in the north of Sinai is considered one of the earth's surface dynamics that impacts infrastructure and farming activities via sand dunes shifting. The ecosystem in Qantara Shark is affected by sand dunes' progress at different rates and directions (Hermas et al. 2012). As shown in Figure 4.8b, the societal feedbacks contributed through the years 2002, 2005, 2008 and 2011 against the desertification, and the spatial distribution of the desertification (MBDI >1.2 and $0.7-1.2$) decreased in the years 2005, 2008 and 2011, which indicated that the environment in this site is improving.

MBDI detected evidences of mitigation investments which decreased desertification and land degradation in the case study. Soil leaching was the strategy for decreasing the salinity in order to improve the physical and chemical soil properties for agriculture production, which was given a high national priority (Galal 2004). Also, planting windbreaks to decrease the wind erosion effects in Qantara Shark has a significant impact to improve the agriculture activity and to minimize the soil erodibility.

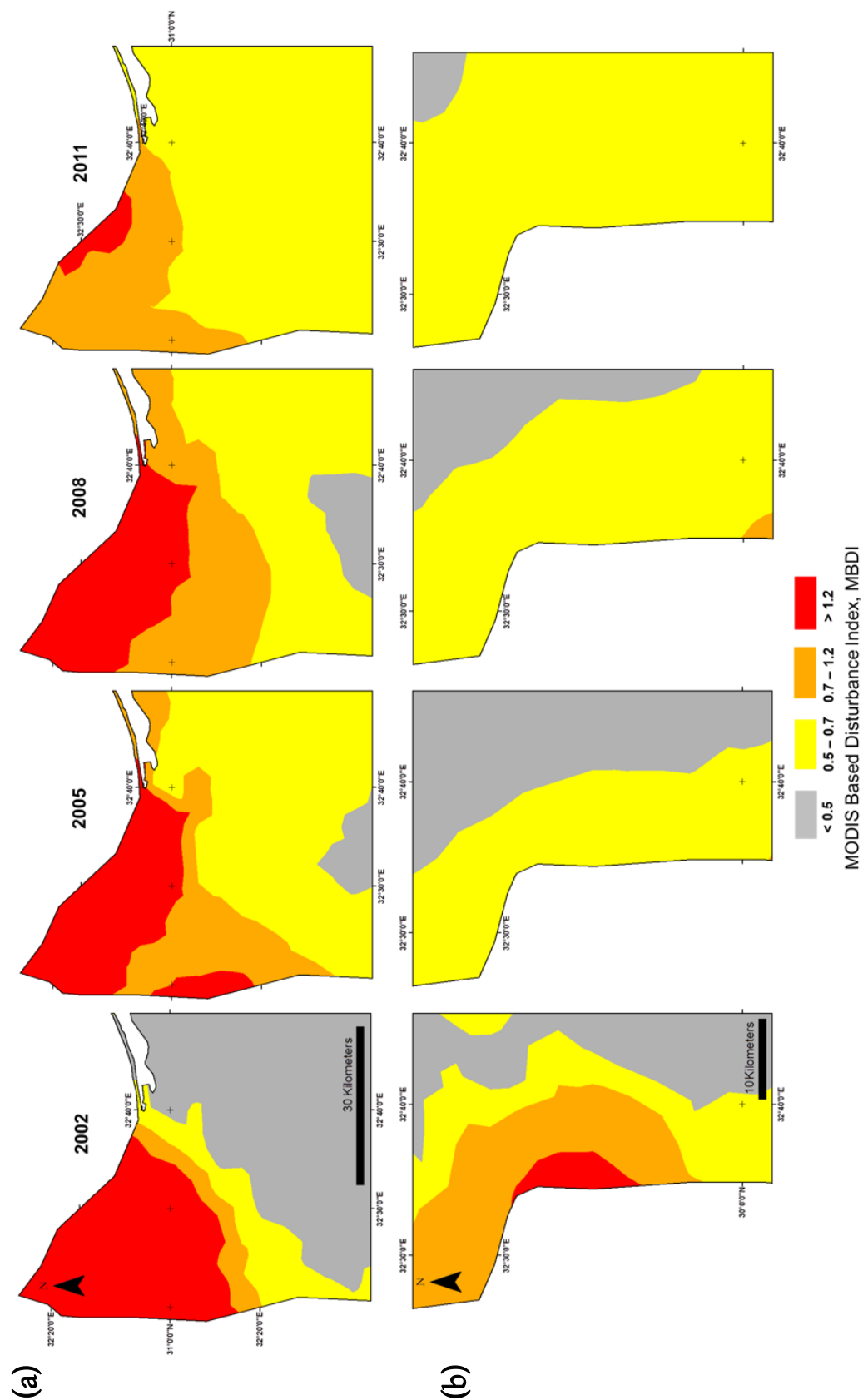


Figure 4.8. The MBDI spatial distribution over the years 2002, 2005, 2008 and 2011; **a)** El-Tina Plain; and **b)** Qanatara Shark. Disturbance recovery is < 0.5 (gray color), the natural variability range is between 0.5–0.7 (yellow color), moderate disturbance 0.7–1.2 (orange color), and extreme disturbance is > 1.2 (red color).

4.4 Conclusion

MBDI algorithm was developed for monitoring the desertification status in an arid environment for regional scales, and based on Aqua/MODIS and Terra/MODIS satellites. This algorithm proved to be a useful method for disturbance detection. The advantages of using MBDI were to provide accurate change detection information about the spatial and temporal departure of disturbance events, and its recovery in arid ecosystems regarding to its natural condition. Mean-maximum LST and SAVI relationship was considered at two different seasons, 1) the most vulnerable biotic condition, when the vegetated areas undisturbed, and 2) the abiotic environment. The relationship between maximum LST and maximum SAVI across different sites in the study area were strongly negatively correlated ($r=-0.88$; $P < 0.001$) after the dry season in September. Classes of MBDI were defined for the natural variability, extreme disturbance, moderate disturbance and recovery status (0.5-0.7, >1.2 , 0.7-0.5 and <0.5 , respectively). MBDI detected anti-desertification change in El-Tina plain and Qanatra Shark through over the studied years 2002, 2005, 2008 and 2011. Soil salinization and wind erosion were the main land degradation that desertified lands in Sinai. Societal drivers in El-Tina plain and Qanatra Shark sites contribute to mitigate and compact desertification process, some of soil remediation practices such soil leaching enhanced salt accumulation in the shallow soils of El-Tina plain.

MBDI provided a powerful tool for monitoring positive and negative changes of desertification in an arid environment in regional level. Also, it can be used for detecting and predicting the effects of the climate change, and deliver accurate information about the environmental risk assessment or the early warning system for decision makers, organizations and public awareness, in order to prevent severe desertification and land degradation events and protect the local natural resources and biodiversity.

4.5 References

- Aboelghar M, Ali A-R, Arafat S (2012) Spectral wheat yield prediction modeling using SPOT satellite imagery and leaf area index. *Arabian Journal of Geosciences*. doi: 10.1007/s12517-012-0772-6
- Adamo SB, Crews-Meyer K a. (2006) Aridity and desertification: Exploring environmental hazards in Jáchal, Argentina. *Applied Geography* 26:61–85.
- Armah F a., Odoi JO, Yengoh GT, et al. (2010) Food security and climate change in drought-sensitive savanna zones of Ghana. *Mitigation and Adaptation Strategies for Global Change* 16:291–306.
- Badreldin N, Goossens R (2013) Monitoring land use/land cover change using multi-temporal Landsat satellite images in an arid environment: a case study of El-Arish, Egypt. *Arabian Journal of Geosciences*. doi: 10.1007/s12517-013-0916-3
- Bannari A, Morin D, Bonn F, Huete AR (1995) A review of vegetation indices. *Remote Sensing Reviews* 13:95–120.
- Carrow RN, Duncan RR (2012) *Best Management Practices for Saline and Sodic Turfgrass Soils: Assessment and Reclamation*. CRC Press, Taylor & Francis Group, FL, p 486.
- Ci L, Yang X (2009) *Desertification and Its Control in China*. Higher Education Press and Springer, Beijing and Dordrecht, p 533.
- Coops NC, Wulder M a., Iwanicka D (2009) Large area monitoring with a MODIS-based Disturbance Index (DI) sensitive to annual and seasonal variations. *Remote Sensing of Environment* 113:1250–1261.
- D’Odorico P, Bhattachan A, Davis KF, et al. (2013) Global desertification: Drivers and feedbacks. *Advances in Water Resources* 51:326–344.
- Dames, Moore (1981) Sinai development study - phase 1: Land classification and capability in Sinai. 167.
- Dawelbait M, Morari F (2012) Monitoring desertification in a Savannah region in Sudan using Landsat images and spectral mixture analysis. *Journal of Arid Environments* 80:45–55.
- Diouf a., Lambin EF (2001) Monitoring land-cover changes in semi-arid regions: remote sensing data and field observations in the Ferlo, Senegal. *Journal of Arid Environments* 48:129–148.
- FAO (2005) *Fertilizer use by crop in Egypt, Land and Plant Nutrition Management Service Land and Water Development Division*. Rome, p 62.
- G.Kepner W, Rubio JL, Mouat DA, Pedrazzini F (2006) Desertification in the Mediterranean Region. A Security Issue. *Proceedings of the NATO Mediterranean Dialogue Workshop on Desertification in the Mediterranean Region. A Security Issue*. Springer, Dordrecht, NL, p 606
- Galal ME (2004) Estimating Soil Hydraulic Parameters In El-Tina Plain Using RETC Program. *International Conf. on Water Resources & Arid Environment*. p 5
- Grainger A, Smith MS, Squires VR, Glenn EP (2000) Desertification and climate change: the case for greater convergence. *Mitigation and Adaptation Strategies for Global Change* 5:361–377.
- Greenwood NH (1997) *The Sinai: a physical geography*. University of Texas Press, Austin, p148.
- Gunderson LH (2000) Ecological resilience - in theory and application. *Annual Review of Ecology and Systematics* 31:425–439.
- Hall FG, Townshend JR, Engman ET (1995) Status of remote sensing algorithms for estimation of land surface state parameters. *Remote Sensing of Environment* 51:138–156.
- Hassan MAE-RAE-A (2002) Environmental studies on coastal zone soils of the north Sinai peninsula (Egypt) using remote sensing techniques. *Technischen Universität Carolo-Wilhelmina*, p 247.
- Hermas E, Leprince S, El-Magd IA (2012) Retrieving sand dune movements using sub-pixel correlation of multi-temporal optical remote sensing imagery, northwest Sinai Peninsula, Egypt. *Remote Sensing of Environment* 121:51–60.
- Herrmann SM, Anyamba A, Tucker CJ (2005) Recent trends in vegetation dynamics in the African Sahel and their relationship to climate. *Global Environmental Change* 15:394–404.
- Huete A. (1988) A soil-adjusted vegetation index (SAVI). *Remote Sensing of Environment* 25:295–309.
- Kaiser MF (2009) Environmental changes, remote sensing, and infrastructure development: The case of Egypt’s East Port Said harbour. *Applied Geography* 29:280–288.
- Kassas M (1977) Arid and semi-arid lands: problems and prospects. *Agro-Ecosystems* 3:185–204.
- Kassas M (1995) Desertification: a general review. *Journal of Arid Environments* 30:115–128.
- Kottek M, Grieser J, Beck C, et al. (2006) World Map of the Köppen-Geiger climate classification updated. *Meteorologische Zeitschrift* 15:259–263.
- Laity J (2008) *Deserts and desert environments*. John Wiley & Sons, Inc. , Chichester , p 357.

- Mildrexler DJ, Zhao M, Heinsch FA, Running SW (2007) A new satellite-based methodology for continental-scale disturbance detection. *Ecological applications*: a publication of the Ecological Society of America 17:235–50.
- Misra A (2013) Climate change impact, mitigation and adaptation strategies for agricultural and water resources, in Ganga Plain (India). *Mitigation and Adaptation Strategies for Global Change* 18:673–689.
- Natural Resources Conservation Service (NRCS) (1999) *Soil Taxonomy: A Basic System of Soil Classification for Making and Interpreting Soil Surveys*, 2nd ed. United States Department of Agriculture (USDA), Washington , p 871.
- Nawar S, Reda M, Farag F, El-nahry A (2011) Mapping Soil Salinity in El-Tina Plain in Egypt Using Geostatistical Approach. *Geoinformatics Forum*. Salzburg, Austria, pp 81–90
- Nemani R, Running S (1997) Land cover characterization using multitemporal red, near-IR, and thermal-IR data from NOAA/AVHRR. *Ecological Applications* 7:79–90.
- Othman A a., Rabeh S a., Fayez M, et al. (2012) El-Salam canal is a potential project reusing the Nile Delta drainage water for Sinai desert agriculture: Microbial and chemical water quality. *Journal of Advanced Research* 3:99–108.
- Peel MC, Finlayson BL, McMahon TA (2007) Updated world map of the Köppen-Geiger climate classification. *Hydrology and Earth System Sciences* 11:1633–1644.
- Pickett STA, White PS (1987) *The ecology of natural disturbance and patch dynamics*. Academic Press, New York, p 472.
- Rengasamy P (2006) World salinization with emphasis on Australia. *Journal of experimental botany* 57:1017–23.
- Richards JA (2013) *Remote Sensing Digital Image Analysis: An Introduction*, 5th ed. Springer-Verlag, Berlin, Heidelberg. pp494.
- Salinas C, Mendieta J (2012a) The cost of mitigation strategies for agricultural adaptation to global change. *Mitigation and Adaptation Strategies for Global Change* 1–9.
- Salinas CX, Mendieta J (2012b) Effectiveness of the strategies to combat land degradation and drought. *Mitigation and Adaptation Strategies for Global Change*. doi: 10.1007/s11027-012-9421-3
- Salinas CX, Mendieta J (2012c) Mitigation and adaptation investments for desertification and climate change: an assessment of the socioeconomic return. *Mitigation and Adaptation Strategies for Global Change*. doi: 10.1007/s11027-012-9380-8
- Stiles D (1984) Desertification: The time for action. *The Environmentalist* 4:93–96.
- Thomas DSG (2011) *Arid Environments: Their Nature and Extent*. Arid Zone Geomorphology. John Wiley & Sons, Ltd, pp 1–16
- Tilman D (1985) The resource-ratio hypothesis of plant succession. *The American Naturalist* 125:827–852.
- U.S. Geological Survey (2011a) *Vegetation Indices Monthly L3 Global 1km*. URL. https://lpdaac.usgs.gov/products/modis_products_table/mod13a3.
- U.S. Geological Survey (2011b) *Surface Reflectance 8-Day L3 Global 250m*. URL. https://lpdaac.usgs.gov/products/modis_products_table/mod09Q1.
- U.S. Geological Survey (2011c) *Global Multi-resolution Terrain Elevation Data 2010 (GMTED2010)*. URL. http://eros.usgs.gov/#/Find_Data/Products_and_Data_Available/GMTED2010.
- U.S. Salinity Laboratory (1954) *Diagnosis and Improvement of Saline and Alkali Soils*, Handbook 6. U.S. Government Printing Office, Washington , p172.
- Wang XD, Zhong XH, Liu SZ, et al. (2008) Regional assessment of environmental vulnerability in the Tibetan Plateau: Development and application of a new method. *Journal of Arid Environments* 72:1929–1939.
- Waring RH, Running SW (2007) *Forest ecosystems: analysis at multiple scales*, 3rd ed. Elsevier Academic Press, San Diego, p 420.
- Weng Q (2002) Land use change analysis in the Zhujiang Delta of China using satellite remote sensing, GIS and stochastic modelling. *Journal of Environmental Management* 64:273–284.
- WFP (2006) *Country Programme-Egypt (2007–2011)*. Rome, p25. World Bank (2013) *Climate baseline*. Egypt dashboard. URL. http://sdwebx.worldbank.org/climateportal/index.cfm?page=country_historical_climate&ThisRegion=Africa&ThisCCode=EGY.
- Yang J, Weisberg PJ, Bristow N a. (2012) Landsat remote sensing approaches for monitoring long-term tree cover dynamics in semi-arid woodlands: Comparison of vegetation indices and spectral mixture analysis. *Remote Sensing of Environment* 119:62–71.
- Zahrán MA, Willis AJ (2009) *The Vegetation of Egypt*, 2nd ed. Springer, Heidelberg, p 451
- Zar JH (2010) *Biostatistical analysis*, 5th ed. Prentice Hall, New Jersey, p 960.

Chapter 5

Monitoring Land Use / Land Cover Change Using Multi-Temporal Landsat Satellite Images in Arid Environment: A Case Study of El-Arish, Egypt

This chapter is modified from:

Nasem Badreldin and Rudi Goossens (2013) Monitoring Land Use / Land Cover Change Using Multi-Temporal Landsat Satellite Images in Arid Environment: A Case Study of El-Arish, Egypt. *Arabian Journal of Geosciences*. DOI: 10.1007/s12517-013-0916-3.

5.1 Introduction

Land Use and Land Cover (LULC) datasets are important sources for many applications, such as environmental monitoring, urban management, and socioeconomic studies (Weng 2010). LULC dynamics can be observed in terrestrial characteristics at local and global scales (Abdel Kawy and Abou El-Magd 2012; Du et al. 2010; Kelarestaghi and Jafarian Jeloudar 2009; Mohamed et al. 2012). Remote sensing technology is supporting research in LULC dynamics with data sources from space that provide information to monitor and estimate the changes on the surface (Jiyuan et al. 2002; Masoud and Koike 2006; Yan et al. 2009). Data from the Landsat satellite images are frequently used in LULC research (Matinfar et al. 2011; Rozenstein and Karnieli 2011), particularly from the Enhanced Thematic Mapper Plus (ETM+). The multispectral bands of ETM+ cover visible, and near infrared and short-wave infrared spectral regions with a ground resolution of 30 m, the thermal infrared spectral region with a ground resolution of 60 m, and a panchromatic channel with a ground resolution of 15 m (Donegan and Flynn 2004; Xian et al. 2009).

The main methods used for monitoring the LULC dynamics are image differencing, rationing, principle component analysis, and post-classification comparison (PCC) (Khalifa and Arnous 2010). The PCC was used to calculate changes in multi-temporal satellite images through comparison between each multi-temporal pairs of classified maps, which result from the supervised classification (Batisani and Yarnal 2009; Qin et al. 2006; Xian et al. 2009; Zhou et al. 2008).

This investigation will provide a multi-temporal LULC maps for years (1999, 2001, 2005 and 2010) and monitor trend of change in El-Arish city of Egypt, based on the integration between the supervised maximum likelihood classification method and visual interpretation of remote sensing data. The layouts will help to identify the causes of change for each period.

5.2 Study area description and field survey

About 95% of the total area of Egypt is covered by desert, while about 85 million inhabitants depend on the remaining 5% of the land. However, this 5% yield only very poor food resources (Abd El-Kawy et al. 2011; Shalaby and Tateishi 2007). The case study is conducted in El-Arish city which is the headquarter of North Sinai Governorate, Egypt ($31^{\circ} 12' 29.63''$, $30^{\circ} 57' 59.18''$ N and $33^{\circ} 40' 56.08''$, $33^{\circ} 58' 7.98''$ E). The study area is approximately 570 km², as shown in Figure 5.1. From the east to the west, sand dunes with different shapes (Barchans, Longitudinal, and Transverse) are found. The area represents the typical biogeography of an arid region with more than 10 different species of flora such as *Arthrocnemum glaucum* “Glaucous Glasswort”, *Juncus subulatus* “Somerset Rush”, and *Zygophyllum album* “White bean-caper” (El-Bana et al. 2010). The major agricultural activity in the study area is horticulture. The climate is a Mediterranean arid type, where the temperature is between 25-35 °C in the summer (June to August) and 10-15 °C in the winter (December to February), and rainfall is only in winter season about 200 mm/year. The local community is mainly Bedouin; they are living in tradition desert environment.

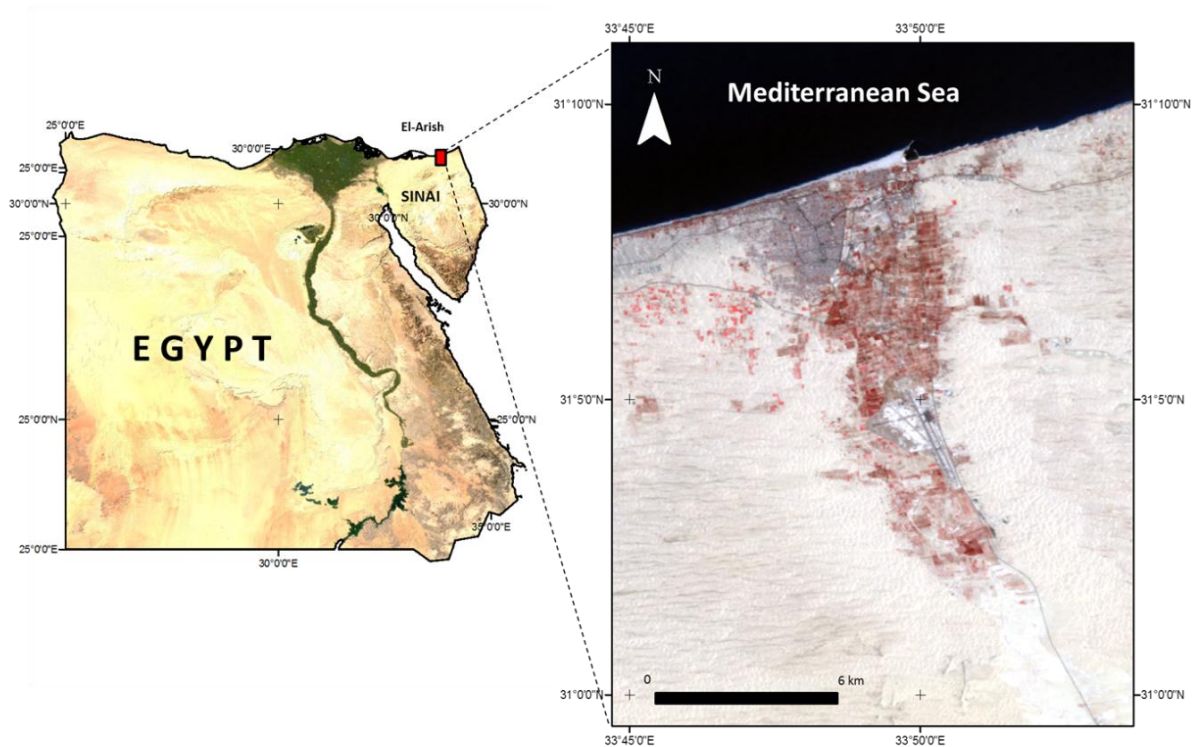


Figure 5.1. The location of the study area, El Arish, Egypt.

We started the field work in April 2009 and continued in October 2010 in order to collect the ground truth data, 75 sample points were selected based on a stratified sampling approach, in which five classes were chosen for the study (Bare soil, Fertile soil, Sand dune, Urban and Vegetation), these classes were the most important categories in the case study because of the possibility to distinguish the changes over the time with using multi-temporal Landsat satellite images. As shown in Figure 5.2a, bare soil class is the land where no agriculture activities are carried out and which are mainly and frequently affected by sand storms or water logging such as saline soils. Secondly, fertile soil class is the piece of land that has been used before in agriculture or formed by flood's sedimentation and is mainly located in Wadi El-Arish, the southern part of this case study, Figure 5.2b. Thirdly, sand dune class is formed by Aeolian deposits and found in different shapes Figure 5.2c. Fourthly, urban class is the place where you find buildings, roads and other infrastructure, and mainly located in the northern part of the case study, Figure 5.2d. Finally, vegetation class is the cultivated areas and the natural palm trees, see Figure 5.2e and f.

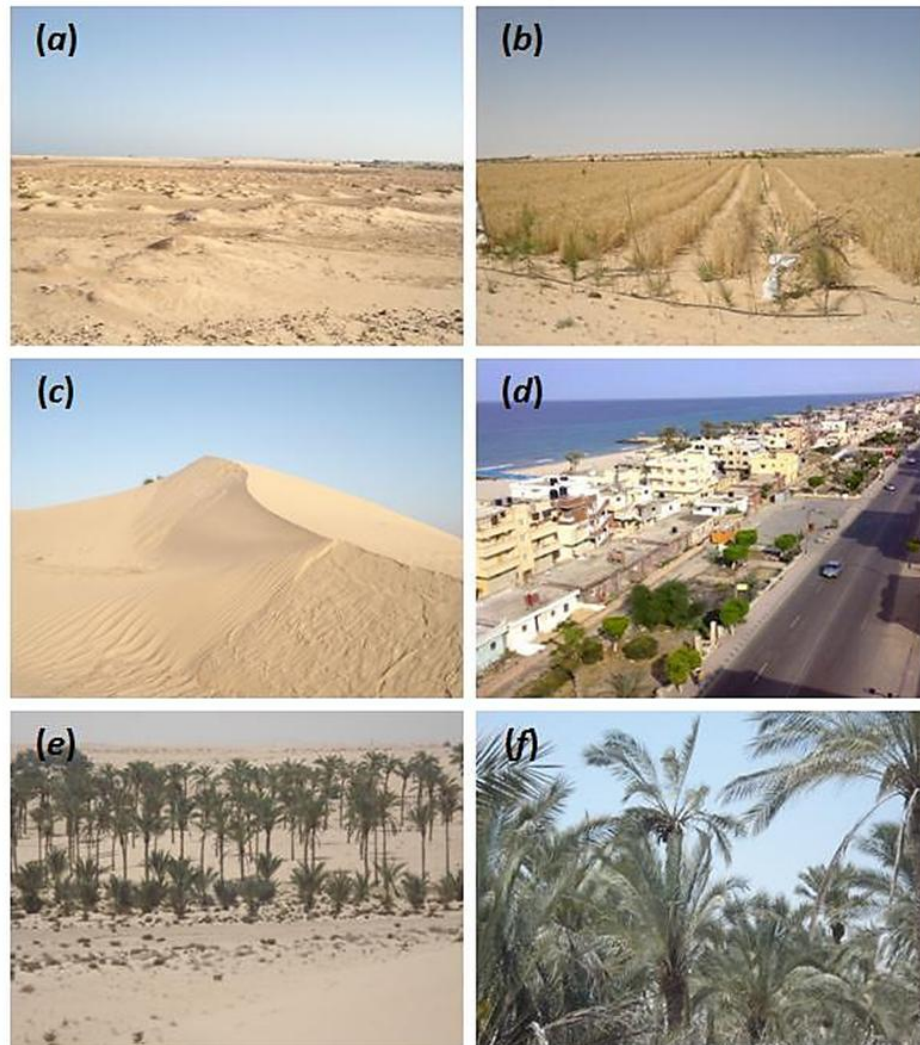


Figure 5.2. Photos taken in the case study during April 2009 and October 2010, **(a)** bare soil; **(b)** fertile soil; **(c)** sand dunes; **(d)** urban; **(e)** and **(f)** vegetation.

5.3 Materials and methods

5.3.1 Data sets

This study is based on Enhanced Thematic Mapper Plus (ETM+) satellite images, which is the third Landsat series in Landsat 7 (15/04/1999) with 30m resolution. The satellite images were acquired in clear atmospheric conditions, the description is shown in Table 5.1:-

Table 5.1. Satellite image information for data acquisitions corresponding to path 176/row 38 and 39

Satellite	Sensor	Bands	Resolution	Acquisition date	Path	Row
Landsat7	ETM+	7	30 x 30 m	August 1999	176	38/39
				July 2001	176	38/39
				May 2005	176	38/39
				April 2010	176	38/39
				June 2010	176	38/39

The satellite images were obtained from Warehouse Inventory Search Tool (WIST) in the USGS Earth Resources Observation and Science (EROS), which is a web-based tool to search and order earth science data from NASA Land Processes Distributed Active Archive Centre User Services. These multi-temporal data were necessary for change detection analysis, in order to provide information about the amount and possible reasons of change, especially in arid environment condition where the natural resources are limited.

5.3.2 Image pre-processing

Satellite images pre-processing is essential for LULC change detection research in order to establish the direct link between the image and the case study (Abd El-Kawy et al. 2011; Coppin et al. 2004). Various image pre-processing operations have been considered, including: geometric correction, ETM+ SLC off and gap filling, and image enhancement. ENVI 4.5 software was used for all images processing in this study.

5.3.2.1 Geometric correction

LULC change detection studies require geometric corrections in order to exploit image usefulness and in order to extract accurate information (Knorn et al. 2009). The 2010 image was geo-referenced using a set of 23 ground control points (GCPs) which are obtained by GPS of Garmin etrex vista, Root Mean Square Error (RMSE) = 0.213 pixels. The images of 1999, 2001, and 2005 were geometrically corrected to 2010 image (RMSE) < 0.4 pixels. The locations of GCPs were chosen assuming that they

were obvious and permanent on the satellite images, such as (road corners, airport and lighthouses). The case study was extended over two senses for each studied year. And in order to achieve a full coverage for the region of interest which is El-Arish city, we mosaicked the images based on geo-referencing.

5.3.2.2 Image enhancement

The purpose of this stage is to improve subjectively the satellite images for better analysis. The classical method of enhancement is to manipulate the histogram of the image in order to increase the contrast. Filtering to remove noise, and principle component analysis (PCA) provide the maximum possible contrast from the multispectral images (Petrou and Bosdogianni 1999). The dark Object Subtraction (DOS) technique was used for the radiometric correction tool to improve image visualization. The dark object has uniformly zero radiance for all bands and any non-zero measured radiance due to atmospheric scattering into the object's pixels (Chavez 1988; Wrigley et al. 1992; Zheng et al. 2007).

5.3.2.3 ETM+ SLC off and gap filling

On 31st of May, 2003 the Scan Line Corrector SLC in Landsat 7 stopped working permanently and ETM+ sensor produces satellite images with gaps about 22% pixels for each scene. These missing pixels are affecting the image quality and they are distributed from one pixel or less near centre of the image to 14 pixels along the east edge of the image as shown in Figure 5.3a. Fortunately there is no influence on the radiometric performance of these images (Chander et al. 2010; Chen et al. 2011). Three SLC-off ETM+ images with different acquisition dates were overlapped (March, April, and June 2010) in order to remove the gaps and reduce the missing pixels Figure 5.3b. The image of May 2005 was processed by NASA Land Processes Distributed Active Archive Centre User Services and provided without any gaps.

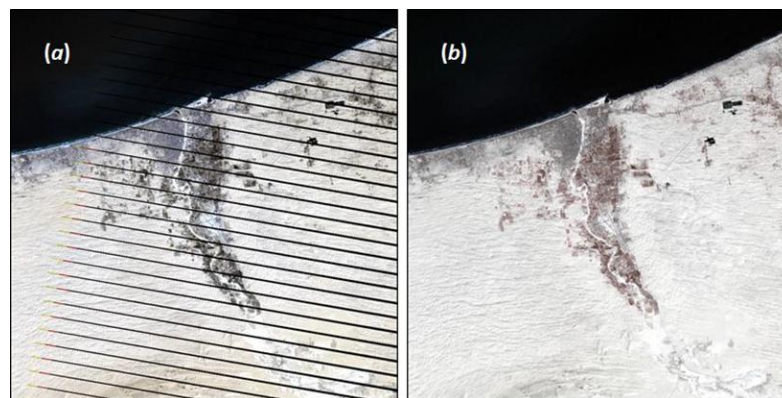


Figure 5.3. ETM+ of the case study in true colour composition, **a)** the image when SLC is off; **b)** after covering the gabs in the same image.

5.3.3 Supervised classification

This method is mostly used for satellite image classification in quantitative analysis (Etteieb et al. 2012). It categorizes all pixels in the raster image in order to represent ground cover classes. The classification depends on the chosen algorithm. The maximum likelihood classification method was considered as one of the commonly used methods in supervised classification (Richards 2013). We passed through several steps in order to obtain the supervised classified maps for the case study: 1- obtaining information about the number of classes that could be recognized by both image and ground observation, 2- choosing training sets (prototype pixels) for each class based on previous adequate field survey and 3- pixel's signature analysis provide information about the expected classes regarding to the pixel's reflectance. The classification improvement depends on the number of training pixels for each class. Davis and Swain (1978) proposed that the minimum training pixels per spectral class is $10N$ (pixel dimensional), increasing to $100N$ if possible per class. Visual interpretation was applied to increase the classification accuracy and the quality of the produced LULC maps (Abd El-Kawy et al. 2011). Vegetation cover has been identified through the Normalized Difference Vegetation Index (NDVI) (Huete 1988; Lyon et al. 1998).

$$NDVI = \frac{(NIR-RED)}{(NIR+RED)} \quad (5.1)$$

Where NIR is the reflectance value of the near infrared band, RED is reflectance of the red band.

5.3.4 Post-Classification Comparison (PCC)

Two comparisons were analyzed by using PCC (i.e., 1999-2005 and 2005-2010). The comparison was based on the difference between the same classes in the multi temporal maps, which was delivered by the supervised classification. The difference between each pair will provide data on the LULC change of the study area (Rahdari et al. 2012; Yeganeh et al. 2012).

5.3.5 Classification accuracy assessment

The classification accuracy is considered to be one of the important factors in LULC change detection research. The term of accuracy in remote sensing data refers to correctness of classification, which is how well the region of interest represents the reality (Foody 2002; Zheng et al. 2007). The confusion/error matrix is the most used method to assess the accuracy of

classification and characterizing errors, which is helping the investigation to refine the classification (Foody 2010).

The accuracy assessment was performed based on random points that were identified and located using a stratified random method in ENVI software to represent the different LULC classes of the area. For performing a proper accuracy assessment, the points used in our study represented the field survey and checkpoints, topographic maps, archived data, and previous field survey studies as reference data. The reference data and the classification results were compared and statistically analyzed using the confusion/error matrix.

The minimum acceptable overall accuracy in LULC studies is 85% with no class less than 70% (Thomlinson et al. 1999). User's accuracy corresponds to commission errors, while producer's accuracy is responsible for the omission errors. The overall accuracy can be used in order to give a general idea about quality of classification. Pontius and Millones (2011) recommended to report quality and allocation disagreement rather than the kappa indices, which are not useful for accuracy assessment and map comparison. The reasons to abandon Kappa are (1- introducing problems in calculation and interpretation; (2- testing the accuracy due to randomness, which is misleading some times and (3- it is more useful to focus on the disagreement in order to explain the error ,instead of focusing on the agreement and the randomness that explain the correctness, which Kappa does. The disagreement quantity is representing the difference between reference and classified maps that is caused by the less than perfect match in the proportions of the categories. And the disagreement based on the allocation is the amount of the difference between the reference and classified map that causes the less than optimal match in the spatial allocation of the categories.

5.4 Results and discussions

Before depending on the classification results which are delivered from satellite images analysis for LULC change, we need to evaluate the validity of the layouts via testing the results against the reference data (Foody 2002; Herold et al. 2008; Weng 2002). The image enhancement and the radiometric correction provided a better visualization of classification processes and increased the overall accuracy of the classification for the 1999, 2001, 2005, and 2010 classified images to 94.92%, 93.26%, 92.02%, and 90.97%, respectively, as shown in Table 5.2. The quantity and allocation disagreements results were met by comparing the acceptable accuracy to reference data with providing less quantity of disagreement, as shown in Figure 5.4.

Table 5.2. Cross-tabulation matrix of classified vs. reference data (the errors of commission: user's accuracy, omission, producer's accuracy, and the overall accuracy).

Classified data	Reference data					Producer's accuracy (%)	User's accuracy (%)	Overall accuracy (%)
	Bare soil	Fertile soil	Sand dune	Urban	Vegetation			
1999								
Bare soil	437	12	1	2	4	97.11	95.83	94.92
Fertile soil	7	502	6	1	2	97.29	96.91	
Sand dunes	1	0	104	17	1	84.55	84.55	
Urban	5	2	9	397	10	94.75	93.85	
Vegetation	0	0	3	2	149	89.76	96.75	
2001								
Bare soil	778	20	7	5	10	95.11	94.88	93.26
Fertile soil	15	264	3	6	8	88.89	89.19	
Sand dunes	10	8	129	3	1	86.00	85.43	
Urban	9	3	10	371	1	96.11	94.16	
Vegetation	6	2	1	1	242	92.37	96.03	
2005								
Bare soil	888	20	4	7	12	92.12	95.38	92.02
Fertile soil	34	724	8	15	11	89.71	91.41	
Sand dunes	7	57	233	10	2	93.95	75.40	
Urban	11	5	2	714	20	94.95	94.95	
Vegetation	24	1	1	6	404	89.98	92.66	
2010								
Bare soil	253	16	2	1	9	82.14	90.04	90.97
Fertile soil	14	310	4	9	9	86.83	89.60	
Sand dunes	2	20	98	6	1	90.74	77.17	
Urban	9	3	3	517	16	95.04	94.34	
Vegetation	30	8	1	11	575	94.26	92.00	

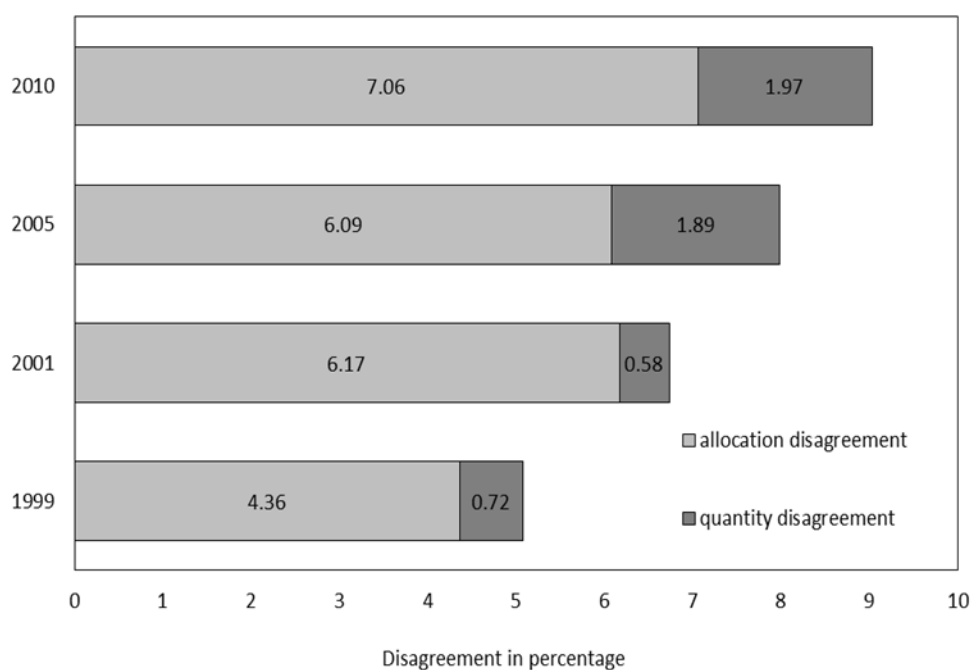


Figure 5.4. Allocation disagreement and quantity disagreement for years (1999, 2001, 2005 and 2010).

5.4.1 LULC trend of changes over decade

The case study noted the development in the past two decades, after long period of war and conflict started in year 1967 and ended in early 80's. The Egyptian government considered North Sinai as the future food basket of the country, helping to narrow the gap between population growth and food productivity (WFP 2006). The trend of change in the LULC in El-Arish is a function of the anthropological and environmental factors, as it is the case in most of the arid environment (Kassas 1977). The human impacts in the case study show how affects the water management and agricultural technology, which is quit poor. Arid environment made a kind of limitation of the suitable species to exist; these species have to be tolerant to drought and salinity as well. As shown in Figure 5.5, data representing the distribution of the LULC classes in (1999, 2001, 2005, and 2010). Bare soil was the largest area in the case study at all studied years, which was occupying approximately 78% (439.2 km²) in 1999 and changed to be 60% (339.7 km²) in 2010. The Urban class slightly increased from 4.75% (5.5 km²) in 1999 to be 5.40% (30.7km²) in 2010. A dramatic increase was monitored in year 1999 for the vegetation cover from 1.08% (6.1 km²) to be 7.94% (45.2 km²) in year 2010, the main causes of the vegetation increase during 1999-2010 are: (1- agriculture development and land reclamation and (2- population growth in North Sinai, list of the vegetation in the study area, as shown in Table 5.3. The fertile soil class rapidly increased over years from 5.12% in 1999 and reached 18.38% (104.7km²) in 2010. The sand dune class changed according to the wind storms events which occurring from January to April. These events can decrease the vegetation cover by affecting the marketability of the vegetables and fruits and increase the phyto-pathogens through the scratches.

Table 5.3. List of vegetation in the study area

- Date Palm	- Cucumber
- Peach	- Eggplant
- Apricot	- Zucchini
- Almonds	- Watermelon
- Calamondins	- Cantaloupe

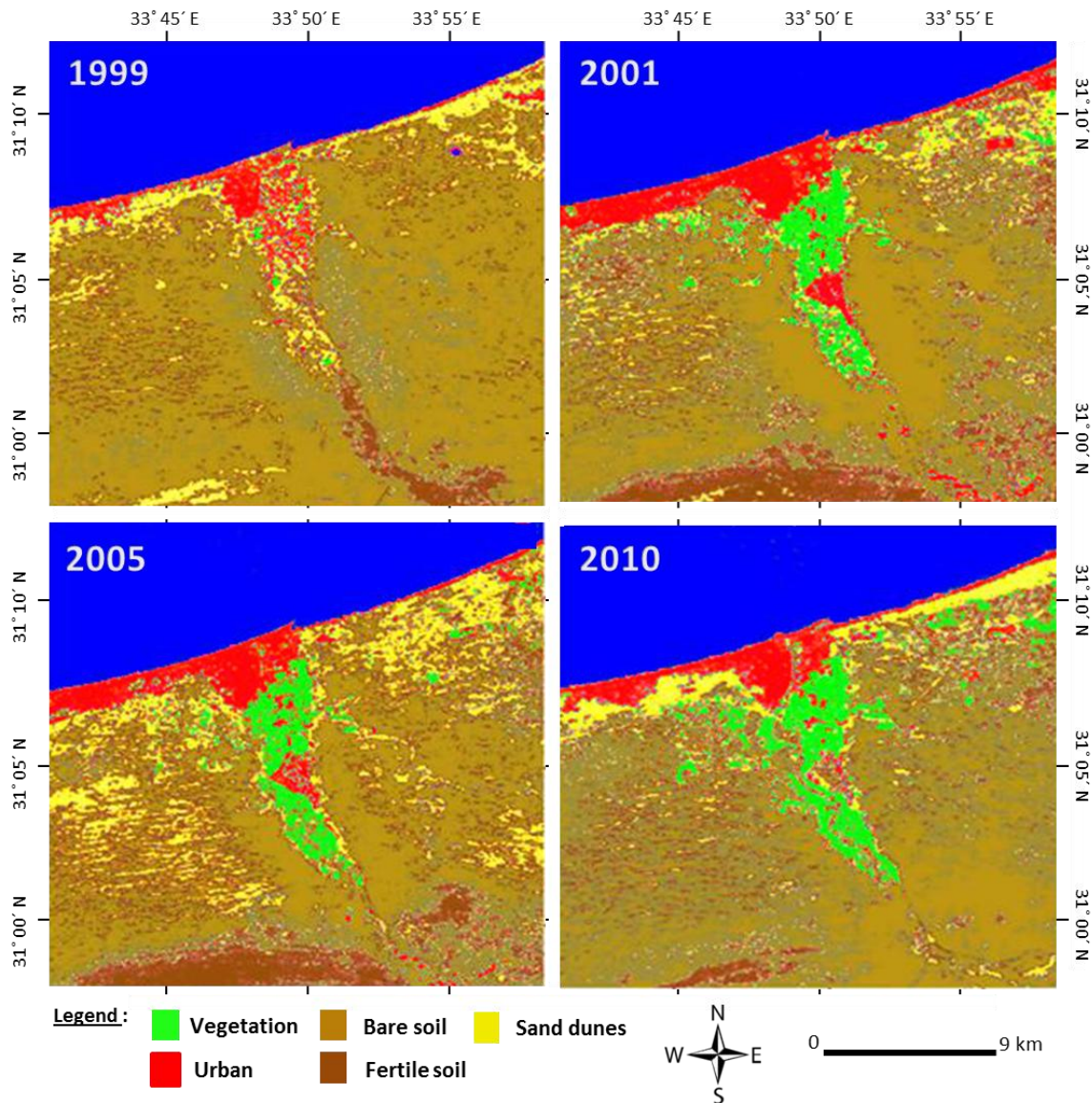


Figure 5.5. The distribution of LULC in percentage for E-l Arish city years (1999, 2001, 2005 and 2010).

5.4.2 Causes of LULC change trajectory

During the period of change (1999-2005) the government started a national project called “El-Salam Canal”. This project aimed to transport fresh water to North of Sinai for agricultural activities. In the year 1991 the immigration rate from other cities in Egypt to El-Arish was 0.6% and resulted in a 3.5% total population growth. In the end of 2001 this number jumped to 1.4% from 4% total population growth. The increase of vegetation cover (+4.07%) and fertile soil (+12.47%) responded positively to the increase of the urban expansion (+1.39 %), comparing to the decrease in bare soils (-22.46%), as shown in Figure 5.6a. Anthropological activities such as agricultural development, fresh water supply and land reclamation in the case study contributed to a dramatical decrease of the bare soils. Soil surface in the case study is vulnerable to wind motion, with less vegetation to cover

the soil it becomes more wind erodible. Wind speed records were high during February 2003, as shown in Figure 5.7, causing less visibility, blocking road networks, and defecting fruits marketability. The sand dunes increased (+4.53%) as a result of wind motion and palm trees, cultivated lands and roads were buried.

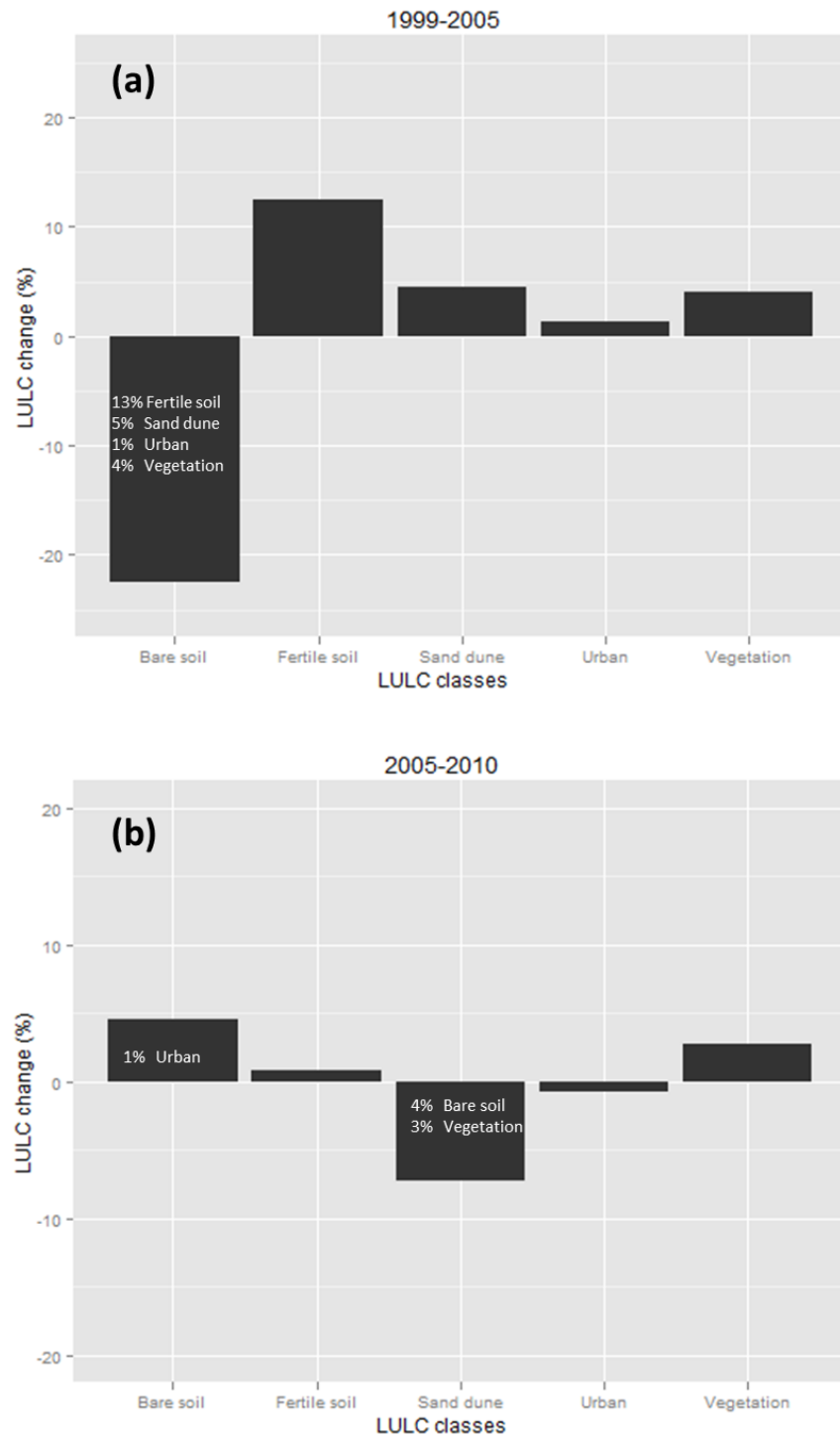


Figure 5.6. LULC change over the periods; **a)** the period between 1999-2005; and **b)** the period between 2005-2010.

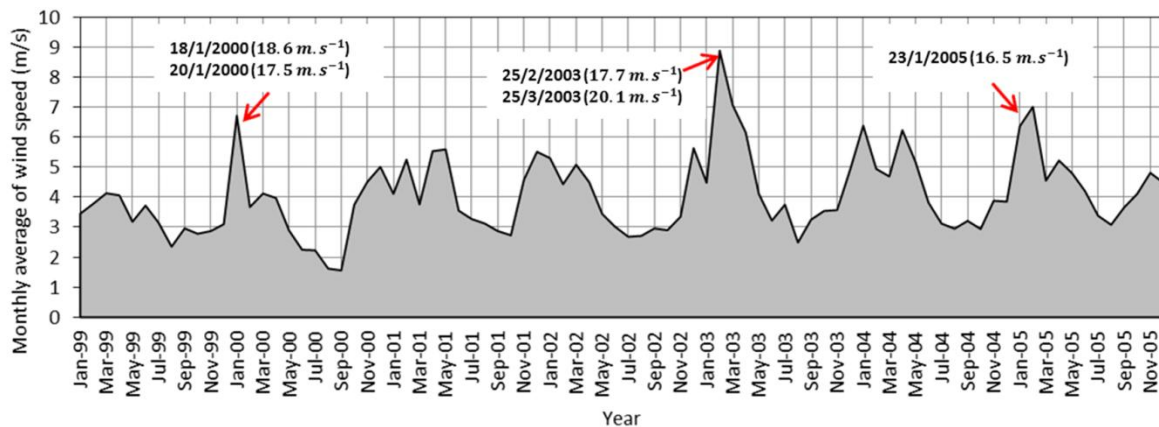


Figure 5.7. Monthly average of wind speed over period (1999-2005).

LULC in period of (2005-2010) were more distributed around the city centre and agricultural activities were densely located near the urban areas and expanded over Wadi El-Arish, where the soil is more suitable for cultivation. In January 2010, flash flood strike the case study, caused by heavy rains in the south and massive movement of this water to the north, as shown in Figure 5.8, this event destroyed most of the urban areas (-0.78%) which are located around Wadi El-Arish basin, as shown in Figure 5.6.b Vegetation (+2.79%) and fertile soil (+0.77%) increased furthermore with a slow pattern of change.



Figure 5.8. Photos taken during the field work in case study, **a)** the flood covered the public market in the valley, first day of flood; **b)** the second day of the flood when it's destroyed the houses on the beach.

5.5 Conclusion

Generally, the integration of Image enhancement, maximum likelihood supervised classification and visual interpretation are providing LULC data with better accuracy of ~95% to ~ 90% and is thus an effective method to monitor LULC changes. El-Salam Canal project has taken place during the last decade and obviously affected the LULC changes in the case study. Land degradation in El-Arish has been slowing down the agriculture development during the past 11 years.

In particular, the period of (1999-2005) has a major decrease in bare areas which is used for agriculture activities and urban settlement. Bare lands in the period of (2005-2010) have increased as a result of slow development policies such as land reclamation and natural hazard assessment. The vegetation cover shows remarkable changes over a decade as a result of two major factors, namely the human impact “anthropogenic activities” and the climate impact “wind and water erosion”. These changes in LULC are reflecting the impact of regional policies and the human dynamics and have resulted in increased food production, which can generate more future employment and a decline of the high population density in the Nile delta. Probably environmental sanitation and anti-desertification strategies will help the local community to avoid or decrease the natural hazards that might affect the agriculture production in the case study.

5.6 References

- Abd El-Kawy OR, Rød JK, Ismail H a., Suliman a. S (2011) Land use and land cover change detection in the western Nile delta of Egypt using remote sensing data. *Applied Geography* 31:483–494.
- Abdel Kawy WAM, Abou El-Magd IH (2012) Use of satellite data and GIS for assessing the agricultural potentiality of the soils South Farafr Oasis, Western Desert, Egypt. *Arabian Journal of Geosciences*. doi: 10.1007/s12517-012-0518-5
- Batisani N, Yarnal B (2009) Urban expansion in Centre County, Pennsylvania: Spatial dynamics and landscape transformations. *Applied Geography* 29:235–249.
- Chander G, Xiong X (Jack), Choi T (Jason), Angal A (2010) Monitoring on-orbit calibration stability of the Terra MODIS and Landsat 7 ETM+ sensors using pseudo-invariant test sites. *Remote Sensing of Environment* 114:925–939.
- Chavez PS (1988) An improved dark-object subtraction technique for atmospheric scattering correction of multispectral data. *Remote Sensing of Environment* 24:459–479.
- Chen J, Zhu X, Vogelmann JE, et al. (2011) A simple and effective method for filling gaps in Landsat ETM+ SLC-off images. *Remote Sensing of Environment* 115:1053–1064.
- Coppin P, Jonckheere I, Nackaerts K, et al. (2004) Digital change detection methods in ecosystem monitoring: a review. *International Journal of Remote Sensing* 25:1565–1596.
- Davis PH, Swain SM (1978) *Remote Sensing: The Quantitative Approach*. McGraw-Hill College, NY. pp396.
- Donegan SJ, Flynn LP (2004) Comparison of the response of the Landsat 7 Enhanced Thematic Mapper Plus and the Earth Observing-1 Advanced Land Imager over active lava flows. *Journal of Volcanology and Geothermal Research* 135:105–126.
- Du P, Li X, Cao W, et al. (2010) Monitoring urban land cover and vegetation change by multi-temporal remote sensing information. *Mining Science and Technology (China)* 20:922–932.
- El-Bana M, Shaltout K, Khalafallah A, Mosallam H (2010) Ecological status of the Mediterranean *Juniperus phoenicea* L. Relicts in the desert mountains of North Sinai, Egypt. *Flora - Morphology, Distribution, Functional Ecology of Plants* 205:171–178.
- Etteieb S, Louhaichi M, Kalaitzidis C, Gitas IZ (2012) Mediterranean forest mapping using hyper-spectral satellite imagery. *Arabian Journal of Geosciences*. doi: 10.1007/s12517-012-0748-6
- Foody GM (2002) Status of land cover classification accuracy assessment. *Remote Sensing of Environment* 80:185–201.
- Foody GM (2010) Assessing the accuracy of land cover change with imperfect ground reference data. *Remote Sensing of Environment* 114:2271–2285.
- Herold M, Mayaux P, Woodcock CE, et al. (2008) Some challenges in global land cover mapping: An assessment of agreement and accuracy in existing 1 km datasets. *Remote Sensing of Environment* 112:2538–2556.
- Huete A. (1988) A soil-adjusted vegetation index (SAVI). *Remote Sensing of Environment* 25:295–309.
- Jiyuan L, Mingliang L, Xiangzheng D, et al. (2002) The land use and land cover change database and its relative studies in China. *Journal of Geographical Sciences* 12:275–282.
- Kassas M (1977) Arid and semi-arid lands: problems and prospects. *Agro-Ecosystems* 3:185–204.
- Kelarestaghi A, Jafarian Jeloudar Z (2009) Land use/cover change and driving force analyses in parts of northern Iran using RS and GIS techniques. *Arabian Journal of Geosciences* 4:401–411.
- Khalifa IH, Arnous MO (2010) Assessment of hazardous mine waste transport in west central Sinai, using remote sensing and GIS approaches: a case study of Um Bogma area, Egypt. *Arabian Journal of Geosciences* 5:407–420.
- Lyon JG, Yuan D, Lunetta RS, Elvidge C (1998) A change detection experiment using vegetation indices. *Photogrammetric Engineering and Remote Sensing* 64:143–150.
- Masoud a. a., Koike K (2006) Arid land salinization detected by remotely-sensed landcover changes: A case study in the Siwa region, NW Egypt. *Journal of Arid Environments* 66:151–167.
- Matinfar HR, Alavi Panah SK, Zand F, Khodaei K (2011) Detection of soil salinity changes and mapping land cover types based upon remotely sensed data. *Arabian Journal of Geosciences*. doi: 10.1007/s12517-011-0384-6
- Mohamed ES, Belal A, Saleh A (2012) Assessment of land degradation east of the Nile Delta, Egypt using remote sensing and GIS techniques. *Arabian Journal of Geosciences*. doi: 10.1007/s12517-012-0553-2
- Petrou M, Bosdogianni P (1999) *Image Processing: The Fundamentals*. John Wiley & Sons, Ltd., Chichester, UK. pp 347.

- Pontius RG, Millones M (2011) Death to Kappa: birth of quantity disagreement and allocation disagreement for accuracy assessment. *International Journal of Remote Sensing* 32:4407–4429.
- Qin D, Jianwen M, Yun OY (2006) Remote sensing data change detection based on the CI test of Bayesian networks. *Computers & Geosciences* 32:195–202.
- Rahdari V, Abadi SMN, Amiri F, et al. (2012) Detection of land use/cover changes over Chah Nimeh in Iran using Landsat TM images. *Fresenius Environmental Bulletin* 21:3825–3835.
- Richards JA (2013) *Remote Sensing Digital Image Analysis: An Introduction*, 5th ed. Springer-Verlag, Berlin, Heidelberg. pp494.
- Rozenstein O, Karnieli A (2011) Comparison of methods for land-use classification incorporating remote sensing and GIS inputs. *Applied Geography* 31:533–544.
- Shalaby A, Tateishi R (2007) Remote sensing and GIS for mapping and monitoring land cover and land-use changes in the Northwestern coastal zone of Egypt. *Applied Geography* 27:28–41.
- Thomlinson J, Bolstad P, Cohen W (1999) Coordinating methodologies for scaling landcover classifications from site-specific to global: steps toward validating global map products. *Remote Sensing of Environment* 70:16 – 28.
- Weng Q (2010) *Remote Sensing and GIS Integration Theories, Methods, and Applications*. The McGraw-Hill, NY. pp433.
- Weng Q (2002) Land use change analysis in the Zhujiang Delta of China using satellite remote sensing, GIS and stochastic modelling. *Journal of Environmental Management* 64:273–284.
- WFP (2006) *Country Programme-Egypt (2007–2011)*. World Food Programme, Rome. pp25.
- Wrigley RC, Spanner MA, Slye RE, et al. (1992) Atmospheric correction of remotely sensed image data by a simplified model. *Journal of Geophysical Research* 97:18797.
- Xian G, Homer C, Fry J (2009) Updating the 2001 National Land Cover Database land cover classification to 2006 by using Landsat imagery change detection methods. *Remote Sensing of Environment* 113:1133–1147.
- Yan CZ, Song X, Zhou YM, et al. (2009) Assessment of aeolian desertification trends from 1975's to 2005's in the watershed of the Longyangxia Reservoir in the upper reaches of China's Yellow River. *Geomorphology* 112:205–211.
- Yeganeh H, Khajedain S jamale, Amiri F, Shariff ARBM (2012) Monitoring rangeland ground cover vegetation using multitemporal MODIS data. *Arabian Journal of Geosciences*. doi: 10.1007/s12517-012-0733-0
- Zheng W, Liu C, Zeng Z, Long E (2007) A Feasible Atmospheric Correction Method to TM Image. *Journal of China University of Mining and Technology* 17:112–115.
- Zhou W, Troy A, Grove M (2008) Object-based Land Cover Classification and Change Analysis in the Baltimore Metropolitan Area Using Multitemporal High Resolution Remote Sensing Data. *Sensors* 8:1613–1636.

Chapter 6

Object-based image analysis for monitoring the spatial distribution of a halophytic species in an arid coastal environment

This chapter is modified from:

Nasem Badreldin, J. Uria-Diez, J. Mateu, Ali Youssef, Cornelis Stal, Magdy El-Bana, Ahmed Magdy and Rudi Goossens (2013) Object-based image analysis for monitoring the spatial distribution of a halophytic species in an arid coastal environment. *Applied Geography*. “Submitted”

6.1 Introduction

The spatial distribution of natural plants in an arid environment such as the Halophytic Species (HS) is usually not random, and there is a variety of factors that influence this distribution, these factors are classified into two general classes: (1) environmental factors that are spatially heterogeneous such as soil properties and microtopography; and (2) genetic factors that make the natural plants tolerance to survive in adverse environmental conditions (Dale 1999). Many studies found a relationship between the natural plants distribution and environmental heterogeneity, such as soil depth (Kenneth A. Kershaw 1959), topography (Greig-Smith 1961), soil nutrients (Galiano 1985), positions of subsurface rocks (Usher 1983), and soil salinity, which is considered as the most abiotic factors associated with HS distribution (Rubio-Casal et al. 2001; Ungar et al. 1977).

In the past 10 years, digital image processing proved to be a useful approach in ecological and environmental sciences via improving image quality (Schowengerdt 2007). Such this improvement can be established using the standard image processing techniques, which can represent the case study as digital dataset with more than 90% accuracy (Liu and Mason 2009; Quets et al. 2013). Developing an appropriate and powerful image processing algorithms are depending on the transformations of functionalities by neighborhood processing techniques, which allowed the parallel processing of images in real time with conceptually high-level operations (Shih 2010).

Satellite images were often used as datasets for environmental monitoring, and the main approach was to capture numerically the coordinates of the studied points or habitats. The digital image processing techniques deliver additional information about environment status, which required a data validation from the field survey (Blaschke 2010; Illian et al. 2008; Vincent and Soille 1991; Winkler 2006). Google Earth provided a high resolution satellite images and freely accessible to the public, many researchers found these images were valuable for environmental studies, because of its exceptional quality (Frankl et al. 2013; Sadr and Rodier 2012; Sheppard and Cizek 2009; Taylor and Lovell 2012; Yang et al. 2012; Quets et al. 2013).

In ecological studies the explicit considerations of spatial structures played an important role in understanding and managing ecological processes. If we include the spatial component of the studied community, we could characterize the nature and intensity of spatial relationships between organisms and their environment (Fortin and Dale 2009). Investigation of the spatial structure using point pattern analysis can therefore be a first step providing important insights into the processes affecting community ecology (Perry et al. 2006). Spatial point processes (as Gibbs models) exhibit

spatial interactions at only a single spatial scale, whereas natural processes exhibit dependence at multiple scales.

The specific objectives for this investigation were 1)- to improve Google Earth image using different digital image processing operators, in order to obtain the HS spatial distribution, and understand the local environmental variables impact, and then 2)- to analyze the spatial distribution of the community of halophyte species in El-Zaraniq Protected Area, North Sinai, Egypt, providing a combination of models that best reflect the observed structures.

6.2 Case study description, field survey and data collection

About 95% of the total area of Egypt is covered by desert, while about 85 million inhabitants depend on the remaining 5% of the land (Abd El-Kawy et al. 2011; Shalaby and Tateishi 2007). The case study is conducted in the northern side of El-Zaraniq Protected Area in North Sinai Governorate, Egypt, between latitudes 31° 7' 12.38", 31° 7' 1.46"N and longitudes 33° 30' 18.44", 33° 30' 29.99"E. The study area is about 10.25 hectare, as shown in Figure 6.1. Based on the classification system (soil taxonomy) that was developed by the United States Soil Conservation Services (USSCS), the major soil group that has been found in the case study is Entisols (Greenwood 1997), Natural Resources Conservation Service, NRCS (1999) described the soils of Entisols order as having little or no development of pedogenic horizons which consists mainly of quartz. According to climate classification of Kotttek et al. (2006) and Peel et al. (2007), Sinai is generally classified as (Bwh) arid-desert-hot climate, however the climate of El-Zaraniq is a Mediterranean arid type; temperature in the summer is above 35 °C and ~ 15 °C in the winter, the mean annual precipitation is about 150 mm with ±50 mm. The vegetation in Zaraniq comprises over 150 plant species (El-Bana et al. 2002).

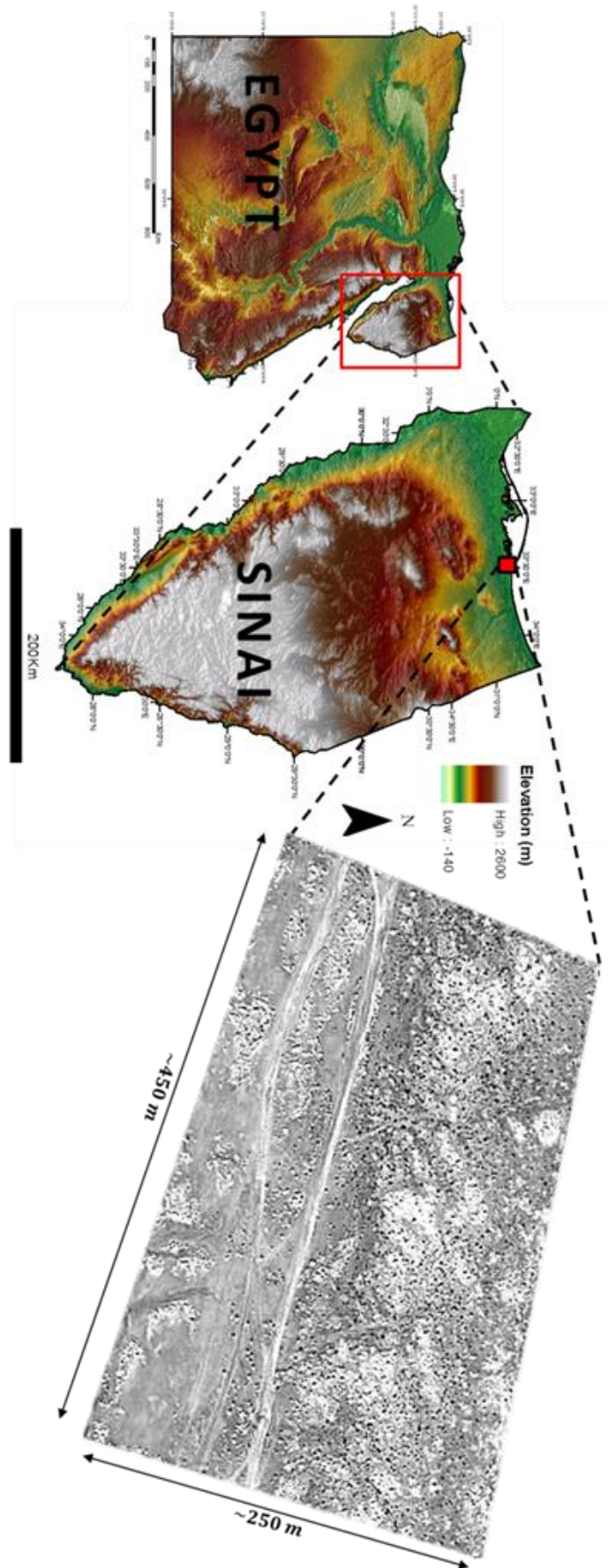


Figure 6.1 . The geographical location and dimension of the case study.

The field survey and data collection were carried out during January 2012. At this time of the year, the vegetation covers at its maximum growth stage. Also, the minimum accumulation of salts at the soil surface offered better living conditions to the HS that investigated in the case study.

The data collection is based on unbiasedness and representativeness in order to control sampling error. Soil surface characteristics, HS distribution and available measuring tools are considered carefully for further statistical analysis and data mapping. Ground control points and soil samples were selected by means of a systematic sampling technique at the corners of an about 1000 m square grid.

90 soil samples were obtained from the top soil surface (25cm depth) during the field work. The soil samples were analyzed in the laboratory using 1/5 diluted extracts for soil salinity and 1/2.5 for soil pH analysis (U.S. Salinity Laboratory, 1954). The soil salinity refers to the total concentration of dissolved salts per unit volume, salt concentration is actually indicated in Electrical Conductivity (EC) which is expressed in units of DeciSiemens/m (Rhoades, 1992). pH measurement is a parameter used for indicating the acidity status of soil, the ranges of pH is from 0 to 14, 7 is the neutral status, below 7 is acidic, and basic is above 7 (Blanco-Canqui and Lal 2010). Elevation of case study is delivered from high resolution topographic maps.

6.3 Materials and methods

6.3.1 Image pre-processing

The study was based on a Google Earth image with resolution of about 0.5 m, which was provided via Google Earth. The satellite image was acquired for a date of January, 2012 in a clear atmospheric condition with no presence of clouds or sandstorms, which could affect the image visualization.

Image pre-processing is an essential treatment for object-based image analysis research in order to establish the direct link between the image and the case study (Badreldin and Goossens 2013a; Coppin et al. 2004). Various image pre-processing operations were considered, including image enhancement, and geometric correction. ENVI 4.5, MatLab and R software were used for digital image analysis in this investigation.

6.3.1.1 Image enhancement

The purpose of this stage was to improve subjectively the images for better analysis. Manipulating the image histogram was carried out in order to increase the highest possible contrast and remove noises (Petrou and Bosdogianni 1999). Point operation for modifying the image histogram is considered as the most powerful technique to optimize the best brightness and contrast for highlighting information in particular DN ranges without changing the image size, as shown in Figure 6.2.

$$y_{ij} = f(x)_{ij} \quad (6.1)$$

Where y_{ij} is the output pixel value, which is a function f of $(x)_{ij}$ DN of a pixel at line i and column j

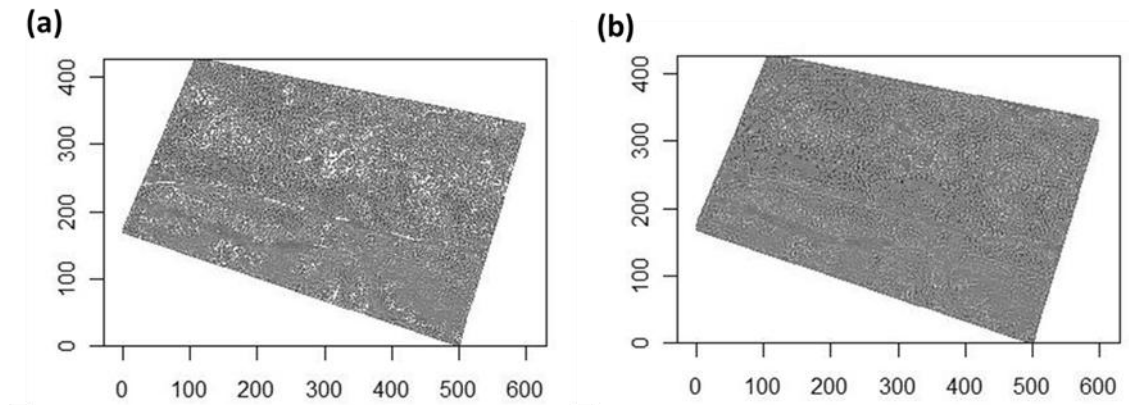


Figure 6.2. The radiometric correction of the satellite image of the case study; **a)** the original satellite image ; and **b)** after the image enhancement.

6.3.1.2 Geometric correction

Object-based image studies required geometric corrections in order to exploit image usefulness and obtain accurate results (Knorn et al. 2009). geo-referencing Google Earth image was based on Keyhole Markup Language (KML), which was converted later to a shapefile using ESRI ArcGIS 9.3, Google Earth image was rectified with shapefile that contained the exact coordinates of the case study, the root mean square error (RMSE)<0.015 pixels.

6.3.2 Object - pixels relationship

The extracted objects from the image were based on the assumptions that explained the spectral response for each plant within that pixel. We assumed that each plant location is represented in the image with a distinctive spectral response, most of HS were observed on the top of sand accumulation called “phytogenic hummocks” with 0.5 m height average (El-Bana et al. 2007). The illustration draws of this phenomenon, as shown Figure 6.3a, b, are explained the difference in solar

radiation reflectance between HS and hummocks' edges. The plant position gave more reflectance than the surrounded area which is exposed "barren soil" and cause scattering to most of the incident solar radiation that is received from the sun (Figure 6.3c).

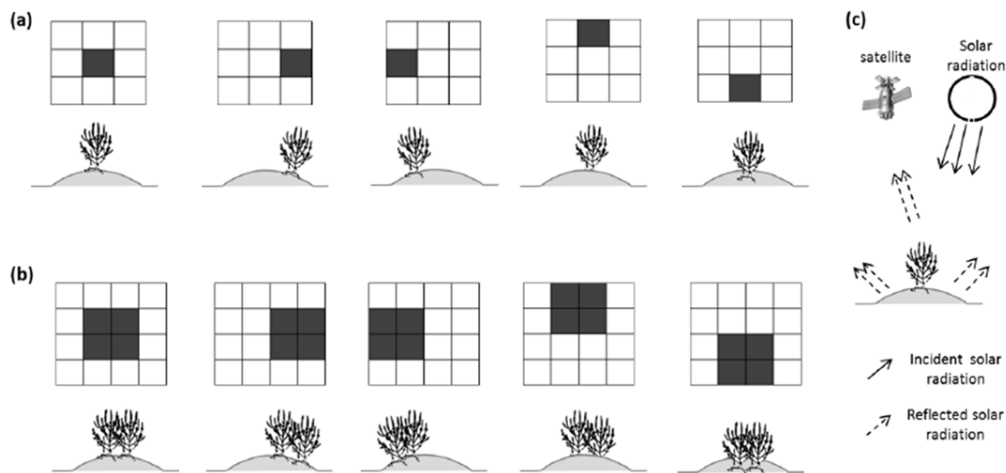


Figure 6.3. Illustration draws of the target objects "HS"; **a)** single object position; **b)** group of objects positions; and **c)** the reflectance and absorbed solar radiation pattern. Object extraction analysis.

We implemented three different types of operators in image processing and spatial filtering to extract the target objects by image convolution, which are the standard operators in digital image processing, and based on moving identified kernels over all pixels within the image boundaries. In the context of image processing, 3×3 kernel size was used as an input array and multiplied with grey level scale image; the resultant image presented both characteristics, as shown in Figure 6.4

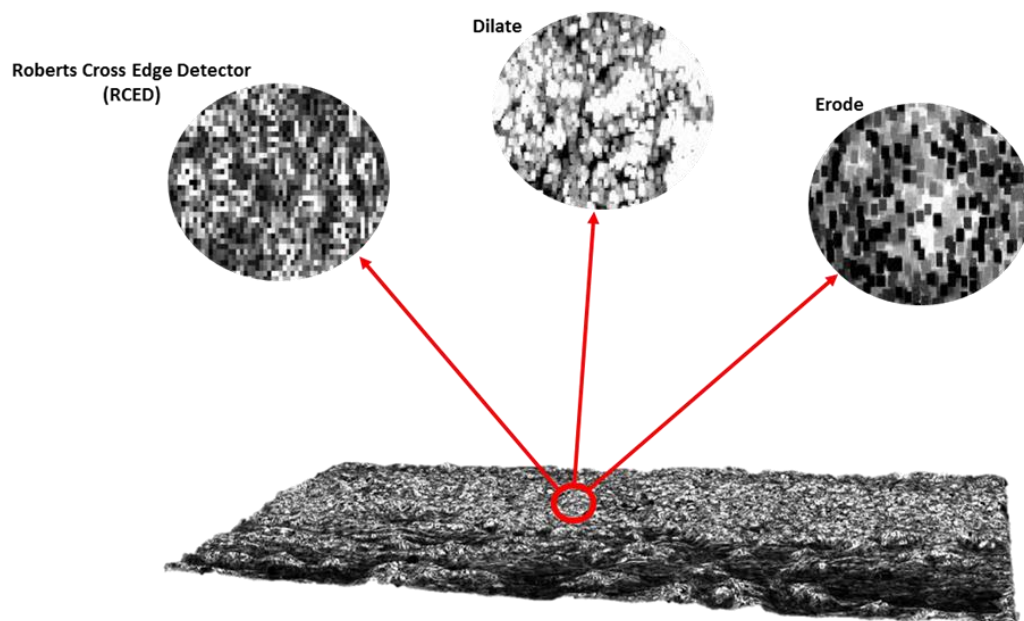


Figure 6.4 Three different types of operators (RCED, Dilate and Erode) for image processing and spatial filtering to extract the plant positions target objects by image convolution.

6.3.2.1 Roberts Cross Edge Detector (RCED)

RCED is a non-linear filter that is similar to the Sobel operator, standard and quick to compute on a greyscale image are the advantages of this operator. Also, this method is based on 2D differencing for sharpening edges and object isolation, and it is not possible to change filter size and edit kernels. In theory, the operator consists a pair of 3x3 convolution kernel masks, one kernel is simply the other rotated by 90 degree. The masks was applied separately in the studied image in order to produce a separate measurements of the gradient component in each orientation (call these Rx and Ry), these masks can then be combined to find the absolute magnitude of the gradient. The gradient magnitude was given by:

$$|R| = \sqrt{Rx^2 + Ry^2} \quad (6.2)$$

An approximate gradient magnitude was computed using:

$$|R|=|Rx|+|Ry| \quad (6.3)$$

6.3.2.2 Dilate Operator (DO)

DO was used to expand bright pixels and enhances dark spots in the image. The output was built on principle of filling the holes smaller than the structural kernel in our panchromatic image. Brining every pixel in the studied image into a line with the darkest pixels of the 8 neighbouring in 3x3 matrix.

$$d=i\oplus k \quad (6.4)$$

6.3.2.3 Erode Operator (EO)

EO was used to reduce the clustered bright pixels and expand dark ones. The values of the output pixels are the minimum values of all the pixels in the input pixel's neighbourhoods.

$$e=i\ominus k \quad (6.5)$$

6.3.3 Data validation

In order to evaluate the results of the object extraction analysis, the field survey data was used as a reference. If this experimental data set totally correlates with the estimated generated by the edge

detectors, the Euclidean distance between a field measurement and an estimated point should be equal to zero. Since the estimated locations were determined using a prior kernel size and the edge detectors are sensitive to noise, there will be a deviation between the measured and estimated locations. For each measured point, the nearest location from each edge detector was selected. The distances between this measured point and its nearest counterpart were analyzed, resulting in a mean distance and standard deviation as demonstrated in Table 6.1.

Table 6.1. Summary statistics of the field survey data and the estimated object's location

	Robert	Erode	Dilate
Count	87	87	87
Mean [m]	7.70	23.31	12.60
St. Dev [m]	5.96	17.56	8.35

Intuitively, it will be clear that the distribution of these deviations will not be normal, but will rather follow a gamma distribution. This distribution is illustrated by Figure 6.5, where the cumulative frequencies are plotted against the distance between a measured point and estimated point. Each edge detector is represented by a curve. Based on this figure, as well as the Table 6.1, it becomes clear that RCED is the best operator that represents the HS locations in this particular case study.

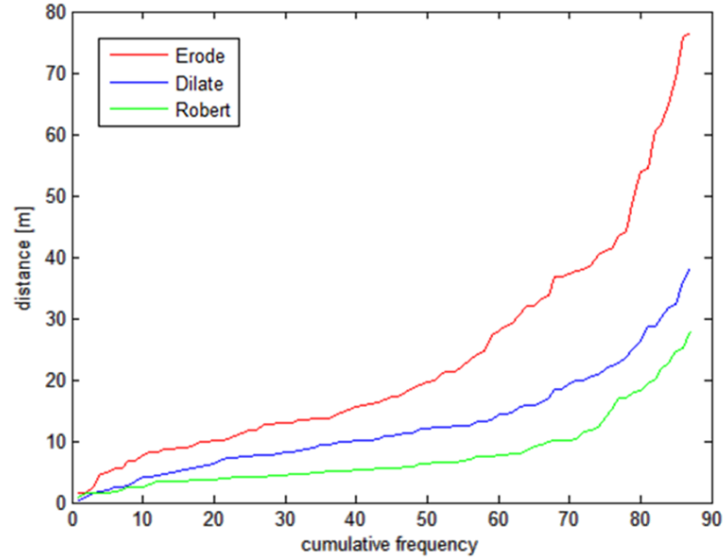


Figure 6.5. Cumulative frequencies distribution and distance between the measured estimated points.

The obtained soil samples that represent soil salinity and pH are denoted $z(x_1), z(x_2), \dots, z(x_n)$, Where x_i is location vector and n is the number of observations, which were used for predicting the uncollected soil samples inside each grid over all case study area using Ordinary Kriging (OK) (Webster and Oliver 2007).

$$Z(x_0) = \sum_{i=1}^m \lambda_i z(x_i) \quad (6.6)$$

Where m is the number of neighbours that have been observed and λ_i are the weights.

90 soil samples were used for cross-validation, and 22 independent soil samples were collected randomly from the case study for validating EC and pH maps. Two accuracy assessment parameters were used, 1) Root Mean Square Error (RMSE) to indicate how far the predicted values from the data measurement and 2) Root Mean Square Standardized Error (RMSSE) to identify whether the predicted values are under/overestimation (Webster and Oliver 2007).

$$RMSE = \sqrt{\frac{1}{n} \sum_{i=1}^m \{Z(x_0) - z(x_i)\}^2} \quad (6.7)$$

$$RMSSE = \sqrt{\frac{\sum_{i=1}^m [Z(x_0) - z(x_i)]^2 / \sigma(x_i)}{n}} \quad (6.8)$$

Where $\sigma(x_i)$ is the estimated error variance and n is the sample size

Validation results of OK method confirm the accuracy of the predicted EC and pH maps, the correlation coefficient calculated between measured and estimated EC and pH values, as shown in Table 6.2.

Table 6.2. Statistical parameters (RMSE and RMSSE) for soil EC and pH validation, based on cross validation (n=90) and separate datasets (n=22).

	Statistical parameter	EC	r^2	r	pH	r^2	r
Cross validation	RMSE	0.3993	n=90		0.4199	n=90	
	RMSSE	0.7678	0.8323	0.912	0.9526	0.3647	0.607
Separate dataset	RMSE	0.4053	n=22		0.2459	n=22	
	RMSSE	1.0840	0.8614	0.928	0.6034	0.7929	0.882

The spatial distribution of soil salinity and pH are essential to understand the spatial distribution patterns of HS in the case study. As shown in Figure 6.6, the eastern side of the case study is more affected by high soil salinity (> 4 dS/m) and alkalinity (pH >9), which are representing a serious land degradation condition in the study site.

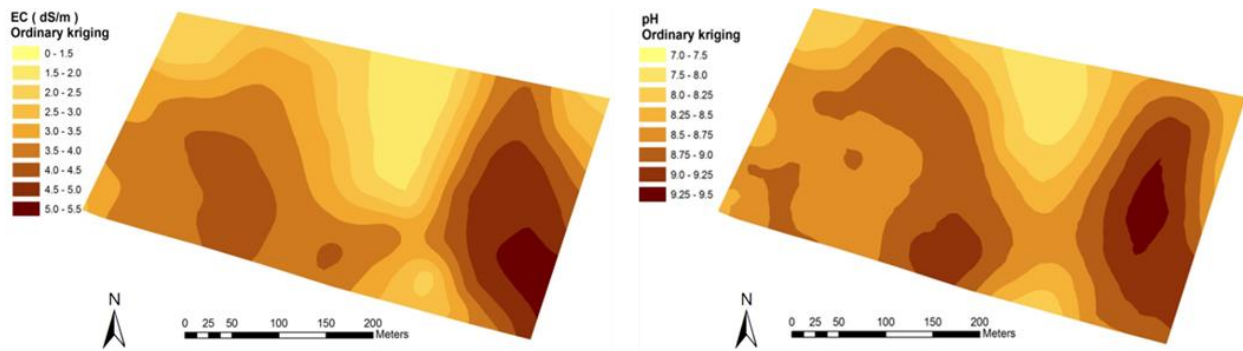


Figure 6.6. The spatial distribution of the soil salinity (EC) and pH in the case study.

6.3.4 Spatial analysis and statistical modelling

A point process is a random collection of points in some space. Point processes are useful statistical tools that can be applied in a variety of scientific fields such as forestry, epidemiology or ecology. Modeling and inference for spatial point processes is an issue that has been investigated broadly in the last few years. The wide range of application fields has been the main engine driving such raised interest.

In the statistical analysis of spatial point pattern data, a parametric modelling approach requires a supply of stochastic models for point patterns. One important source of models is the class of finite Gibbs point processes. Many models of this class can be fitted rapidly to real data sets containing large numbers of points (Baddeley and Turner 2000, 2006; Diggle 2003; Geyer 1999; Moller and Waagepetersen 2003).

However, in practice, Gibbs models currently available for use in data analysis are few in number and limited in scope. The most commonly used Gibbs models exhibit spatial interaction at only a single spatial scale, whereas most natural processes exhibit dependence at multiple scales. The key problem is that the construction of new Gibbs models *ab initio* is not trivial. Gibbs models are usually defined using the un-normalised probability density h . While it is easy to write down a new functional form for h , it is not always obvious whether h is integrable, so that the normalising constant is finite and the process is well-defined.

This paper considers a practical technique for constructing new Gibbs models from existing ones. The un-normalised densities (h_1, h_2) of two existing models are multiplied together, to form a new hybrid un-normalised density $h(x) = h_1(x) \cdot h_2(x)$. This is called hybridisation and it defines a way to construct new point process models to be fitted to data. Hybrids are particularly useful for modelling interactions at multiple scales. This method has been demonstrated to be useful on a real dataset on human social interaction (Baddeley et al. 2013). Here we give another example based on

real data from object-based image for a high resolution Google Earth satellite image of HS in a protected area from the coastal desert of North Sinai in Egypt.

The analysis and construction of hybrids models run through several modeling steps. We first investigated the spatial inhomogeneity, and then the evidence of any interaction between points. Then, with this previous analysis we start building models of increasing complexity with the aim to describe the observed behavior of the data. The spatial trend was modeled using a parametric estimation with a linear combination of the EC covariate and a log-cubic function of the cartesian coordinates. This linear function was fitted by maximum likelihood using the Berman-Turner device (Berman and Turner 1992; Baddeley and Turner 2000). We checked its goodness-of-fit by smoothed partial residual diagnostics, which is a useful diagnostic for transformation of a covariate in a Poisson point process model. Then, considering the estimated degree of inhomogeneity through the fitted parametric first-order intensity function, we estimated the inhomogenous pair correlation function (Baddeley et al. 2000). Available Gibbs processes are able to model interpoint interaction and tend to have simple mathematical structure that cannot model complex patterns. In this paper we take three existing (and widely used) models (Hardcore, Geyer and Strauss spatial point processes), we multiplied the probability densities together and renormalise to obtain a new probability density. The resulting model is a hybrid, particularly useful for point patterns which exhibit interaction at different spatial scales.

6.4 Results and discussions

6.4.1 Soil salinity and microtopography relationship

Soil salt accumulation in an arid climate condition is a dominant land degradation process in the case study, where the evaporation is higher than the precipitation. This arid condition with the seepage of Mediterranean Sea water causing water logging to salty ground, which formed surface salt crust and increased soil salinity (Badreldin and Goossens 2013b; Goossens and Van Ranst 1998). The microtopographical characteristics are influencing the distribution of soil salinity in the case study, the lower micro-elevation the higher salt concentration and vice versa, as shown in Figure 7. Waterlogging is found in lower elevation < 2 meters (Figure 6.7, point 1) and between phytogenic

hummocks (Figure 6.7, points 2); these points are the most affected spots by the upraising of salty ground water, and more probably it will become more salinized in dry seasons. The soil salinity in (Figure 6.7, points 3) are $<3.8 \text{ dS.m}^{-1}$, which are provided a better environmental conditions for HS growth and survival.

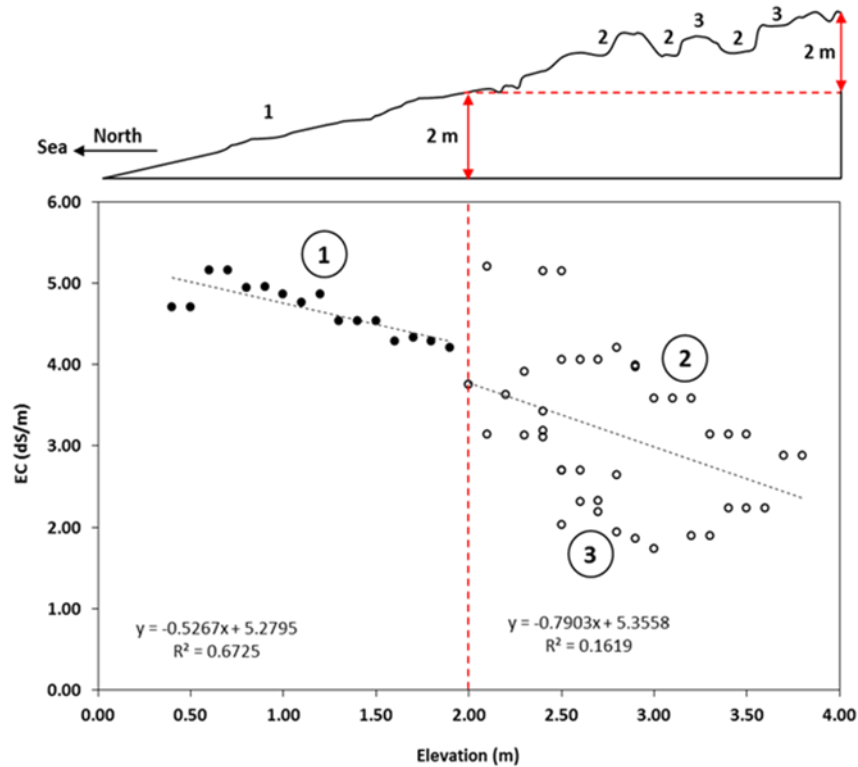


Figure 6.7. The relationship between the soil salinity (EC) distributions along with the micro-topography of the case study.

6.4.2 HS spatial distribution along with EC and pH

HS are distributed in different densities over the entire study site, as shown in Figure 6.8. The south eastern side of the case study contained low plant density ($<3 \text{ plants/m}^2$), unlike the northern side that had higher density ($>5 \text{ plants/m}^2$).

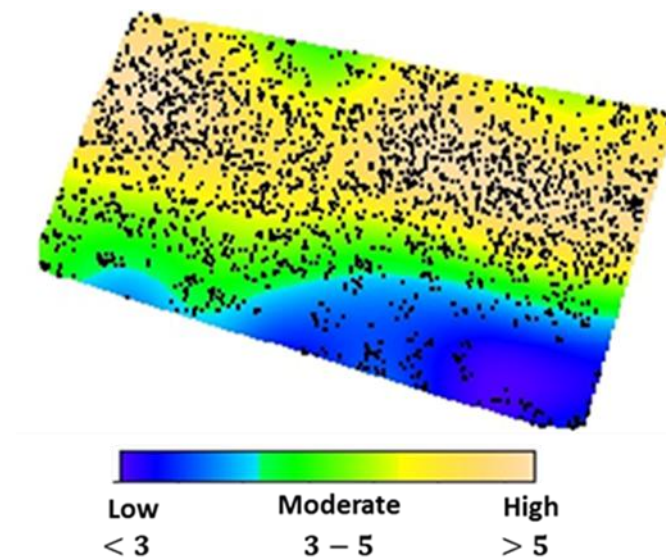


Figure 6.8. HS spatial distribution and density per m² in the case study

Soil salinity and pH are considered to be the local environmental variables that influenced the HS spatial distribution in the case study with the association of the microtopography. As shown in Figure 6.9, about 82% of HS in the case study were found in elevation of > 2m. Microtopography showed significantly negative correlations with pH and EC ($r = -0.79$ and -0.81 , respectively), the less elevation the higher soil salinity and soil alkalinity at each HS location. The spatial pattern of the extracted objects shown that the HS are avoided the severe abiotic spots which contained higher soil salinity and alkalinity in the case study.

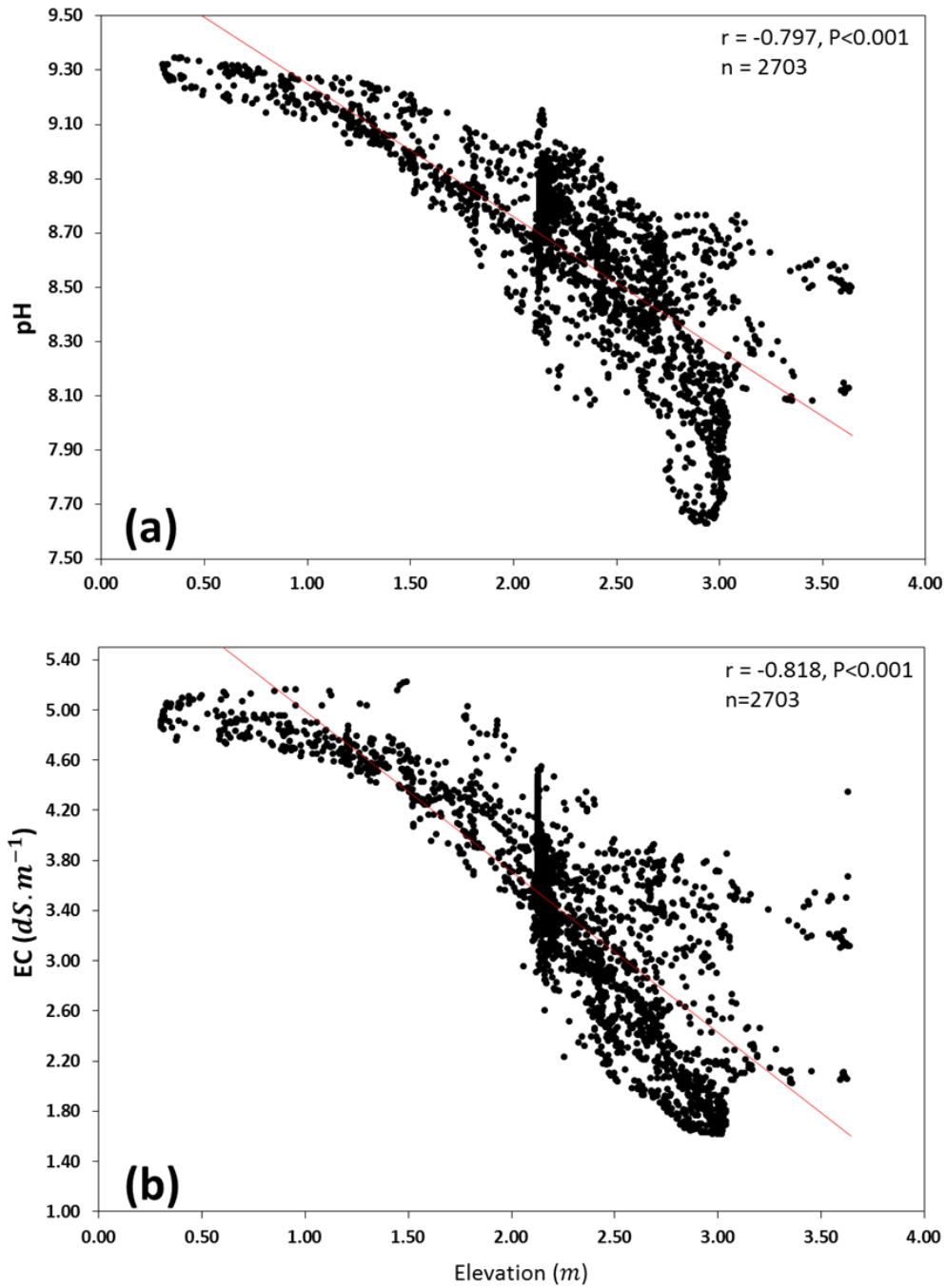


Figure 6.9. HS distributions over different micro-topography and it's relation with; **a)** pH; and **b)** EC.

The analysis of spatial structure and construction of hybrids starts studying the spatial inhomogeneity by providing a model for the first-order intensity function. The left panel in (Figure 6.10) shows the parametric estimation of the intensity modeled through a linear function of EC and a log-cubic function of the cartesian coordinates, fitted by maximum likelihood using the Berman-Turner device (Berman and Turner 1992; Baddeley and Turner 2000). The right panel (Figure 6.10) confirms the goodness-of-fit of this fitted model to the halophyte community intensity.

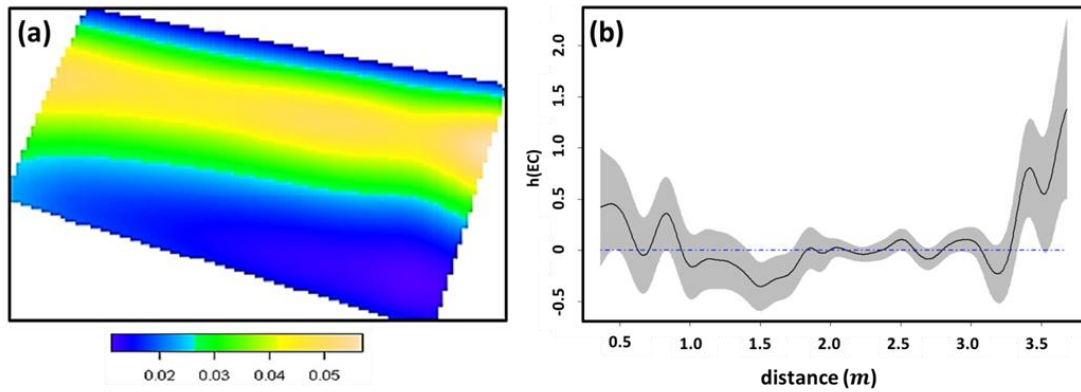


Figure 6.10. Spatial inhomogeneity of the halophyte community data; **a)** kernel smoothing estimates of ρ at different values of EC, Intensity units are individuals' shrubs per square meter in the halophyte community in El-Zaraniq protected area, North Sinai, Egypt; and **b)** Parametric estimate of intensity described by the spatial trend of EC and log-cubic function of coordinates fitted by maximum likelihood.

Figure 6.11, shows the estimate of the inhomogeneous pair correlation function (Baddeley, Moller, and Waagepetersen 2000) for the halophyte community using the fitted intensity function given in the right panel of (Figure 6.10). This function shows clear evidence of a “hard core” effect at distances less than about 1.3 m, combined with a strong attraction between distances between 1.3 and 10 m. Then for higher values it is shown a random spatial behavior of the halophyte community.

The hybrid procedure consists of the addition of different Gibbs models to capture the three observed behaviors (Figure 6.11, Table 6.3). We first fit an inhomogeneous hard core process with a spatial trend of EC and log-cubic function of the coordinates (Figure 6.12a). The simulated pattern (Fig 6.12a) does not appear to exhibit the same strong clustering as the data (Figure 6.8). The k-residual from the first model suggests a positive association between points, as it lies outside the confident intervals at a range from about 10 to 20 meters. The second model added to the previous hardcore process is a Geyer process (Figure 6.12b, Table 6.3). This second hybrid process has parameters of interaction radius at 1.4 meters and number of neighbors of 2, with a gamma parameter of 2.001. However, after including another Gibbs process, the second hybrid does not capture the low level of clustering of the process at these scales. Differences between AIC values were significant (Table 6.3) indicating that the addition of the Geyer clustering structure was significant. Our procedure was completed by a third step adding a Strauss process to the second hybrid model. With this third model we were able to capture the random pattern, as the fitted Strauss model showed a gamma parameter value of 1.002 (Table 6.3) for a range from 10 to 70 meters. This hybrid built with the three models is clearly the best among the previous ones taking into account the AIC values.

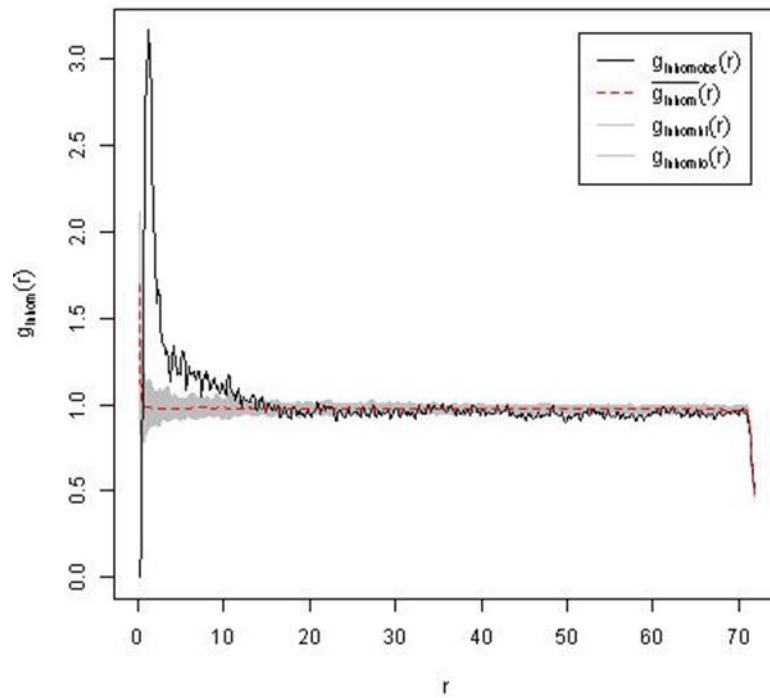


Figure 6.11. Graph showing pcf(r) functions with parametric kernel intensity with a spatial trend described by the EC and log-cubic function of coordinates, fitted by maximum likelihood in inhomogeneous version. The observed $g_{inhom}(r)$ values are expressed as a black solid line, and the grey polygon represents the limits of the 95% confidence intervals generated by Monte Carlo simulations, where r represents the distance examined in the halophyte community in El-Zaraniq protected area, North Sinai, Egypt.

Table 6.3. Parameters and comparison of values of Akaike's information criterion (AIC) among the three multi-scale hybrid models used to understand the spatial structure of halophyte community in El-Zaraniq protected area, North Sinai, Egypt. Parameters are r_0 radius of the hardcore process; r_1 interaction radius, sat is saturation threshold that is the number of close neighbors and γ is the interaction parameter of the Geyer process; r_2 is the interaction radius and γ is the interaction parameter of the Strauss process.

gamma (γ) is the interaction parameter of the Strauss process.						
	Hardcore	Geyer		Strauss		AIC
	r0	r1/sat	gamma (γ)	r2	gamma (γ)	
First model (a)	1.2	-	-	-	-	23313.99
Second model (b)	1.2	1.4/2	2.128	-	-	18927.55
Third model (c)	1.2	1.4/2	2.001	12	1.022	14245.2

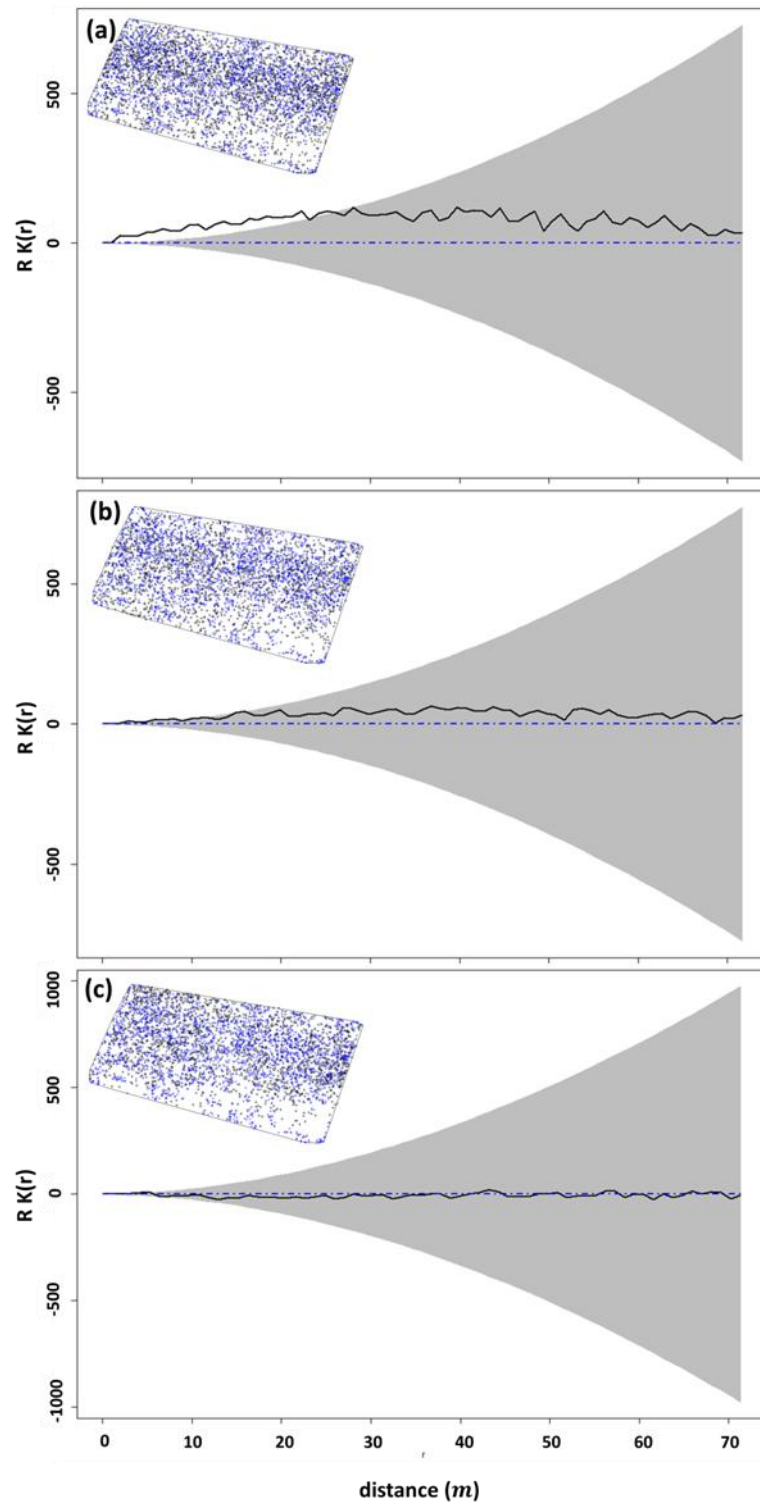


Figure 6.12.

Diagnostics for models of the halophyte community data for k -residual function and simulated realizations, the plus symbols “extracted point pattern”, and the blue circle “simulated point pattern” using; **a)** hardcore; **b)** hardcore plus geyer; and **c)** hardcore plus geyer and Strauss processes with parametric intensity estimation used in the halophyte community in El-Zaraniq protected area, North Sinai, Egypt.

6.5 Conclusion

The integration between field survey, digital image processing, and point pattern analysis provided better understanding to the local environment conditions and explaining more accurately the HS spatial distribution in the case study. RCED is proven to be the best object extraction operator which provide accurate information about HS distribution and met the assumption design that explained the local environmental condition of the case study.

Generally, about 82% of HS are found on elevation > 2m, the microtopography found to be strongly correlated with both soil pH and EC ($r = -0.79$ and -0.81 ; $p < 0.001$, respectively). Using the new hybrids Gibbs point process model, we demonstrated that the joint effects of biotic processes at different scales and abiotic heterogeneity could explain the spatial pattern of the halophyte community. Soil salinity alone was not responsible for the distribution of halophyte community (Naz et al. 2010). Also, the relative importance of edaphic factors on the spatial structure of halophytic communities is scale-dependent (Pan et al. 1998) but biotic interactions play an important role in structuring these communities (Quets et al. 2013).

A medium-size shrub (2.4 meters of diameter) is found. Shrub canopy diameter is related to the presence of nebkhas size, and these vegetation islands are a function of the microtopography (El-Bana et al. 2002), highly correlated to soil salinity (Figure 9b). There is a positive interaction at 1.4 meters between two individuals, showing a process of facilitation described for hard arid conditions (Bertnessa and Callaway 1994). As there is no information in the species identity of each individual, we cannot interpret if the facilitation is between conspecifics or interspecific individuals. The spatial structure shows a random effect at 12 meters showing that these groups of two individuals are randomly distributed. This structure is showing that the studied community is in transition from aggregates at early stages to a regular pattern due to self-thinning response. This study is a start point for understanding the spatial structure of this halophyte community. It will be necessary more biotic information such as: species composition of the community, and also at temporal scales to a better understanding of the self-regeneration strategy of the halophyte community.

6.6 References

- Abd El-Kawy, O. R., Rød, J. K., Ismail, H. a., & Suliman, a. S. (2011). Land use and land cover change detection in the western Nile delta of Egypt using remote sensing data. *Applied Geography*, 31(2), 483–494.
- Baddeley A, Turner R. (2000). Practical maximum pseudolikelihood for spatial point patterns. *Australian and New Zealand Journal of Statistics*, 42:283–322
- Baddeley, A.J., Turner, R. (2006), *Modelling Spatial Point Patterns in R in Case Studies in Spatial Point Process Modelling*, Springer , USA. pp316
- Baddeley A, Møller J, Waagepetersen R. (2000). Non- and semiparametric estimation of interaction in inhomogeneous point patterns. *Statistica Neerlandica*, 54:329–350
- Badreldin, N., & Goossens, R. (2013a). Monitoring land use/land cover change using multi-temporal Landsat satellite images in an arid environment: a case study of El-Arish, Egypt. *Arabian Journal of Geosciences*. doi:10.1007/s12517-013-0916-3
- Badreldin, N., & Goossens, R. (2013b). A satellite-based disturbance index algorithm for monitoring mitigation strategies effects on desertification change in an arid environment. *Mitigation and Adaptation Strategies for Global Change*. doi:10.1007/s11027-013-9490-y
- Blanco-Canqui, H., & Lal, R. (2010). *Principles of Soil Conservation and Management*. Dordrecht: Springer Netherlands. doi:10.1007/978-1-4020-8709-7
- Blaschke, T. (2010). Object based image analysis for remote sensing. *ISPRS Journal of Photogrammetry and Remote Sensing*, 65(1), 2–16.
- Berman M, Turner TR. (1992). Approximating point process likelihoods with GLIM. *Journal of the Royal Statistical Society*, 41:31–38
- Bertness, M.D. & Callaway, R. (1994). Positive interactions in communities. *Trends in Ecology & Evolution*. 9: 191–193.
- Coppin, P., Jonckheere, I., Nackaerts, K., Muys, B., & Lambin, E. (2004). Digital change detection methods in ecosystem monitoring: a review. *International Journal of Remote Sensing*, 25(9), 1565–1596.
- Dale, M. R. T. (1999). *Spatial Pattern Analysis in Plant Ecology*. Cambridge, UK: Cambridge University Press. pp. 337.
- Diggle PJ., (2003). *Statistical analysis of spatial point patterns*, 2nd edn. Edward Arnold, London
- El-Bana, M., Khedr, A., Hecke, P. Van, & Bogaert, J. (2002). Vegetation composition of a threatened hypersaline lake (Lake Bardawil), North Sinai. *Plant Ecology*, (1937), 63–75.
- El-Bana, M.I., Li, Z.Q. and Nijs, I (2007). Role of host identity in effects of phytogenic mounds on plant assemblages and species richness on coastal arid dunes. *Journal of Vegetation Science*, 18: 635–644.
- Fortin M-J, Dale M., (2009). Spatial autocorrelation in ecological studies: a legacy of solutions and myths. *Geographical Analysis*, 41:392–397
- Frankl, A., Zwervaegher, A., Poesen, J., & Nyssen, J. (2013). Transferring Google Earth observations to GIS-software : example from gully erosion study. *International Journal of Digital Earth*, 6(2), 196–201.
- Galiano, E. F. (1985). The small-scale pattern of *Cynodon dactylon* in Mediterranean pastures. *Vegetatio*, 63(3), 121–127.
- Geyer CJ., (1999). Likelihood inference for spatial point processes, in: OE Barndorff-Nielsen, WS Kendall and MNM van Lieshout (eds), *Stochastic Geometry: Likelihood and Computation*, Chapman and Hall/CRC, London, pp 79–140.
- Goossens, R., & Van Ranst, E. (1998). The use of remote sensing to map gypsiferous soils in the Ismailia Province (Egypt). *Geoderma*, 87(1-2), 47–56.
- Greenwood, N. H. (1997). *The Sinai: a physical geography* (p. 148). Austin: University of Texas Press.
- Greig-Smith, P. (1961). Data on Pattern within Plant Communities: I. The Analysis of Pattern. *Journal of Ecology*, 49(3), 695–702.
- Illian, J., Penttinen, A., Stoyan, H., & Stoyan, D. (2008). *Statistical Analysis and Modelling of Spatial Point Patterns*. Chichester, UK: John Wiley & Sons, Ltd. pp. 557.
- Kenneth A. Kershaw. (1959). An Investigation of the Structure of a Grassland Community: II. The Pattern of *Dactylis Glomerata*, *Lolium Perenne* and *Trifolium Repens*: III. Discussion and Conclusions. *Journal of Ecology*, 47(1), 31–53.
- Knorn, J., Rabe, A., Radeloff, V. C., Kuemmerle, T., Kozak, J., & Hostert, P. (2009). Land cover mapping of large areas using chain classification of neighboring Landsat satellite images. *Remote Sensing of Environment*, 113(5), 957–964.
- Kottek, M., Grieser, J., Beck, C., Rudolf, B., & Rubel, F. (2006). World Map of the Köppen-Geiger climate classification updated. *Meteorologische Zeitschrift*, 15(3), 259–263.

- Liu, J. G., & Mason, P. J. (2009). *Essential Image Processing and GIS for Remote Sensing*. Chichester, UK: John Wiley & Sons, Ltd. pp. 462.
- Møller, J. and Waagepetersen, R. (2003). *Statistical inference and simulation for spatial point processes*. Chapman and Hall/CRC Press.
- Natural Resources Conservation Service (NRCS). (1999). *Soil Taxonomy: A Basic System of Soil Classification for Making and Interpreting Soil Surveys*, 2nd Ed., Washington, DC: United States Department of Agriculture (USDA), p871.
- Naz N, Hameed M, Sajid Aqeel Ahmad, M. Ashraf, M. Arshad M. (2010). Is soil salinity one of the major determinants of community structure under arid environments? *Community Ecology*, 11, 84-90.
- Pan, D., Bouchard, A., Legendre, P. and Domon, G. (1998), Influence of edaphic factors on the spatial structure of inland halophytic communities: a case study in China. *Journal of Vegetation Science*, 9: 797-804.
- Peel, M. C., Finlayson, B. L., & McMahon, T. A. (2007). Updated world map of the Köppen-Geiger climate classification. *Hydrology and Earth System Sciences*, 11, 1633-1644.
- Perry GLW, Miller BP, Enright NJ. (2006). A comparison of methods for the statistical analysis of spatial point patterns in plant ecology. *Plant Ecology*, 187:59-82
- Petrou, M., & Bosdogianni, P. (1999). *Image Processing: The Fundamentals*. Chichester, UK: John Wiley & Sons, Ltd. pp 347.
- Quets J., Temmerman S., El-Bana M.I., Al-Rowaily S., Assaeed A. M., Nijs I. (2013). Unravelling landscapes with phytogenic mounds (nebkhas): an exploration of spatial pattern. *Acta Oecologica*, 49: 53-63.
- Rhoades, J. D. (1992). *Instrumental Field Methods of Salinity Appraisal*. Advances in Measurement of Soil Physical Properties: Bringing Theory into Practice, Vol. SSSA. Soil Science Society of America. pp347.
- Rubio-Casal, a. E., Castillo, J. M., Luque, C. J., & Figueroa, M. E. (2001). Nucleation and facilitation in salt pans in Mediterranean salt marshes. *Journal of Vegetation Science*, 12(6), 761-770.
- Sadr, K., & Rodier, X. (2012). Google Earth, GIS and stone-walled structures in southern Gauteng, South Africa. *Journal of Archaeological Science*, 39(4), 1034-1042.
- Schowengerdt, R. A. (2007). *Remote Sensing: Models and Methods for Image Processing*, 3rd Ed., Amsterdam, NL: Elsevier. pp 558.
- Shalaby, A., & Tateishi, R. (2007). Remote sensing and GIS for mapping and monitoring land cover and land-use changes in the Northwestern coastal zone of Egypt. *Applied Geography*, 27(1), 28-41.
- Sheppard, S. R. J., & Cizek, P. (2009). The ethics of Google Earth: crossing thresholds from spatial data to landscape visualisation. *Journal of environmental management*, 90(6), 2102-17.
- Shih, F. Y. (2010). *Image Processing and Pattern Recognition: Fundamentals and Techniques*. Hoboken, NJ, USA: John Wiley & Sons, Inc. p. 552
- Taylor, J. R., & Lovell, S. T. (2012). Mapping public and private spaces of urban agriculture in Chicago through the analysis of high-resolution aerial images in Google Earth. *Landscape and Urban Planning*, 108(1), 57-70.
- U.S. Salinity Laboratory. (1954). *Diagnosis and Improvement of Saline and Alkali Soils* (Handbook 6., p. 172). Washington, DC: U.S. Government Printing Office.
- Ungar, I. A. ., Benner, D. K. ., & McGraw, D. C. . (1977). The Distribution and Growth of *Salicornia Europaea* on an Inland Salt Pan. *Ecology*, 60(2), 329-336.
- Usher, M. B. (1983). Pattern in the Simple Moss-Turf Communities of the Sub-Antarctic and Maritime Antarctic. *Journal of Ecology*, 71(3), 945-958.
- Vincent, L., & Soille, P. (1991). Watersheds in digital spaces: an efficient algorithm based on immersion simulations. *IEEE Transactions on Pattern Analysis and Machine Intelligence*, 13(6), 583-598.
- Webster, R., & Oliver, M. A. (2007). *Geostatistics for Environmental Scientists*, 2nd Ed., Chichester, UK: John Wiley & Sons, Ltd. p. 333
- Winkler, G. (2006). *Image Analysis, Random Fields and Markov Chain Monte Carlo Methods: A Mathematical Introduction (Stochastic Modelling and Applied Probability)*. Retrieved from <http://dl.acm.org/citation.cfm?id=1206577>
- Yang, X., Jiang, G.-M., Luo, X., & Zheng, Z. (2012). Preliminary mapping of high-resolution rural population distribution based on imagery from Google Earth: A case study in the Lake Tai basin, eastern China. *Applied Geography*, 32(2), 221-227.

Chapter 7

General conclusions and recommendations

This chapter is modified from:

Nasem Badreldin and Rudi Goossens (2013) Bi-stable ecosystem balance and satellite-based algorithms: New approaches for assessing desertification in arid lands. Journal of Arid Environments. "Submitted"

7.1 General conclusion

Desertification is the major environmental threat in the arid regions. In **Chapter 3**, SAVI was used as an indicator to monitor the desertification change in Egypt. A multi-temporal satellite data of MODIS were used to estimate SAVI and LST. Also, GMTED2010 and climatic data were used for the analysis. This research focuses on assessing the trend of the vegetation cover change in the seasons of January, March, June, September and December for the years 2002, 2005, 2008 and 2011. The magnitude of the vegetation cover change in periods 2002-2005, 2005-2008 and 2008-2011 at ≤ 100 and > 100 meters elevation were analyzed. A major increase in the vegetation cover occurred in the period 2002-2005 was about 3400 km², as a result of two national mega-projects (Toshka Project and El-Salam Canal). In contrast, vegetation cover decreased by 5500 km² in March during the period 2005-2008, coinciding with the period when the management of the mega-projects failed. Vegetation cover changed again 1500 km² in the period of 2008-2011, the vegetated areas in the Nile Delta were affected by the sea level rising which was responsible for the soil salinization. Three sites were chosen in this investigation (Kom Ombo, El-Oweinat and Nile Delta) in order to observe the difference of desertification dynamics and to understand relationship between the vegetation cover distribution and other environmental variables. Anti-desertification policies and advanced agricultural management are highly required in Egypt to decrease any environmental crises and food shortage.

In **Chapter 4**, a new satellite-based algorithm for monitoring desertification in an arid environment was proposed in order to deliver useful information about the desertification hazards dynamic at sub-regional scale. A multi-temporal remote sensing data of MODIS were used for SAVI and LST, based on monthly data during the years 2002, 2005, 2008 and 2011. MBDI was improved by estimating the long-term variation in the ratio of annual maximum composite LST and SAVI on a pixel-by-pixel basis. A significant correlation ($r=-0.88$; $P<0.001$) was found between the mean-maximum SAVI and mean-maximum LST in the dry season. The response of the MBDI to land degradation was assessed by comparing the obtained soil salinity data to the algorithm outcomes. The results showed that the proposed new satellite-based algorithm has a high potential to detect the spatial extent of prime land degradation in an arid environment. Also, this algorithm was able to recognize the difference between the natural variability and instantaneous/non-instantaneous desertification symptoms in an arid environment. The mitigation strategies in the case study decreased the desertification development and combat the land degradation in the last decade.

Environment in arid conditions is dynamic and needs more investigation to understand the complexity of change in moderate spatial scale. This spatio-temporal study will help to assess and monitor LULC change in the arid region of El-Arish area (**Chapter 5**), where the climate and human activities are the major threat to the rural development. In the past 11 years dramatic changes of environment have been recorded in this case studies. The post classification comparison method was used to observe the changes using multi-temporal satellite images which were captured in the years 1999, 2001, 2005, and 2010. The overall accuracy of the produced thematic images was assessed regarding to the quantity and allocation disagreements. Five classes were defined in this investigation: Bare soil, vegetation, urban, sand dunes and fertile soil. From the year 1999 to 2010, fertile soil was increased by 13%. Bare soil class occupied more than 50% of land in the case study during for over a decade. From year 1999 to 2010 vegetation cover witnessed dramatic increase. Soil and water management are the keys of land development and positive Land Use and Land Cover dynamics. Changing agricultural policies of using the available water resources are needed in the case study to prevent severe food shortage in the future.

In small spatial scales, obtaining information about the horizontal distribution of desert plants is considered as a serious challenge for ecologists and environmental modeling due to the required intensive field work and infrastructures in harsh and remote arid environments. In **Chapter 6**, a new method was applied for assessing the spatial distribution of the HS in an arid coastal environment. This method was based on object-based image analysis for a high resolution Google Earth image. The integration of image processing techniques and field work provided accurate information about the spatial distribution of HS. The extracted objects were based on assumptions that explained plant-pixel relationship. Three different types of digital image processing techniques were implemented and validated in order to obtain accurate HS spatial distribution. 2703 of the HS were found in the case study, about 82% were located above 2m elevation. The microtopography showed a significant negative relationships with pH and EC ($r = -0.79$ and -0.81 , respectively, $p < 0.001$). The spatial structure was modeled using stochastic point processes, in particular a hybrid family of Gibbs processes. A new model is proposed which is handled a hard-core structure at very short distances, together with a cluster structure in short-to-medium distances and a Poisson one for larger distances. This model found to fit the data perfectly well.

7.2 Bi-stable ecosystem balance for assessing desertification status

The Bi-stable ecosystem balance explained the status of desertification in arid environment (Chapters 3 & 4). Based on the spatial and temporal changes of the land cover, this system has two possible stable states – with vegetation cover (biotic environment) and desertified (abiotic environment), and these states are both locally stable to some arid environmental perturbations. Two aspects of environmental stability were considered: resistance (the amount a variable changes in response to a given disturbance) and resilience (stable state recovery duration). Lenton (2002) reported that the abiotic state in arid environment is uninhabitable “desertified”, locally stable to the addition of some life, and the biotic state is habitable “vegetated”, locally stable to the removal of some life, then the system is bi-stable, and an unstable state will also exist between the two stable states. The arid ecosystem exhibit the resistances to change to a certain range of impacts via the unstable states, thresholds are at the edges of the resistance ranges, where the system leads to stable or transition state (Figure 7.1).

The non-desertified area in this investigation was the most biotic condition, which is “vegetated” or stable to be cultivated, as a result of the homeostatic environmental conditions of Egypt in the period January to March. The suitable climatic conditions were recovering any decline in vegetation cover distribution during this period of time (Chapter 5, Figure 5.6), unless it is disturbed by sudden events, such as the flash food that occurred in January 2011 in El-Arish city, as shown in (Chapter 5; Figure 5.8). 90% of the vegetation in Egypt were located in the Nile delta and valley, where the freshwater and fertile soil were highly available (Chapter 3, Table 3.1). The slightly –desertified status occurred mostly in the period between March and June, where the vegetation cover started to decrease dramatically. In this particular status the environmental conservation and local mitigation strategies were effective in order to prevent desertification and land degradation to move to a permanent desertified status. Semi-desertified status is a result of reaching environmental resistance threshold, over consumption of natural resource such as water, can lead to dramatic decrease in the vegetation cover in the Nile Delta. Also, The usage of the limited available land resources regardless the sustainability caused more damage to soil, water logging and soil salinization feedbacks are one of major land degradation effects in arid regions like Egypt (Frihy and El-Sayed 2012; Mohamed et al. 2012), Zahran and Willis (2009) reported that the differences in rainfall were seen in the growth of ephemerals and the appearance of seedlings of perennials in the wet season which may or may not continue to grow, depending on the volume of water resources. In the “Moderately-desertified” status the human impact is the most effective factor that move the arid environment to more permanent degradation and desertification, such as low level of precision farming in Kom Ombu which caused directly by over consumption to the limited natural resources regardless the sustainability and damage to soil (Chapter 3; Figure3.9).

Many sites were affected with permanent land degradation and desertification, such as the case in the northwestern side of the Nile Delta and the northeastern side of El-Zaraniq Protected Area, where the desertification status reached to the extremely-desertified degree. The soil salinity and sand dunes movement exterminate all habitats, and only tolerant species survive the extreme soil salinity and drought (Figure 7.1).

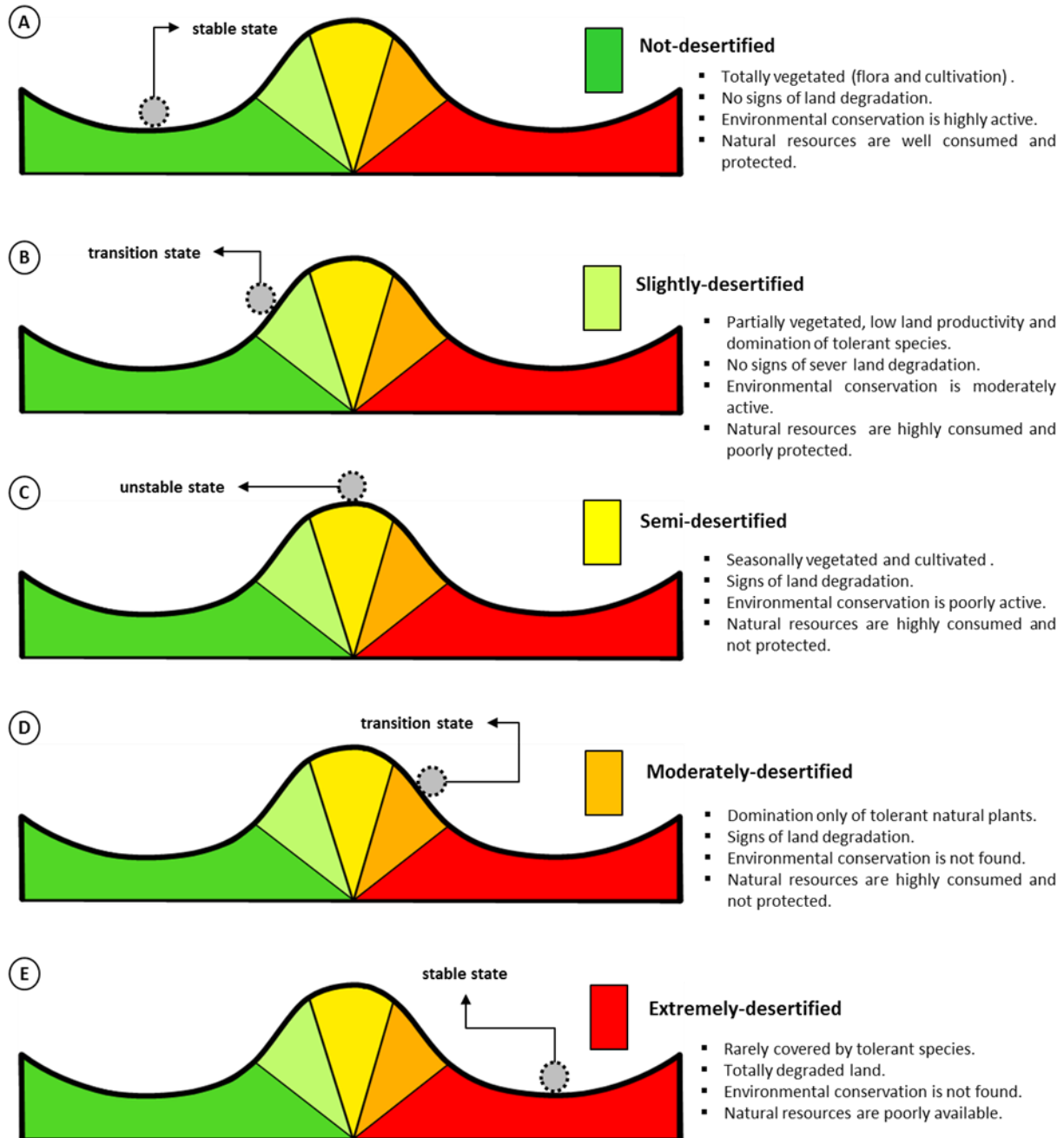


Figure 7.1. Illustration draws of the bi-stable ecosystem balance for an arid environment.

7.3 MODIS Based Disturbance Index (MBDI) for monitoring the desertification development

The MBDI is the ratio of annual maximum composite LST and SAVI, which was based on a multi-temporal MODIS satellite data. This algorithm was designed to capture long-term variations on a pixel-by-pixel basis for detecting the significant in the inter-annual changes of surface energy. Usually these changes were responsible for the natural variability of instantaneous and non-instantaneous desertification symptoms in arid environment like Egypt (e.g., erosion, overgrazing, climate change and drought) (Mildrexler et al. 2007). In order to detect the disturbance the success of this algorithm was depending on two major factors: 1) sufficiently strong and frequent signals to detect disturbance and 2) obtaining signals greater than the natural variability of the case study (Coops et al. 2009; Mildrexler et al. 2007).

It is important to determine the natural condition for any case study in arid environments in order to understand the pattern of the environmental changes such as desertification development. The natural variability window was defined for each individual pixel that falls within \pm standard deviation for the long-term mean LST/SAVI ratio, as described in (Chapter 4; section 4.2.4). Instantaneous disturbance such as water erosion and floods are responsible for any immediate increase in MBDI from the natural variability range, whereas non-instantaneous disturbance such as drought and soil salinization, will incrementally shift the MBDI over the natural variability range, see Figure 7.2.

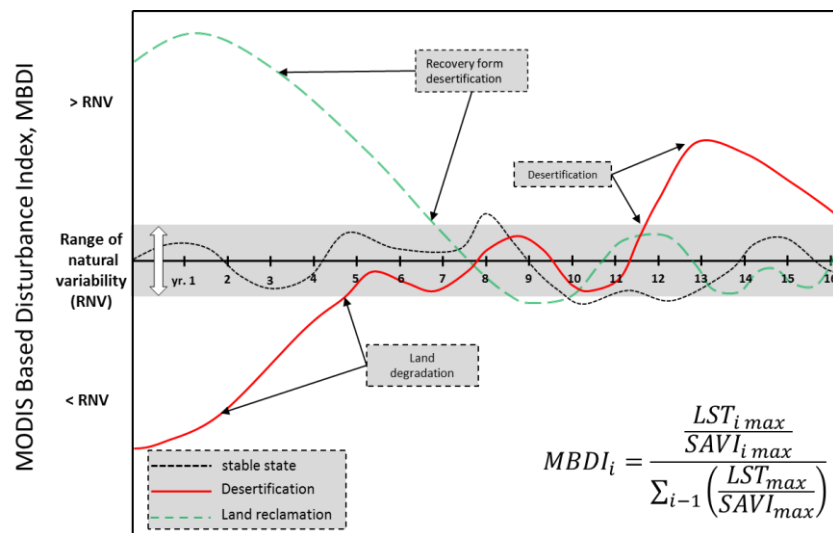


Figure 7.2. The MODIS Based Disturbance Index (MBDI) algorithm with a bi-directional aspect, for tracking the disturbance that caused by desertification in an arid environment. The normal environmental condition exist in the range of the natural variability (gray zone), when the studied year LST_{max} and $SAVI_{max}$ have the mean of 0.6. In cases of desertification the LST_{max} increases and the $SAVI_{max}$ decreases (red solid line). The recovery state found when the LST_{max} decreases and the $SAVI_{max}$ increases (green dashed line).

The accuracy assessment to the MBDI algorithm was highly required in order to trust the results. The soil salinity was considered as the major disturbance agents that found in Sinai Peninsula (Nawar et al. 2011). 44 soil samples were collected from different sites in North Sinai for analyzing soil salinity and compared with the MBDI values that represent the disturbance in the case study for the same temporal-frame (2011) and spatial location, as shown in Figure 7.3; soil salinity classification was based on (Chapter 4; Table 4.3). A strong relationship between the measured data and the estimated values of disturbance MBDI ($r = 0.79$; $p < 0.001$), which approved using the algorithm for monitoring the desertification in this particular case study.

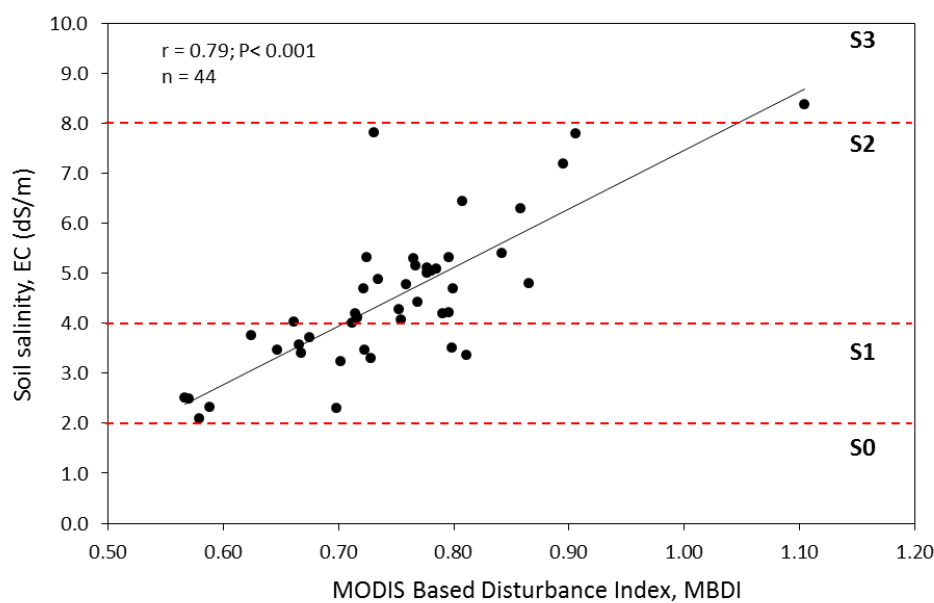


Figure 7.3 Soil salinity, EC (dS/m) and the MODIS-Based Disturbance Index, MBDI relationship; $n=44$ soil samples were obtained during field survey in 2011, the soil salinity classified into four major groups, see table 4. S0: Non-saline (< 2 dS/m); S1: Slightly-saline (2-4 dS/m); S2: Moderately-saline (4-8 dS/m); S3: Highly-saline (8-16 dS/m).

The MBDI algorithm detected a recovery from desertification at two sites in the case study (El-Tina plain and Qanatra Shark), MBDI detected evidences of mitigation activities which decreased desertification and land degradation. Soil leaching was the strategy for decreasing the salinity in order to improve the physical and chemical soil properties for agriculture production in the case study, which was given a high national priority (Galal 2004). This algorithm provided a useful and accurate information for monitoring desertification development in regional scales. It is important for detecting and assessing the natural and human impacts on arid environments. Also, it can be used for environmental risk assessment or early warning system for decision makers, organizations and public awareness, in order to avoid severe desertification events in arid environments

7.4 A decade of LULC change in El-Arish city

This study was based on a multi-temporal ETM+ satellite images, which was the suitable datasets for change detection analysis in El-Arish, (Chapter 5). The general goal was how to provide accurate information about the amount and possible reasons of change such in an arid environment condition, where the natural resources are limited. It is highly required to preprocess the satellite images in LULC change detection research in order to establish the direct link between the image and the case study (Abd El-Kawy et al. 2011; Coppin et al., 2004). The minimum acceptable overall accuracy in LULC research is 85 % (Thomlinson et al. 1999), which was achieved, as shown in (Chapter 5; Table 5.2). Pontius and Millones (2011) recommended the using of quality and allocation disagreement for the accuracy assessment, this method was used in order to avoid introducing problems in the calculation and interpretation processes and to prevent testing the accuracy due to randomness, as shown in (Chapter 5; Figure 5.4).

Over the studied years (1999, 2001, 2005, and 2010) LULC classes showed different trends of changes according to the human activity and the environmental situation. A dramatic increase was monitored in year 1999 for the vegetation cover from 1.08% (6.1 km²) to be 7.94% (45.2 km²) in year the 2010, bare soil class was the largest area in the case study at all studied years, which was occupying approximately 78% (439.2 km²) in the year 1999 and changed to be 60% (339.7 km²) in the year 2010, urban class slightly increased from 4.75% (5.5 km²) to be 5.40% (30.7km²), fertile soil class rapidly increased over the years from 5.12% in 1999 and reached 18.38% (104.7km²) in 2010, and sand dunes class has decreased about (-2%) between the period of 1999 – 2010, as shown in (Chapter 5; Figure 5.5).

The wind erosion was the major environmental threat, as shown in climatic records in February 2003 (Chapter 5; Figure 5.7), the sand dunes distribution increased +4.53% of the case study area. However, El-Salam Canal was one of the mega national projects that influenced positively the agricultural activities in the period of (1999–2005).

El-Arish city was vulnerable to any environmental perturbations, which indicate that the local agricultural area in this case study was poorly designed and protected, in January 2010 a flash flood struck the most vegetated area and part of urban areas in El-Arish city, beside losing a massive amount of fresh water and fertile soils, which were the most precious environmental element in such arid environment, as shown in (Chapter 5; Figure 5.8). In the period of (2005-2010) the urban area decreased about -0.78%, the vegetation cover and fertile soils were slowly increased +0.77% and +2.79%, respectively, as shown in (Figure 7.4)

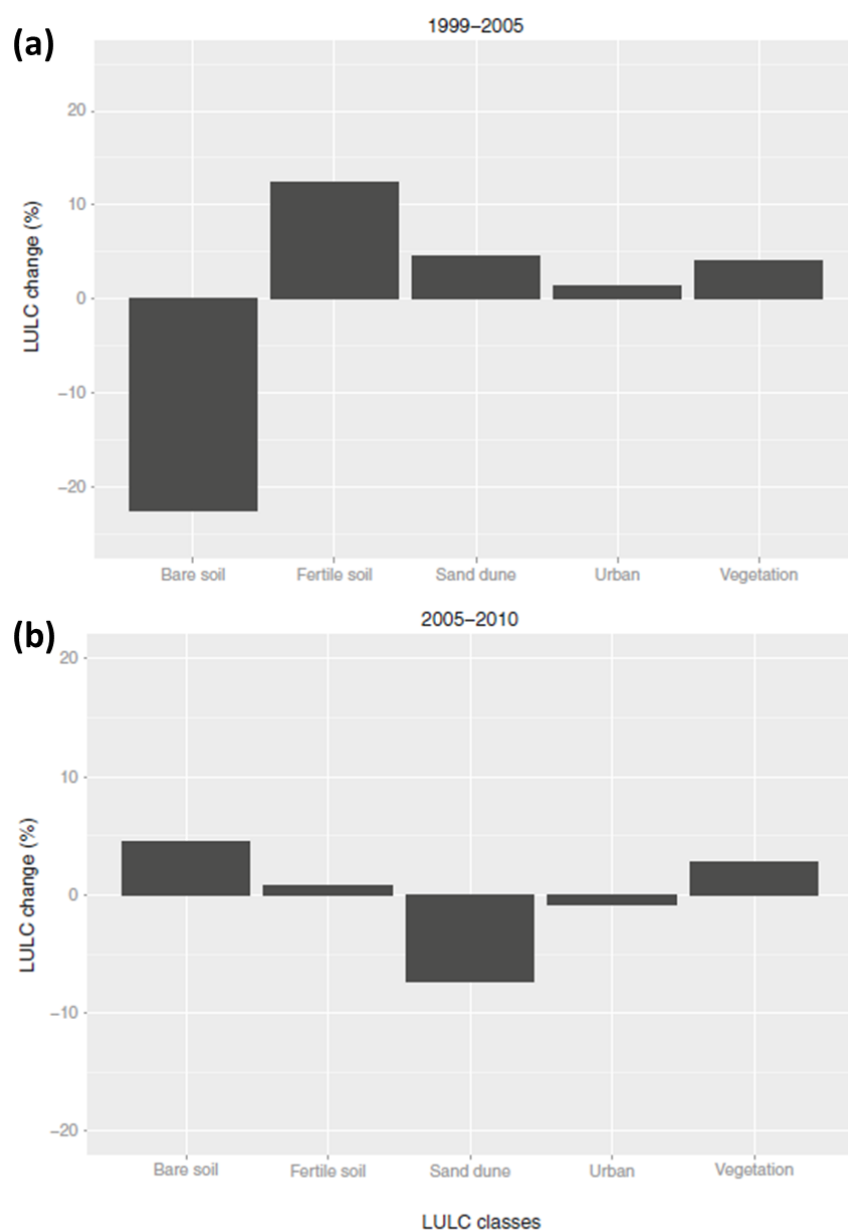


Figure 7.4. LULC change over the period, **a)** 1999–2005; and **b)** 2005–2010.

7.5 Google Earth images for spatial pattern analysis

Many researchers found that Google Earth images were valuable for different environmental studies (Frankl et al. 2013; Sadr and Rodier 2012; Sheppard and Cizek 2009; Taylor and Lovell 2012; Yang et al. 2012). Improving the quality of satellite images via advanced techniques of digital image processing has a significant impacts on the field of ecology and environmental sciences (Blaschke 2010; Illian et al. 2008; Liu and Mason 2009; Schowengerdt 2007; Shih 2010; Vincent and Soille 1991; Winkler 2006).

7.5.1 Object-pixel relationship and extraction in arid environment

Building a suitable assumption that explains accurately the object-pixel relationship during the field survey will help to select the appropriate image processing model. During the field work a unique relationship between HS and soil was indicated, this relationship affected the spectral response of the satellite images for this particular case study, as shown in (Chapter 6; section 6.2), the observed HS was found on the top of sand accumulation called “phytogenic hummocks” with 0.5 m height average (El-Bana et al. 2010). The illustration draws of this phenomenon, as shown in (Figure 7.5a and b) explained the difference in solar radiation reflectance between HS and hummocks’ edges, the plant position gave more reflectance than the surrounded area which was exposed “barren soil” and cause scattering to most of the incident solar radiation that was received from the sun (Figure 7.5c).

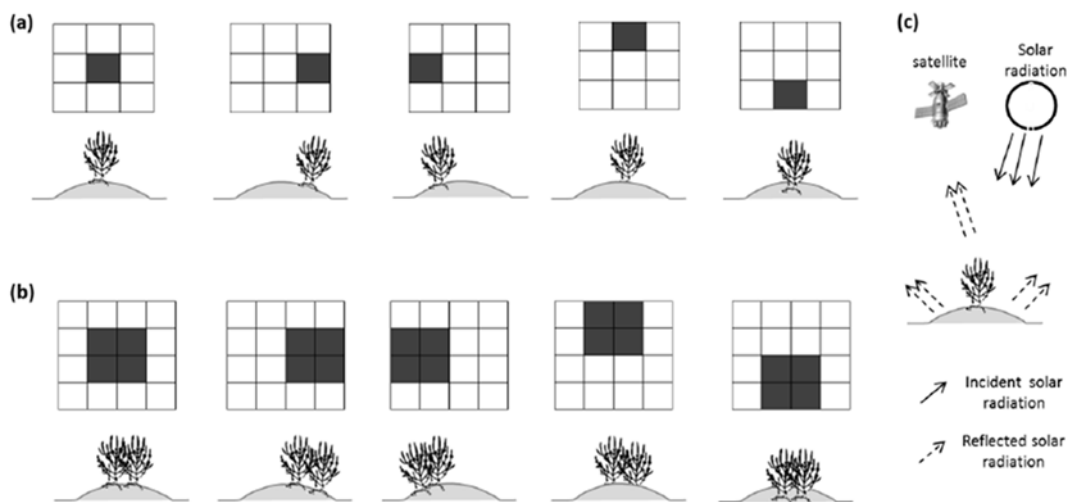


Figure 7.5. Illustration draws of the target objects "HS"; **a)** single object position; **b)** group of objects positions; and **c)** the reflectance and absorbed solar radiation pattern. Object extraction analysis.

Based on previous assumption three different image processing techniques were implemented in order to obtain accurately the HS spatial distribution. Selecting the best HS extraction method was based on validating the digital image analysis with random 90 HS positions which were counted and located in the field survey. RCED proven to be the best object extraction operator which provide accurate information about HS distribution and met the assumption design that explained the local environmental condition of the case study.

7.5.2 Integration system based analysis for HS spatial distribution

The integration between field survey, digital image processing, and point pattern analysis provided better understanding to the local environment conditions and explaining more accurately the HS spatial distribution in the case study. RCED is proven to be the best object extraction operator which provide accurate information about HS distribution and met the assumption design that explained the local environmental condition of the case study.

Generally, about 82% of HS are found on elevation > 2m, the microtopography found to be strongly correlated with both soil pH and EC ($r = -0.79$ and -0.81 ; $p < 0.001$, respectively). Using the new hybrids Gibbs point process model, we demonstrated that the joint effects of biotic processes at different scales and abiotic heterogeneity could explain the spatial pattern of the halophyte community. Soil salinity alone was not responsible for the distribution of halophyte community (Naz et al., 2010). Also, the relative importance of edaphic factors on the spatial structure of halophytic communities is scale-dependent (Pan et al. 1998) but biotic interactions play an important role in structuring these communities (Quets et al. 2013).

A medium-size shrub (2.4 meters of diameter) was found. Shrub canopy diameter is related to the presence of nebkhas size, and these vegetation islands are a function of the microtopography (El-Bana et al. 2002), highly correlated to soil salinity (Chapter 6; Figure 6.9b). There is a positive interaction at 1.4 meters between two individuals, showing a process of facilitation described for hard arid conditions (Bertnessa and Callaway 1994). As there is no information in the species identity of each individual, we cannot interpret if the facilitation is between conspecifics or interspecific individuals. The spatial structure shows a random effect at 12 meters showing that these groups of two individuals are randomly distributed. This structure is showing that the studied community is in transition from aggregates at early stages to a regular pattern due to self-thinning response. This study will be a start point for better understanding to the spatial structure of the halophyte community in arid environment.

7.6 Suggestions for future research

Even as this thesis aimed to develop new methodologies for assessing environmental change in arid regions using remote sensing and GIS, which has so far been achieved, there still remain aspects for future research that will help to perform better investigation.

- MODIS satellite images provide useful data for monitoring arid-environmental change at regional scale. A series of monthly data for a continues 5 years or more will help researchers to identify the most affected locations;
- Assessing the vegetation cover change in arid regions is the first step that should be tested, in order to have a clear visibility for carrying on further research in desertification in a particular case study;
- The integration between remote sensing and GIS tools and analysis with the field survey will support the research to understand the interactions of all drivers and feedbacks. Field survey and sampling must be designed carefully; selecting the most significant parameters to be tested will save more time and money;
- MBDI is a promising algorithm for assessing the desertification in arid regions, developing other algorithms will be helpful to obtain more information about desertification development in a small spatial scale;
- Assessing the LULC change in arid environment required certain accuracy for the image classification, which is the most crucial challenge in this kind of research. More GCPs and statistical data will increase the knowledge of understanding the case study, and will provide image classification with high accuracy and more trustful results;
- For better research in monitoring the LULC change over different years in arid environment, we suggest that such studies must be conducted in the same climatic condition or season for each selected year, such as satellite images, field survey and measurements. Obtaining a monthly data and measurement for a continues 5 years or more will provide a clear information about the actual pattern of LULC change, and will help to identify the vital causes of change; and
- Google earth images are very valuable and accessible data source for studying the spatial pattern analysis of the habitats in arid environment, the field measurements will add useful information that explain the causes of the monitored patterns.

7.7 Clues for decision makers on the use of the research findings

This section elaborates how decision makers can make use the results of the environmental change assessment for Egypt and other locations that have the same aridity condition.

- The GIS statistical results obtained from this research can be used to substantiate claims of the desertification threats to the arid environmental condition of Egypt, and use that to formulate plans and policies for achieving a well-protected environment;
- The findings of this thesis will help decision makers to come to the realization that a healthier environment in arid condition cannot be achieved without adequate involvement of local people who are affected of desertification. It is important to depend on the people who live in the affected environment rather than government policies and regulations;
- The local people are not knowledgeable on issues pertaining to their natural environment. The results of the thesis thus expose how knowledgeable local people are on issues of the environment and the need to tap such resources for policy formulation; and
- In formulating environmental policies, decision makers should not discard the local environmental management practices, but should manage how such practices could be effectively utilized with scientific management practices to realize a greener and more protected environment.

7.8 References

- Abd El-Kawy OR, Rød JK, Ismail H a., Suliman a. S (2011) Land use and land cover change detection in the western Nile delta of Egypt using remote sensing data. *Applied Geography* 31:483–494.
- Bertness, M.D. & Callaway, R. (1994). Positive interactions in communities. *Trends in Ecology & Evolution*. 9: 191–193.
- Blaschke T (2010) Object based image analysis for remote sensing. *ISPRS Journal of Photogrammetry and Remote Sensing* 65:2–16.
- Coops NC, Wulder M a., Iwanicka D (2009) Large area monitoring with a MODIS-based Disturbance Index (DI) sensitive to annual and seasonal variations. *Remote Sensing of Environment* 113:1250–1261.
- Coppin P, Jonckheere I, Nackaerts K, et al. (2004) Digital change detection methods in ecosystem monitoring: a review. *International Journal of Remote Sensing* 25:1565–1596.
- El-Bana M, Khedr A, Hecke P Van, Bogaert J (2002) Vegetation composition of a threatened hypersaline lake (Lake Bardawil), North Sinai. *Plant Ecology* 63–75.
- El-Bana M, Shaltout K, Khalafallah A, Mosallam H (2010) Ecological status of the Mediterranean *Juniperus phoenicea* L. Relicts in the desert mountains of North Sinai, Egypt. *Flora - Morphology, Distribution, Functional Ecology of Plants* 205:171–178.
- Frankl A, Zwertvaegher A, Poesen J, Nyssen J (2013) Transferring Google Earth observations to GIS-software : example from gully erosion study. *International Journal of Digital Earth* 6:196–201.
- Frihy OE, El-Sayed MK (2012) Vulnerability risk assessment and adaptation to climate change induced sea level rise along the Mediterranean coast of Egypt. *Mitigation and Adaptation Strategies for Global Change*. doi: 10.1007/s11027-012-9418-y
- Galal ME (2004) Estimating Soil Hydraulic Parameters In El-Tina Plain Using RETC Program. *International Conf. on Water Resources & Arid Environment*. p 5
- Illian J, Penttinen A, Stoyan H, Stoyan D (2008) Statistical Analysis and Modelling of Spatial Point Patterns. 557.
- Lenton TM (2002) Testing Gaia: the effect of life on earth's habitability and regulation. *Climatic Change* 52:409–422.
- Liu JG, Mason PJ (2009) *Essential Image Processing and GIS for Remote Sensing*. John Wiley & Sons, Ltd., Chichester, UK. pp 462.
- Mildrexler DJ, Zhao M, Heinsch FA, Running SW (2007) A new satellite-based methodology for continental-scale disturbance detection. *Ecological applications : a publication of the Ecological Society of America* 17:235–50.
- Mohamed ES, Belal A, Saleh A (2012) Assessment of land degradation east of the Nile Delta, Egypt using remote sensing and GIS techniques. *Arabian Journal of Geosciences*. doi: 10.1007/s12517-012-0553-2
- Nawar S, Reda M, Farag F, El-nahry A (2011) Mapping Soil Salinity in El-Tina Plain in Egypt Using Geostatistical Approach. *Geoinformatics Forum. Salzburg, Austria*, pp 81–90
- Naz N, Hameed M, Sajid Aqeel Ahmad, M. Ashraf, M. Arshad M. (2010). Is soil salinity one of the major determinants of community structure under arid environments? *Community Ecology*, 11, 84–90.
- Pan, D., Bouchard, A., Legendre, P. and Domon, G. (1998), Influence of edaphic factors on the spatial structure of inland halophytic communities: a case study in China. *Journal of Vegetation Science*, 9: 797–804.
- Pontius RG, Millones M (2011) Death to Kappa: birth of quantity disagreement and allocation disagreement for accuracy assessment. *International Journal of Remote Sensing* 32:4407–4429.
- Quets J., Temmerman S., El-Bana M.I., Al-Rowaily S., Assaeed A. M., Nijs I. (2013). Unravelling landscapes with phytogenic mounds (nebkhas): an exploration of spatial pattern. *Acta Oecologica*, 49: 53–63.
- Sadr K, Rodier X (2012) Google Earth, GIS and stone-walled structures in southern Gauteng, South Africa. *Journal of Archaeological Science* 39:1034–1042.
- Schowengerdt RA (2007) *Remote sensing: models and methods for image processing*, 3rd edn. Elsevier, Amsterdam, pp 558.
- Sheppard SRJ, Cizek P (2009) The ethics of Google Earth: crossing thresholds from spatial data to landscape visualisation. *Journal of environmental management* 90:2102–17.
- Shih FY (2010) *Image Processing and Pattern Recognition: Fundamentals and Techniques*. John Wiley & Sons, Inc., Hoboken, NJ, USA. pp 552.
- Taylor JR, Lovell ST (2012) Mapping public and private spaces of urban agriculture in Chicago through the analysis of high-resolution aerial images in Google Earth. *Landscape and Urban Planning* 108:57–70.
- Thomlinson J, Bolstad P, Cohen W (1999) Coordinating methodologies for scaling landcover classifications from site-specific to global: steps toward validating global map products. *Remote Sensing of Environment* 70:16 – 28.

- Vincent L, Soille P (1991) Watersheds in digital spaces: an efficient algorithm based on immersion simulations. *IEEE Transactions on Pattern Analysis and Machine Intelligence* 13:583–598.
- Winkler G (2006) *Image Analysis, Random Fields and Markov Chain Monte Carlo Methods: A Mathematical Introduction (Stochastic Modelling and Applied Probability)*. 2nd Ed. Springer. Berlin, Heidelberg, pp 381.
- Yang X, Jiang G-M, Luo X, Zheng Z (2012) Preliminary mapping of high-resolution rural population distribution based on imagery from Google Earth: A case study in the Lake Tai basin, eastern China. *Applied Geography* 32:221–227.
- Zahran MA, Willis AJ (2009) *The Vegetation of Egypt*, 2nd ed. Springer, Heidelberg, pp 451.